COUNTERION BINDING TO IONIC AND MIXED IONIC/NONIONIC MICELLES

by

HELEN R. STEWART B.Sc.

A thesis submitted for the
Degree of Doctor of Philosophy

University of Edinburgh

April 1981

I declare that the work described in this thesis has not been submitted for any other degree and is the original work of the author except where acknowledgement is made by reference. The work was carried out in the Chemistry Department of the University of Edinburgh between October 1977 and September 1980 under the supervision of Dr. W.D. Cooper. Some time was also spent at the Unilever Research Laboratories at Port Sunlight.

Postgraduate courses attended include:
Chemistry of the Atmosphere (12 lectures - Prof. R.J. Donovan); E.R.C.C. Fortran B Course (1 week); Chemistry at its Most Colourful (8 lectures - Staff of I.C.I. Organics Division); Detergency and the Design of Surface Active Agents (5 lectures - Dr. W.D. Cooper); Why Chemists Use Neutrons (7 lectures); The Bio-organic Chemistry of Drugs, Toxins and other Xenobiotics (5 lectures - Dr. A.G. Rowley); Catalysis and Chemical Productivity (7 lectures - Staff of I.C.I. Petrochemicals Division); Mass Spectrometry (5 lectures - Prof. J.H. Beynon); Zeolites (5 lectures - Dr. B.M. Lowe).

I would like to place on record my thanks to:

1. Dr. W.D. Cooper for his continued interest, and willingness to discuss and assist throughout the duration of the research project.

2. Dr. A.L. Smith and Dr. T.J. Price of Unilever Research who contributed to some valuable discussions and Mr. E.J. Staples for instruction in the use of the PCS apparatus.

3. The technical staff of the Chemistry Department, in particular Mr. J. Broom who constructed the glassware for the electrokinetic experiments.

4. My husband and parents for their encouragement and support.

5. The SRC and Unilever Research for the provision of a CASE grant.

6. Mrs. J. Gorrie for undertaking the typing of the manuscript.

ABSTRACT

Amphipathic molecules associate into micelles at concentrations in excess of the critical micelle concentration (c.m.c.). The resultant charge on micelles containing ionic surfactant is less than that due to the number of ionised head groups per micelle because of counterion binding to the micelle. In this study aqueous solutions of pure ionic and mixed ionic/nonionic surfactants have been investigated. Using the results of conductivity and dye tracer electrophoresis experiments the degree of dissociation, α, of mixed micelles of cetyl trimethyl-ammonium bromide/hexaoxyethylene n-dodecyl ether ($CTAB/C_{12}E_6$) has been determined as a function of micelle composition. Less detailed investigations of the systems sodium dodecyl sulphate/tetraoxyethylene n-octyl ether (SDS/C_8E_4), CTAB/alcohol, and SDS/alcohol have also been carried out, with ionic strength variation noted for the pure ionic surfactants. In general when nonionic material is added to the ionic surfactant solution it enters the micelles causing a decrease in the surface charge density. This permits the release of bound counterions which is demonstrated by a corresponding increase in α. It is found that for $CTAB/C_{12}E_6$ the adsorption of counterions follows the form of the Langmuir Adsorption Isotherm.

Micellar size has been estimated from measured diffusion coefficients obtained by Photon Correlation Spectroscopy and results indicate that at the c.m.c. the radii of CTAB and $C_{12}E_6$ micelles are identical and furthermore the SDS and C_8E_4 micellar radii are equal.

The collected data have been analysed using simple thermodynamic theories of micellisation and following D. Stigter, recent theories of conductivity and electrophoresis. Values of α calculated by various applicable methods are found to be in good agreement.

CONTENTS

CHAPTER ONE

INTRODUCTION

CHAPTER 1

INTRODUCTION

1.1 The Phenomenon of Micellisation

Molecules which are amphipathic, that is molecules which contain both a hydrophilic and hydrophobic part have unusual properties in aqueous solution. In order to minimise interfacial energy they can become aligned at the solution/air interface with the hydrocarbon tails protruding into the air and the polar head groups immersed in the aqueous environment. However, above a certain critical concentration of material an alternative mechanism exists for the reduction of interfacial free energy. Plots of many physical properties against a function of concentration, c, for example specific conductivity, κ_{sp} against concentration, molar conductivity, Λ against $c^{\frac{1}{2}}$, surface tension, γ against lnc, turbidity, τ against c, show a discontinuity around this critical concentration which is due to the aggregation of monomers into micelles (see figure 1.1.1). The micelles are reversibly formed and contain 20 to 200 monomers for ionic micelles and often over 1000 for nonionic micelles. The critical nature of the onset of micellisation has led to the use of the term 'critical micelle concentration' or 'c.m.c.', but the exact point at which the process occurs is ill defined and depends on the technique of measurement. One definition due to Phillips[1] considers the c.m.c. to be the point at which $\frac{d^3\phi}{dc^3} = 0$, where ϕ is some physical property. Mukerjee and Mysels[2] have

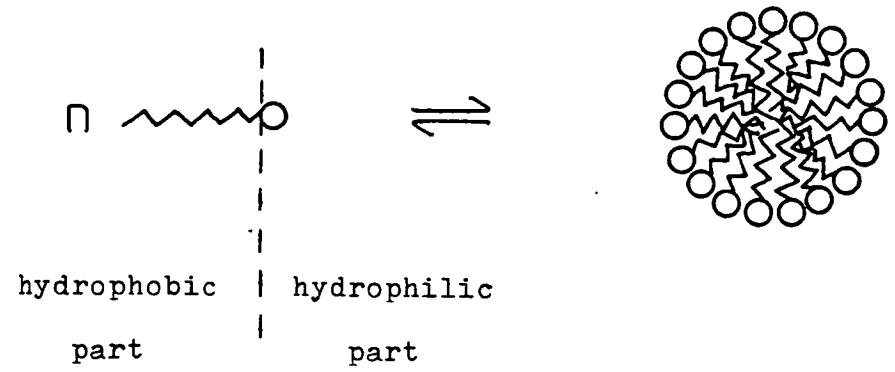

Figure 1.1.1 Schematic representation of micellisation.

Examples of surfactants which form micelles.

$CH_3(CH_2)_{11}OSO_3Na$ (SDS)

$CH_3(CH_2)_{15}N(CH_3)_3Br$ (CTAB)

$CH_3(CH_2)_7(OCH_2CH_2)_6OH$ (C_8E_6)

tabulated results of nearly 5000 c.m.c. determinations for pure and mixed systems.

The driving force for micellisation is therefore the minimisation of hydrophobic interactions[3] between the hydrocarbon chains and water but electrostatic repulsion between head groups is an important factor in determining the size of the micelle and hence its physical properties. These repulsive forces depend on the size, charge, and charge density of the head groups. An ionic micelle consisting of up to 200 monomers would appear to carry a very high surface charge but in fact this is reduced somewhat by the association of a fraction β of counterions where β is defined in equation 1.1.1

$$\beta = \frac{\text{number of bound counterions}}{\text{number of ionic monomers in micelles}} \qquad 1.1.1$$

The precise difference between a bound and an unbound or free counterion is not clear, and as with c.m.c. measurements the value of β depends on the technique employed. The most favoured distinction[4] designates the term 'bound' to those counterions which move with the micelle under the influence of a potential gradient while the remaining counterions constitute an ion atmosphere round the charged micelle.

Since the phenomenon of micellisation was first recognised by J.W. McBain[5] in 1913 much progress has been made in the elucidation of the structure and properties of micellar

solutions.[6-9] Hartley[10] proposed a spherical structure which is indeed the form that many micelles adopt but ellipsoids and rodlike structures also exist (see figure 1.1.2). Light scattering has been the most frequently used technique for studying micelle size but only the dimensions at the c.m.c. are obtained. Most micelles are generally thought to be spherical in this region, the condition for a sphere being that the diameter should not exceed twice the extended length of the hydrocarbon chain. Rod diameters are similarly limited.

1.2 Theories of Micellisation

A successful theory of micellisation must explain the dependence of size, shape and properties of micelles on the various parameters in the system and must demonstrate why aggregates of limited size are formed. External variables are temperature, T, pressure, P, and ionic strength, I, but many changes can be produced in the surfactant itself, such as length and extent of branching of the hydrocarbon chain, size, charge, charge density and position of the head group on the chain, and the valency and size of the counterion. Many data have been accumulated along these lines so that trends can be studied and theories well tested.

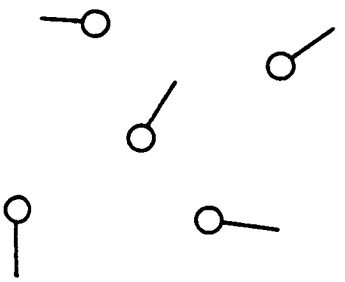

monomers

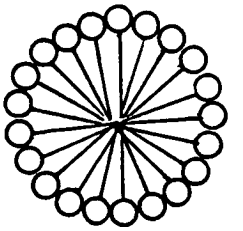

spherical micelle

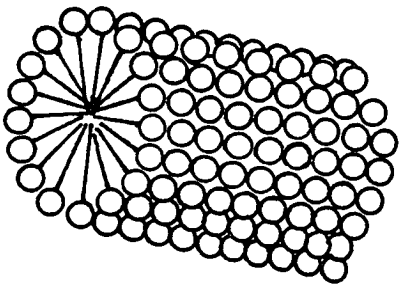

cylindrical micelle

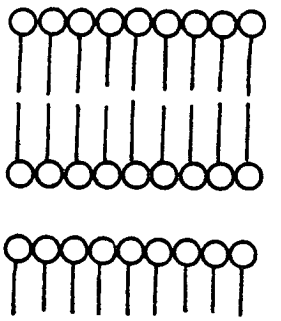

lamellar structure

Figure 1.1.2 Schematic representation of idealised structures that may be encountered in surfactant solutions.

1.2.1. Thermodynamic Theories

(A) Equilibrium Model

(A)(i) Mass Action Model[10,11]

This was the earliest approach developed. Equation 1.2.1 describes an equilibrium whereby micelles form in a single step and equation 1.2.2 gives the equilibrium constant k

$$nS^+ + mC^- \rightleftharpoons [micelle]^{(n-m)+} \qquad .....1.2.1$$

where S^+ denotes a surfactant monomer, C^- a counterion and $n > m$

$$k = \frac{a_{micelle}}{a_{S+}^{\ n}\ a_{C-}^{\ m}} \qquad .....1.2.2$$

where a denotes the activity of the ionic species.
In practice activity coefficients are assumed to be unity and hence concentrations can be substituted in place of activities without introducing serious error. Figure 1.2.1 illustrates that as n increases the concentration of micelles rises rapidly over a narrow range of n, thus predicting a c.m.c. as required, but no degree of polydispersity is allowed for in the mathematical approach.

(A)(ii) Multiple Equilibrium Model[12]

A natural extension of the Mass Action Model is to consider a series of consecutive linked equilibria giving a range of possible micelle sizes. The equilibria are described by equation 1.2.3.

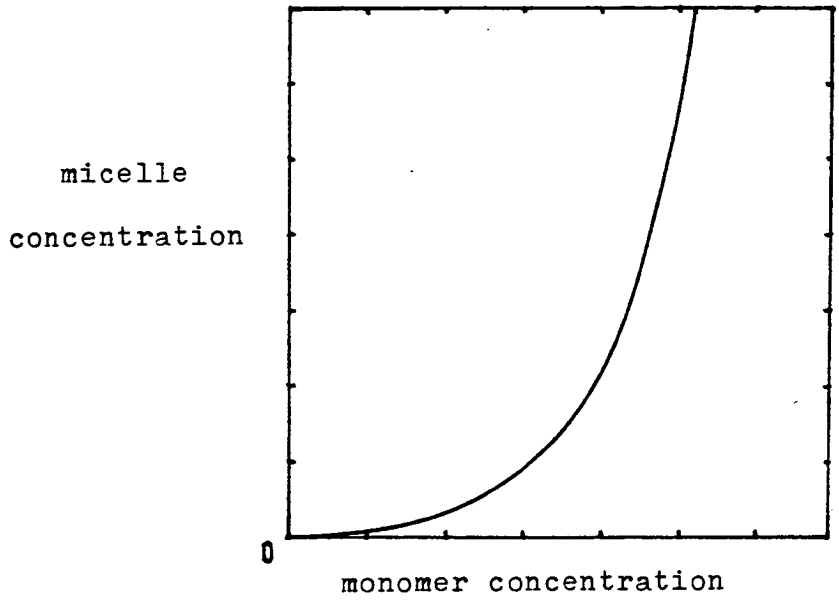

Figure 1.2.1 Graph of micelle concentration against monomer concentration.

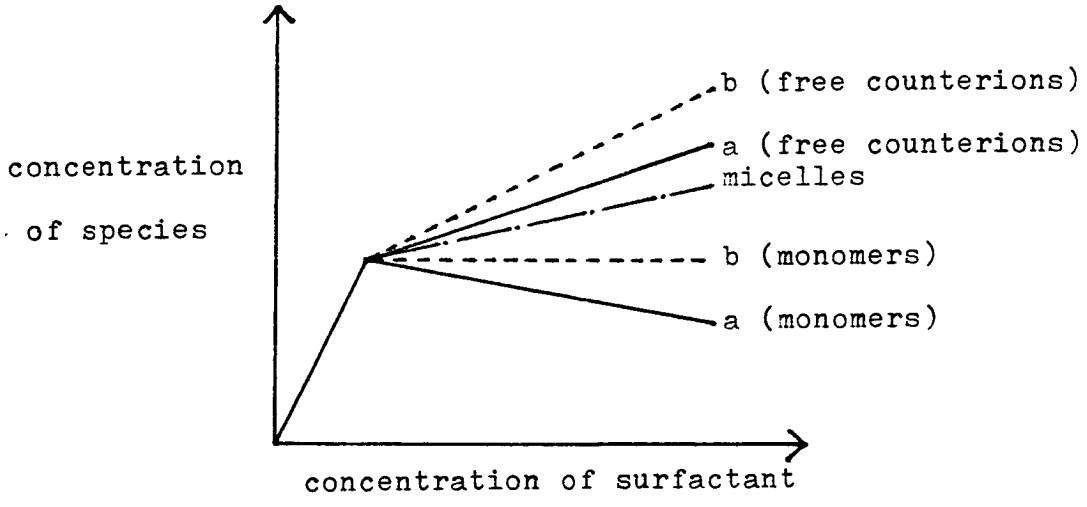

Figure 1.2.2 Concentration of each species in a surfactant solution as a function of total concentration as predicted by a) Mass Action Model

b) Phase Separation Model

$$S + S_{n-1} \overset{K_{S-1,S}}{\rightleftharpoons} S_n \qquad \text{.....1.2.3}$$

This model accounts for polydispersity but there are still drawbacks and for many purposes the simple Mass Action Model is sufficient.

(B)(i) Phase Separation Model[13,14]

This model considers the micelles (and bound counter-ions) as a separate phase with phase separation occurring at the c.m.c. and constant monomer concentration above the c.m.c. Although this simple model is a good approximation for many purposes, it is inadequate for precise work due to the difficulty of rationalising a 'charged phase' in ionic systems and the problem that an infinitely sharp c.m.c. is predicted.

(B)(ii) Small System Thermodynamics

This is an extension of the Phase Separation Model developed by Hill[15] and refined by Hall and Pethica[16] in which thermodynamic quantities are calculated for a single micelle rather than the bulk ensemble using intensive variables temperature, pressure and chemical potential of the monomers and the size distribution of micelles.

Figure 1.2.2 shows graphically the concentration of each species present in a surfactant solution as a function of total concentration as predicted by the Mass Action and Phase Separation Models.

1.2.2. Kinetic Theories

The dynamic aspects of micellisation have been studied extensively by relaxation methods such as temperature jump,[17] pressure jump[18] and stopped flow,[19] and nuclear magnetic resonance (n.m.r.) and electron spin resonance (e.s.r.) spectra provide data on faster processes. Two relaxation times emerge, the first and slower process (of the order of 10^{-2} to 10^{-5} s) is associated with the complete breakdown of a micelle into monomer units and the second faster process (less than 10^{-5} s) is correlated with one step in the monomer micelle equilibrium shown in equation 1.2.3. Aniansson and Wall[20] have provided a theoretical analysis which is now widely accepted.

1.3. The Kinetic Micelle

For many purposes the ionic micelle can be considered as a typical charged colloidal particle. It carries a substantial surface charge and is surrounded by an ion atmosphere or electrical double layer containing the counterions necessary for the neutralisation of that charge. The basis of an electrical double layer is the separation of a layer of positive charges adjacent to a layer of negative charges, thereby producing an uneven charge distribution in an overall neutral entity. Helmholtz[21] first tackled the problem of the counterion distribution near a charged surface in solution, proposing a model similar to a flat condenser with planes of opposite charges rigidly lined up facing each other (see figure 1.3.1). However, thermal motion could make this double layer

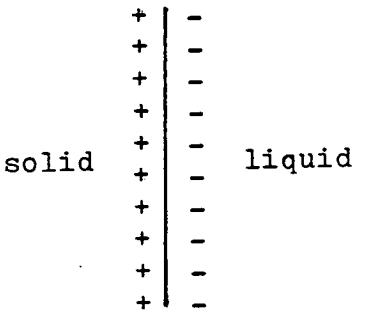

Figure 1.3.1 Electrical Double Layer (Helmholtz).

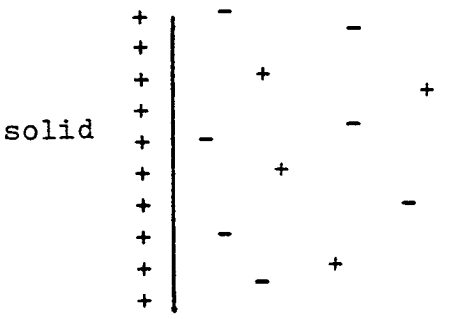

Figure 1.3.2 Electrical Double Layer (Gouy-Chapman).

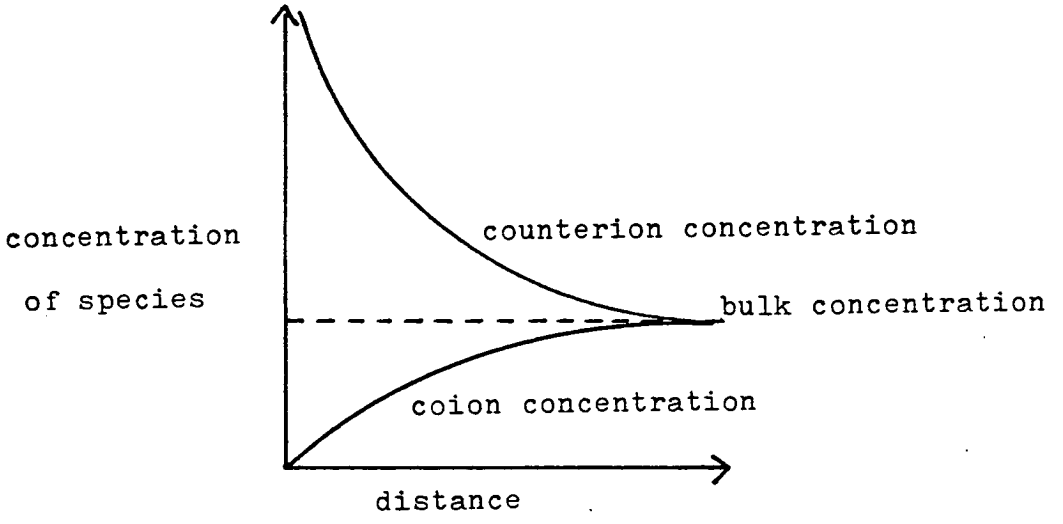

Figure 1.3.3 Concentrations of coions and counterions as a function of distance from the colloid surface.

diffuse as the kinetic energy of the ions in the solution could oppose the electrostatic attractive forces. Later, Gouy[22] and Chapman[23] took account of both the thermal energy and the electrostatic interactions in their theoretical treatment of the problem. A uniform smeared out surface charge was assumed and a space charge built up from an unequal distribution of point sized ions (see figure 1.3.2). In general the electric field strength due to the surface charge decreases moving outwards from the surface because the charge is screened by counterions. As the field strength drops the concentration of the counterions also falls until it reaches that of the bulk solution. Similarly coions are repelled from the surface creating a deficiency in the vicinity of the colloid (see figure 1.3.3). Gouy-Chapman theory therefore provides mathematical solutions for the potential and ion concentration at any point in the system but a discrepancy arises due to the fact that finite ion size is neglected. For example, for a high surface potential of 200 mV and an electrolyte concentration of 0.1 mol dm^{-3} the predicted counterion concentration at the surface is 300 mol dm^{-3} which is physically impossible. Stern[24] modified the theory to allow for the effect of ion size by proposing the restriction that ions cannot approach the surface closer than a minimum distance d. He also introduced the possibility of specific ion adsorption as in Langmuir's[25] adsorption theory. This treatment effectively divides the double layer into two regions - an inner layer or Stern layer and an outer layer or Gouy-Chapman diffuse double layer as described above. The thickness of the

double layer, $^{1}/\kappa$, depends primarily on the ionic strength, I, of the solution and is defined in equation 1.3.1

$$\kappa = \left(\frac{2e^2 n_o z^2}{\varepsilon kT} \right)^{\frac{1}{2}} \qquad 1.3.1.$$

where n_o is the bulk ion concentration, z is the valency, e is the electronic charge, k is the Boltzmann constant and ε is the permittivity of the medium which is equal to $\varepsilon_o \varepsilon_r$ where ε_o is the permittivity of a vacuum and ε_r is the relative permittivity.

It is not readily possible to determine experimentally either the potential at the colloid surface, ψ_o, or the Stern potential, ψ_d, but one accessible parameter is the zeta potential, ζ, which is fundamental in electrokinetic phenomena. These phenomena involve the tangential movement of a liquid relative to a charged interface, for example, electrophoresis, in which the charged colloid moves in one direction under the influence of an electric field while the mobile part of the double layer moves in the opposite direction carrying solvent with it and causing it to flow. A surface of shear, or slipping plane, the potential at which is the zeta potential, can therefore be defined. The exact location $(d + \delta)$ of this plane is uncertain but it is just beyond the Stern plane (see figure 1.3.4).

The model considered for a micelle is that of Stigter[4] in which three distinct regions are defined (see figure 1.3.5).

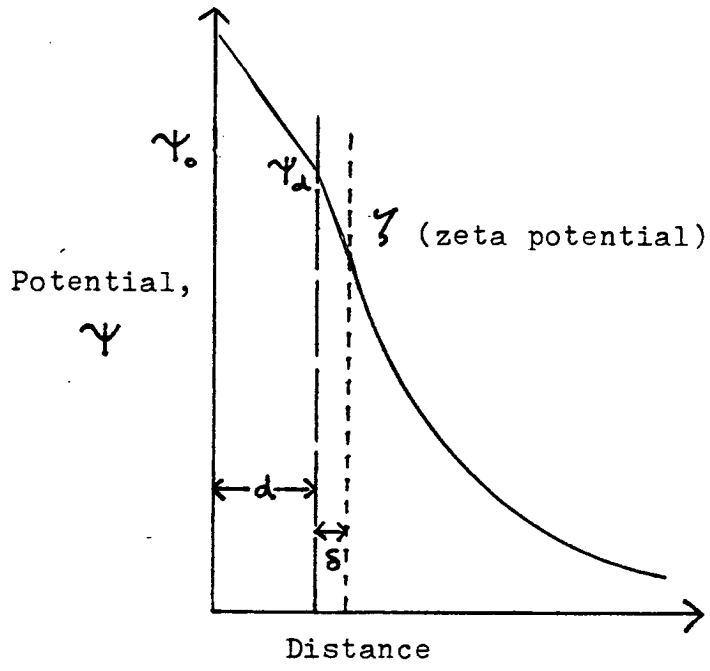

Figure 1.3.4 Potential, ψ as a function of distance from the colloid surface.

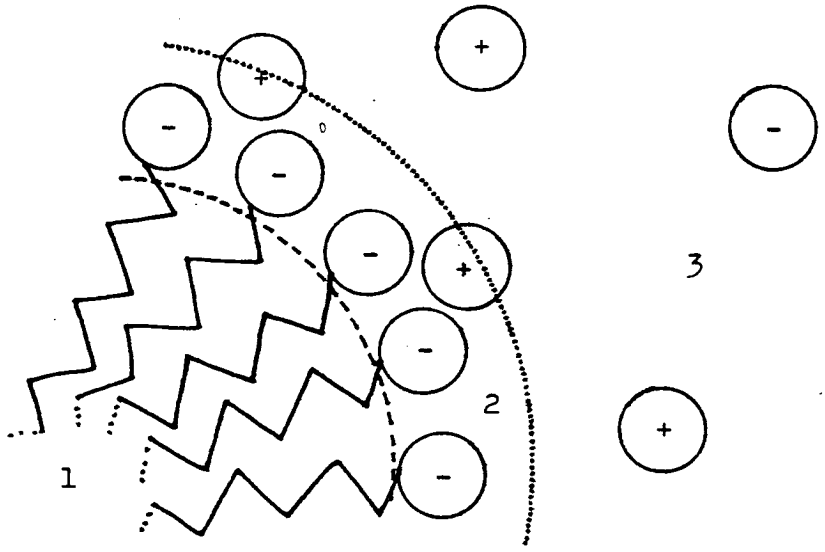

Figure 1.3.5 Model of a micelle (Stigter).

1. Hydrocarbon Core
2. Stern Layer
3. Gouy-Chapman Diffuse Double Layer

A) Hydrocarbon core

B) Stern Layer

C) Gouy-Chapman Diffuse Double Layer

A) Core

The micelle core, which contains the hydrocarbon chains is generally thought to be liquid like[26] but the chains are slightly more restrained than in a pure liquid due to the anchoring effect of the head groups and necessarily restricted cooperative movement of chains in a small volume. Evidence for the liquid nature comes from spin probe experiments in which the motion of a spin labelled atom on the hydrocarbon chain can be monitored. It seems likely that water can penetrate at least as far as the α-CH_2 group,[27] i.e. that adjacent to the head group, but controversy exists over claims that deeper penetration occurs. The core is the position of solubilisation of many purely hydrophobic substances[28] but how the inclusion of these affects micelle structure varies a great deal with the nature of the additive. Water insoluble dyes are frequently used in micelle studies and it is thought that only one molecule enters each micelle and the structure change is undetectable. The size of the core is dependent on the length of the hydrocarbon chains and the aggregation number.

B) Stern layer

The Stern layer contains the n head groups and βn bound counterions in an aqueous environment and extends from the core boundary to the Stern Plane. The thickness of the layer is determined by the size and configuration of the head groups and to a lesser extent by the size and degree of hydration of the adsorbed counterions. Stigter has found that the bound counterions in this region are not significantly dehydrated compared to their free counterparts[4] and that a monomolecular hydration layer explains the results of electrokinetic experiments. He concludes that the distribution of counterions is governed almost entirely by electrostatic and dimensional factors but the lack of knowledge of the permittivity of the region hinders development of a precise theory. Using the Stern-Gouy model of the double layer it was calculated by Levine[29] et al. that it is probable that the zeta potential is equal to the Stern potential for micelles i.e. $\delta = 0$ and the surface of shear is at the plane of the head groups. Negative values of δ (-1 to -2 Å) were also predicted implying that counterions can penetrate the head group region. The core and Stern layer together constitute the kinetic micelle.

C) Gouy-Chapman Diffuse Double Layer

The charge on the kinetic micelle is neutralised by the $(1-\beta)n$ counterions surrounding it and the thickness of the layer is given by equation 1.3.1. It is to be noted

that the ionic strength term includes both the monomeric, unmicellised surfactant concentration and any added salt. It is assumed that in this region the Gouy-Chapman theory of the diffuse double layer holds.

1.4. Mixed Micelles

When two surfactants are mixed in solution either they form separate micelles as in the case of hydrocarbon and fluorocarbon mixtures,[30] or mixed micelles are formed. The composition of the micelles depends not only on the concentration of each surfactant but also on the monomer concentrations in equilibrium with the mixed micelles. Since the forces inducing micellisation are generally non-specific, ionic/ionic or ionic/nonionic micelles can be formed. The inclusion of weakly surface active molecules, for example, alcohols, or even purely hydrocarbon materials which are solubilised within the micelle interior, can also be considered to produce mixed micelles. Although many detailed studies have been performed on single micellar systems there is relatively little definitive information available about mixed micellisation and to date there is no general theory describing the processes involved. However there is much to be gained from the investigation of mixed systems since surfactants in everyday use are almost invariably mixtures of several components and their efficacy depends on this fact. Alternatively when pure systems are used their activity depends on the ability to interact in some manner with a substrate, often leading to the formation of mixed micelles, for example, the removal of greasy dirt in the washing process.

1.5. Uses

The interest in studying micellar systems comes from many branches of science. They are thermodynamically stable, reproducible, and relatively monodisperse colloidal systems which makes them good models for biological macromolecules[31] as well as simpler colloids. Many of their properties depend on their ability to lower surface tension and to solubilise hydrophobic substances[32] which explains their use as detergents, in petroleum recovery[33] and as flotation agents.[34] It is found that many micellar systems can alter the rate of chemical reactions[35] and this has led to their use as catalysts in preparative chemistry and also to a comparison with enzymatic processes which appear similar. The catalytic effect may be due to concentration of reactants within micelles or adsorption near the micelle/solution interface when the molecule contains a hydrophilic part (proximity effect). Such a situation implies the existence of mixed micelles.

1.6. Aim of the Project

The aim of this work is to determine the extent of counterion binding to pure ionic and mixed ionic/nonionic kinetic micelles as a function of surfactant type, mole ratio of components and salt concentration with a view to better comprehension of the fundamental processes involved in surfactant association in solution. The variation of the micellar surface charge density with the above parameters should be explicable using a physical model of the micelle, as in section 1.3, and theories of interactions in the system. Such studies may provide information leading to better

understanding of the role of charged micelles in catalysis, detergency and all other varied uses.

CHAPTER TWO

PREVIOUS WORK

CHAPTER 2

PREVIOUS WORK

2.1. The Determination of Micellar Charge

There are three kinds of micellar charge which can be distinguished

A) native charge

B) kinetic charge

C) thermodynamic charge.

The first is simply the product of the aggregation number and the charge per head group and serves no useful purpose other than as a measure of micelle size. The kinetic charge is the charge on the kinetic unit as defined by Stigter and described in section 1.3, and is the parameter sought in studies of counterion binding. It equals αne where $\alpha = (1-\beta)$. The thermodynamic charge may vary considerably from the kinetic charge depending on the technique of measurement and so it is sometimes called the 'effective' thermodynamic charge. In some methods, for example light scattering, the assumption of constant activity coefficients of species present is wrongly made leading to variations in the calculated extent of counterion binding.

Examples of techniques used to determine α are shown below in table 2.1.1 and several results of such experiments are quoted to demonstrate the range of calculated α values

for sodium dodecyl sulphate (SDS). The reasons for the discrepancies may be due to use of an inaccurate model for the micelle and methods of analysis of the data.

Table 2.1.1 Calculated values of α, the degree of dissociation of SDS micelles in water or NaCl solutions of 298 K

Technique	NaCl concentration/ mol dm^{-3}	α	reference
Light scattering	0	0.17	36
Light scattering	0.4	0.15-0.17	37
EMF	-	0.15	38
EMF	-	0.16	39
EMF	-	0.22	40
electrophoretic mobility and size	-	0.29	41
specific conductance	-	0.49	42
and electrophoretic	-	0.70	43,44
mobility	0.1	0.5	43,44
Mass Action	-	0.31	present study
Diffusion	-	0.33	45
Equilibrium	0.1	0.16	37
ultracentrifugation	0.4	0.20	37
specific conductance		0.28	46

2.1.1 EMF Measurements

Ion activities can be measured in surfactant solutions using specific ion electrodes and 1:1 electrolyte behaviour is demonstrated below the c.m.c. followed by a relative reduction in the free ion concentration above the c.m.c. A typical plot of the activity of the counterion, a_{ci}, against concentration of surfactant is shown in figure 2.1.1. The activity is given by equation 2.1.1

$$a_{ci} = f_1 \text{ c.m.c.} + f_2 \alpha (c - \text{c.m.c.}) \quad \ldots\ldots 2.1.1$$

where f_1 is the free counterion activity coefficient in the bulk solution, f_2 is the free counterion activity coefficient in the ionic atmosphere around the micelles and c is the total surfactant concentration. The linearity of the plot suggests that f_1, f_2 and α are constant above the c.m.c. so the slope of the a_{ci} against concentration plot gives α directly if f_2 if correctly assigned. This is taken as $f_{\text{c.m.c.}}$ which may in fact overestimate the activity leading to low calculated values of α.

2.1.2. Law of Mass Maction

Corrin[47] suggested a method of calculation of α which uses the Mass Action Model of micellisation outlined in section 1.2.1. The equilibrium constant for the process

$$nS^+ + mC^- \rightleftharpoons [\text{micelle}]^{(n-m)+} \quad \ldots\ldots 1.2.1$$

is given by equation 1.2.2.

Concentrations are used in place of activities without the

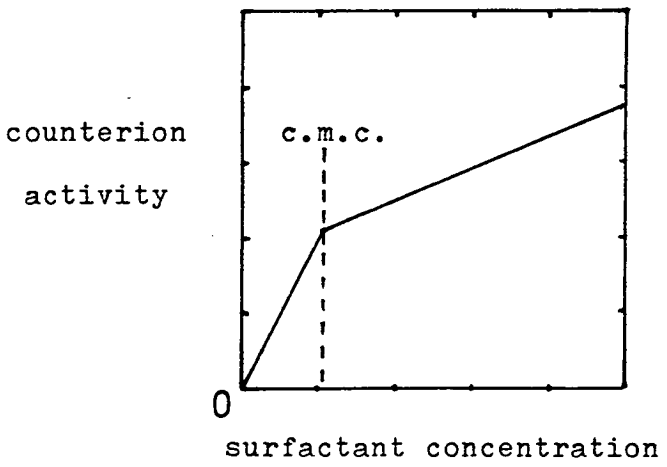

Figure 2.1.1 Graph of counterion activity against surfactant concentration.

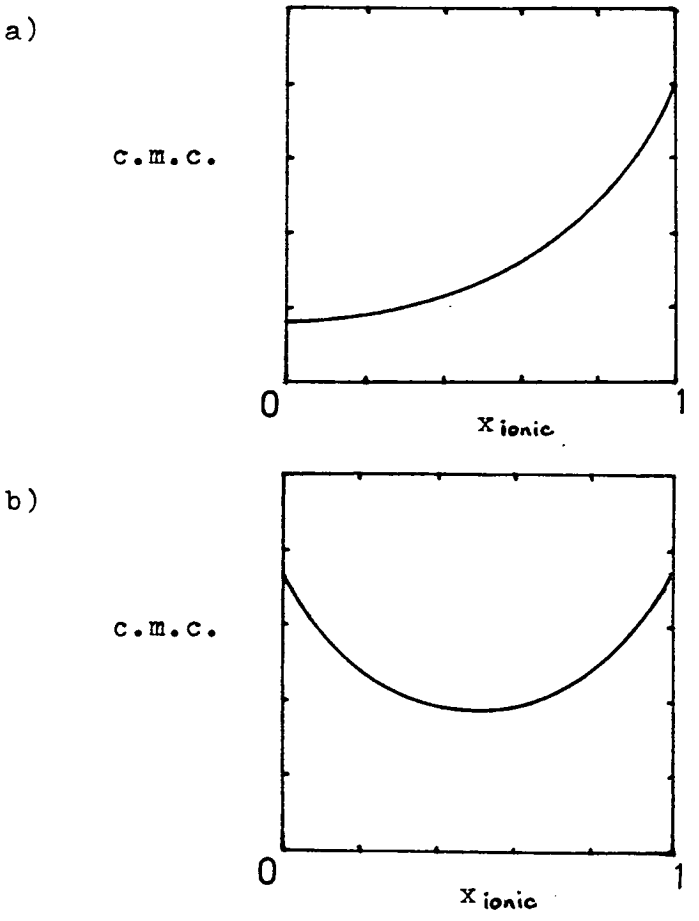

Figure 2.2.1 General shapes of curves of c.m.c. against mole fraction, x for mixed micellar systems.

a) $c.m.c._{ionic} \gg c.m.c._{nonionic}$

b) $c.m.c._{ionic} \doteq c.m.c._{nonionic}$

introduction of much error.

$$k = \frac{[\text{micelle}]}{[S^+]^n[C^-]^m} \quad \ldots\ldots 2.1.2$$

Taking logarithms of equation 2.1.2 and dividing by n gives equation 2.1.3.

$$\frac{1}{n} \log k = \frac{1}{n} \log [\text{micelle}] - \log [S^+] - \frac{m}{n} \log [C^-] \ldots 2.1.3$$

At the c.m.c. the concentration of S^+ is approximately equal to the c.m.c. and the concentration of micelles is negligible. Since k is a constant and $\beta = {}^m/_n$ equation 2.1.4 is derived.

$$\log (\text{c.m.c.}) = -\beta \log[C^-] + \text{constant} \quad \ldots\ldots 2.1.4$$

A plot of log (c.m.c.) against log (ionic strength) is therefore a straight line of slope $-\beta$. Values of α obtained in this way tend to be higher than those for other methods, for example EMF.

2.1.3. Osmotic Coefficient

Methods which can be used include measurement of the freezing point depression or vapour pressure lowering. Assuming that the micelles are of sufficient size so that their contribution to the freezing point depression is negligible, the osmotic coefficient g is given by equation 2.1.5.

$$g = \frac{c_- + c_+}{2c} \quad \ldots\ldots 2.1.5.$$

where c_- includes all the free counterions and c_+ includes all the monomers and coions. Since the concentration of the free counterions is [c.m.c. + α(c-c.m.c.)] and the concentration of free monomer is the c.m.c. then α is given by equation 2.1.6.

$$\alpha = \frac{2(gc - c.m.c.)}{c - c.m.c.} \qquad \ldots\ldots 2.1.6$$

Particle interactions are ignored in this method so that the values of α tend to be low.

2.1.4. Light Scattering

Debye[48] introduced the technique for the study of molecular weights of macromolecules or colloidal electrolytes in solution. Equation 2.1.7 gives the relationship between concentration and turbidity τ.

$$\frac{H(c - c.m.c.)}{\tau - \tau_o} = A + B\,(c - c.m.c.) \qquad .... 2.1.7$$

H is a constant depending on geometric and refractive index factors and A and B are constants for the system. A plot of Hc/τ against c gives a straight line for many colloidal systems and the molecular weight, M is calculated as the reciprocal of the intercept on the y axis i.e. $A = {}^{1}/M$. When the colloid carries a substantial charge there are complications due to particle interactions and the plot of Hc/τ against c depends on the amount of added salt which reduces the interactions. These factors have been dealt

with by Prins and Hermans[49] and Mysels and Princen[50] and expressions for the aggregation number n (equation 2.1.8) and the number of charges, z (equation 2.1.9) on the micelles enable the calculation of α to be performed since $\alpha = {}^{z}/_{n}$

$$n = \tfrac{1}{2}[zE + \frac{1}{1000A}] + \tfrac{1}{2}[\, zE + (\frac{1}{1000A})^2 - (z + z^2)E^2]^{\frac{1}{2}} \quad \ldots. \; 2.1.8$$

$$z = \frac{B(c.m.c. + fc_{salt}) + [(B/500)(c.m.c. + c_{salt})]^{\frac{1}{2}}}{A(1 - 500cE)} \quad \ldots. \; 2.1.9$$

B is the slope and A the intercept of the Hc/τ against concentration plot, f is a refractive index increment and E is defined in equation 2.1.10

$$E = \frac{c.m.c. + fc_{salt}}{c.m.c. + c_{salt}} \quad \ldots. \; 2.1.10$$

Values of α thus calculated tend to fall in the lower end of the range.

2.1.5. Diffusion

Clifford and Pethica[45] measured the self diffusion coefficient of Na^+ in SDS solutions and Stigter and Mysels found that of the micelles. α was calculated from equation 2.1.11

$$D_{Na^+} = [\frac{c.m.c.}{c} + (\frac{c-c.m.c.}{c})\alpha]D + (\frac{c-c.m.c.}{c})(1-\alpha)D_{mic} \quad 2.1.11$$

where D_{Na^+} is the self diffusion coefficient of Na^+ at 298K
D is the self diffusion coefficient of Na^+ below the c.m.c.

and D_{mic} is the self diffusion coefficient of the micelles. For SDS with no added salt a value of α of 0.33 was found but there was some variation with added salt concentration. An alternative electrostatic theory was presented not involving the concept of ion binding which worked well and some electrostatic interaction terms should be employed in the treatment of the diffusion data. Above the c.m.c., the small ions diffuse faster than micelles and tend to accelerate their motion while conversely the micelles tend to slow the ions in their ion atmospheres so results for low ionic strength may be suspect.

2.1.6. Equilibrium Ultracentrifugation

The sedimentation of colloidal particles can be studied in an ultracentrifuge equipped with an optical system for observing behaviour. When the centrifugal force on a particle is balanced by the diffusion tendencies the equilibrium is reached and the molecular weight of the colloid can be calculated from the equilibrium concentrations at different distances from the axis of rotation. Problems in calculating the charge are exactly analogous to those encountered in light scattering and diffusion. The smaller counterions tend to sediment at a slower rate creating a potential difference in the solution which acts to restore the original distribution of material by slowing the colloid. Estimations of α give good agreement with values found using other techniques.

2.1.7 Nuclear Magnetic Resonance

Recently n.m.r. studies have provided information about counterion binding to ionic micelles but most results to date have been merely qualitative in nature. The technique is useful because for ions with magnetic quantum number I where $I \geqslant 1$, for example ^{79}Br, ^{81}Br, ^{23}Na ($I = {}^{3}/2$), the predominant nuclear magnetic relaxation mechanism is due to the coupling of the nuclear quadrupole moment and the fluctuating electric field gradient at the nucleus. If ions adsorb in the Stern layer the electric field gradient is large as the charge distribution is non-spherical and hence the relaxation time gives an indication of the extent of counterion binding. β can be calculated[51] from equation 2.1.12.

$$R = R_f + \beta(R_m - R_f) - \frac{\beta c.m.c.}{c}(R_m - R_f) \quad \ldots\ldots 2.1.12$$

R is the measured relaxation rate, R_f is the intrinsic relaxation rate of the free counterions and R_m is the intrinsic relaxation rate of the micellised counterions.

2.1.8 Conductance, Electrophoretic Mobility and Transport Numbers

These three are so closely linked that they must be considered together as has often been done in the literature. Below the c.m.c. the conductance of a micellar solution demonstrates 1:1 electrolyte behaviour but above the c.m.c. the rate of increase of specific conductance, κ_{sp} with concentration is reduced.
κ_{sp} is given by the sum of the conductivities of the individual species present as in equation 2.1.13.

$$\kappa_{sp} = F \sum_i u_i c_i z_i \qquad \ldots\ldots 2.1.13$$

where u is the electrophoretic mobility and F is the Faraday. For a SDS solution containing monomers, counterions and micelles

$$\kappa_{sp}/F = u_{Na+}c_{Na+}z_{Na+} + u_{DS-}c_{DS-}z_{DS-} + u_{mic}c_{mic}z_{mic} \qquad \ldots\ldots 2.1.14$$

For constant monomer concentration above the c.m.c.

$$\kappa_{sp}/F = u_{Na+}(\text{c.m.c.} + \alpha(c-\text{c.m.c.})) + u_{DS-}\text{c.m.c.} + u_{mic}\,\alpha(c-\text{c.m.c.}) \qquad \ldots\ldots 2.1.15$$

Therefore the slope $\frac{d\kappa_{sp}/F}{dc}$ above the c.m.c. is given by equation 2.1.16.

$$\frac{d\kappa_{sp}/F}{dc} = \alpha(u_{Na+} + u_{mic}) \qquad \ldots\ldots\ldots 2.1.16$$

The linearity of the plot suggests constant α, u_{Na+} and u_{DS-} so if the mobility of the micelles and Na^+ is known, α can be calculated.

Evans[52] predicted the contribution of the micelles to conductance as a first approximation as follows. He calculated the aggregation number, n from the density, d of the micelle and the maximum extended length, l of the hydrocarbon chains.

$$\therefore n = {}^{4}/_{3}\,\pi l^{3}\,\frac{Nd}{10^{24}M} \qquad \ldots\ldots 2.1.17$$

where M is the molecular weight of the hydrocarbon portion. He then deduced, in conjunction with Stokes Law[53] that the conductivity of an ion in unit electric field is proportional to $\frac{\text{charge}^2}{\text{radius}}$, so for n monomers in a spherical micelle of charge (n-m)

$$u_{mic} = \frac{(n-m)^2}{n^{1/3}}\,u_{monomer} \qquad \ldots\ldots 2.1.18$$

Using the equation

$$\lambda_i = Fu_i \qquad \ldots\ldots 2.1.19$$

where λ_i is the ionic molar conductivity, and substituting in equation 2.1.16

$$\frac{d\kappa_{sp}/F}{dc} = \alpha\left(u_{Na+} + \frac{(n-m)^2}{\alpha F n^{4/3}}\,\lambda_{monomer}\right) \qquad \ldots\ldots 2.1.20$$

$$\therefore \quad \frac{d\kappa_{sp}/F}{dc} = \alpha u_{Na+} + \frac{(n-m)^2}{n^{4/3}}\,\lambda_{monomer} \qquad \ldots\ldots 2.1.21$$

$\lambda_{monomer}$ is found by subtracting the counterion contribution from the slope below the c.m.c. This crude method gives a value of α of 0.26 for SDS.

Hartley, Collie and Samis[54] measured transport numbers and conductivities of several micellar solutions and computed α from equation 2.1.22

$$\alpha = \frac{\Lambda}{\lambda_{fci} + \lambda_{surfactant}} \qquad \ldots\ldots 2.1.22$$

Here Λ is the molar conductance of the solution, λ_{fci} the conductance of the free counterion and $\lambda_{surfactant}$ the conductance of the surfactant. The transport numbers for the surfactant species, micelle and monomer, were greater than unity due to the fact that a large fraction of the counterions travel with the micelle in the direction contrary to the expected one, so $\lambda_{surfactant}$ is greater than Λ. λ_{fci} is taken as the value found for that ion in a simple 1:1 electrolyte solution. In this method the presence of surfactant monomer is ignored but will not cause serious error if the c.m.c. is low as in the above study.

Mysels and Dulin[46] combined the results of conductance and counterion mobility experiments to obtain α as follows

$$c = nc_{mic} + c_{mon} = c_{ci} + (n - z)c_{mic} \qquad \ldots\ldots 2.1.23$$

where nc_{mic} is the concentration of monomers in micelles and c_{mon} is the concentration of monomers. The flux of positive particles moving in the negative direction is given by

$$cu_{-} = c_{ci}u_{ci} - (n - z)c_{mic}u_{mic} \qquad \ldots.2.1.24$$

and the flux of negative particles moving in the positive direction is given by

$$cu_+ = nc_{mic}\, u_{mic} + c_{mon}\, u_{mon} \qquad \ldots\ldots 2.1.25$$

Solving for c_{mon} and c_{ci} gives

$$c_{mon} = c(u_+ - u_{mic})/(u_{mon} - u_{mic}) \qquad \ldots\ldots 2.1.26$$

$$c_{ci} = c(u_- + u_{mic})/(u_{ci} + u_{mic}) \qquad \ldots\ldots 2.1.27$$

Recalling that $\kappa_{sp} = F(u_+ + u_-)$ and noting that $\frac{n-z}{n} = \beta$ equation 2.1.28 gives for β

$$\beta = \frac{(u_{ci}-u_-)(u_{mon}-u_{mic})}{(u_{ci}+u_{mic})(u_{mon}-u_- - \kappa_{sp}/Fc)} \qquad \ldots\ldots 2.1.28$$

where u_+ is the average mobility of micellised and free monomer and u_- is the average mobility of bound and free counterions. The results for SDS give $\alpha = 0.28$ at the c.m.c. rising slowly to $\alpha = 0.35$ at 0.1 mol dm^{-3} salt concentration which agrees well with Stigter's estimation of α from electrophoretic mobility and size measurements. Taking the mobility of the micelle as extrapolated to the c.m.c. and the aggregation number from light scattering studies he used various theories to calculate the zeta potential. Those of Smoluchowski,[55] Henry,[56] Booth[57] and Overbeek[58] were used and later the

approach of Loeb, Wiersema and Overbeek[59] was tried. Knowledge of the zeta potential enables calculation of the charge at the micelle surface if a suitable theoretical treatment is employed. Equation 2.1.29 was used in conjunction with the aggregation number and the degree of ionisation $\alpha = {}^{Q}/n$ was found.

$$R = (1 + \kappa a)\ \phi \qquad 2.1.29$$

a is the micellar radius, ϕ is the potential and R is defined in equation 2.1.30. Q is the micellar charge.

$$R = \frac{Qe^2}{4\pi a \epsilon k T} \qquad 2.1.30$$

For SDS in water a value of α of 0.287 was found by this method.

Stigter has combined his mobility results with conductance measurements and modified the simple approach of equation 2.1.16.[42] u_{Na+} is set at $u^{o}_{Na+}\ (u_{mic}/d_1\zeta)$ where $u^{o}_{Na}+$ is the mobility at infinite dilution and $(u_{mic}/d_1\zeta)$ is a factor to correct for the interaction with micelles. Also Λ is corrected for the influence of liquid flow around the micelle in electrophoretic motion. α is then given by equation 2.1.31.

$$\alpha = \frac{\Lambda - I}{Fu + Fu^{o}_{Na}+(u_{mic}/d_1\zeta)} \qquad 2.1.31$$

where $I = F/n\int \nu p d\tau$, ν is the local liquid velocity and p is the excess concentration of counterions. The integration is carried out over the entire Gouy-Chapman double layer. Values of α thus obtained are in the region 0.4 to 0.5 for SDS in salt solutions.

As an extension to all previous approaches Stigter[43] has recently presented a theory of conductance of colloidal electrolytes in univalent salt solutions. The zeta potential has been calculated[44] from the results of mobility measurements by the method of Loeb, Wiersema and Overbeek[59] and the conductance data corrected for excess salt effects caused by the necessity of including an excluded volume term for the micelles. The basic conductivity equation is equation 2.1.32

$$1000\ \kappa_{sp} = c_2\Lambda_2 + c_3\Lambda_3 \qquad 2.1.32$$

where the subscript 2 refers to the colloid and 3 refers to the salt. Due to the expulsion of coions from the vicinity of the micelle the bulk salt concentration is raised from the average value of c_3 to c_3^* so as Λ_3 is a function of c_3^* it is also dependent on c_2

$$c_3 = c_3^* + A_1 c_3^* c_2 \qquad 2.1.33$$

A_1 is the first mixed virial coefficient in the McMillan Mayer solution theory[60] and depends on the interaction between a colloid and a coion.[61] The factor $A_1 c_3^*$ is

negative and is equal to the negative adsorption of moles of salt per colloid charge equivalent. For constant salt concentration,

$$1000 \lim_{c_2 \to 0} \left(\frac{d\kappa_{sp}}{dc_2}\right)_{c_3} = \Lambda_2 + c_3 \left(\frac{d\Lambda_3}{dc_2}\right)_{c_3} \qquad 2.1.34$$

Since Λ_3 depends on c_3^*

$$\Delta\Lambda_2 = c_3 \left(\frac{dc_3^*}{dc_2}\right)_{c_3} \frac{d\Lambda_3}{dc_3^*} \qquad 2.1.35$$

With equation 2.1.34 this gives for $\Delta\Lambda_2$

$$\Delta\Lambda_2 = -A_1 c_3 \, c_3^* \frac{d\Lambda_3}{dc_3^*} \qquad 2.1.36$$

For $c_2 \to 0$ and $c_3^* \to c_3$ equation 2.1.34 gives

$$\Lambda_2 = \lim_{c_2 \to 0} 1000 \left(\frac{d\kappa_{sp}}{dc_2}\right)_{c_3} + A_1 c_3^2 \frac{d\Lambda_3}{dc_3} \qquad 2.1.37$$

Noting that $c_2 + c_3 = c$, rewriting 2.1.32

$$1000 \, \kappa_{sp} = c_3^* \Lambda_3 + \frac{(c - c_3^*)(\Lambda_2 + A_1 c_3^* \Lambda_3)}{1 + A_1 c_3^*} \qquad 2.1.38$$

Above the c.m.c. $\frac{d\kappa_{sp}}{dc}$ becomes essentially constant indicating constant monomer activity, that is constant c_3^* and constant Λ_3 so equation 2.1.38 reduces to

$$\Lambda_2 = 1000\left(\frac{d\kappa_{sp}}{dc}\right)(1 + A_1 c_3^*) - A_1 c_3^* \Lambda_3 \qquad \ldots. 2.1.39$$

A further term is required for solutions containing added salt. This term is $A_1 c_3^* (d\Lambda_3/dc_3)$ and is added to the right hand side of equation 2.1.39. Thus Λ_2 is calculated from the experimental slope of conductance plots below and above the c.m.c. and is greater than the slope above the c.m.c. The conductance is also calculated theoretically on the following basis.

$$I = \kappa_{sp} XA \qquad \ldots. 2.1.40$$

where I is the current, X is the field strength and A the cross sectional area through which current flows. From equation 2.1.32 for a colloidal solution in a rectangular volume V

$$(c_2\Lambda_2 + c_3\Lambda_3)/1000 = \frac{1}{V}\int \frac{I}{X}\, dV \qquad \ldots. 2.1.41$$

At infinite dilution for a relatively large volume V of salt solution containing one colloid particle with n native charges.

$$\frac{n\Lambda_2}{N} = \int_V \frac{I}{X}\, dV - \frac{c_3\Lambda_3 V}{1000} \qquad \ldots. 2.1.42$$

Λ_2 is the value calculated from experimental data and the other terms are expressed in the charge transport of individual ions. For the micelle of aggregation number, n, charge ze, and mobility u/X, the contribution to conductance is zeu/X. For the bulk salt concentration $u_{ion} = \frac{eX}{f}$ where f is a friction factor

$$\therefore \quad \Lambda_3 = Fe\left(\frac{1}{f_+} + \frac{1}{f_-}\right) \qquad \ldots. \ 2.1.43$$

The current density i in the solution is therefore

$$i = e(\nu_+ u_+ + \nu_- u_-) \qquad \ldots. \ 2.1.44$$

where ν is the local salt concentration. Combination of these results gives

$$\frac{n\Lambda_2}{N} = \frac{zeu}{X} - \frac{Fec_3V}{1000}\left(\frac{1}{f_+} + \frac{1}{f_-}\right) + \frac{e}{X}\int_V (\nu_+ u_+ - \nu_- u_-)\,dV \qquad \ldots. \ 2.1.45$$

On deeper analysis this becomes for colloid cylinders

$$n\Lambda_2 = \frac{zFu}{X} - z\lambda_- + \frac{FL}{X}\int_a^b (\nu_+^o - \nu_-^o) \langle u \rangle 2\pi r dr - \frac{2L}{3}\int_a^b (\nu_+^o \lambda_+ L_+ - \nu_-^o \lambda_- L_-) 2\pi r dr \qquad \ldots. \ 2.1.46$$

where L is a dimensionless function depending on the orientation of the cylinder and r is the radius of the cylinder. A similar expression is available for spheres.

In equation 2.1.46 separate contributions from the colloid and counterion can be seen along with interaction integrals. These terms can be equated with electrophoretic hindrance and relaxation effects so equation 2.1.46 can be written simply as

$$n\Lambda_2 = z\lambda_{coll} + z\lambda_- + z\lambda_{eh} + z\lambda^+_{rel} + z\lambda^-_{rel} \quad \ldots\ldots 2.1.47$$

Mathematical expressions are available for these terms. Stigter has tabulated computer calculated results of determinations of these quantities for a range of reduced surface potential, reduced radius of the colloid, and reduced mobility of the simple ions enabling their evaluation for any set of parameters. α is then calculated from equation 2.1.48

$$\alpha = \frac{z}{n} = \frac{\Lambda_2}{\lambda_{coll} + \lambda_- + \lambda_{eh} + \lambda^+_{rel} + \lambda^-_{rel}} \quad \ldots\ldots 2.1.48$$

Stigter obtains values of α of 0.7 for SDS in water and 0.5 to 0.6 in salt solutions up to 0.1 mol dm^{-3}. These are considerably higher values than are given for many other methods and even allowing for the fact that it is admitted that the theory may fail at low salt concentrations, the calculated results seem excessively high. This raises the suspicion that Stigter's α values represent a different quantity from the α normally described for ionic micelles due to some variation in the definition of a 'bound' counterion.

2.2 Mixed Micelles

The study of mixed systems has received increasing attention in recent years since the existence of mixed micelles was first proved in 1957.[62] Most of the work in the area has concentrated on the determination and theoretical prediction of the c.m.c. but other useful information has also been obtained. One main problem lies in the determination of the composition of the mixed micelles. Mysels and Otter[63] studied the system sodium decyl sulphate/sodium dodecyl sulphate using conductance measurements and employed an empirical extrapolation method to determine the monomer concentrations in equilibrium with the micelles at any bulk concentration and composition. Shedlovsky[40] did further work on similar systems using the same method. The success of the approach depended on the similarity between the constituents and most early experiments were done and theories developed for homologous series of surfactants.

2.2.1 c.m.c.'s of Mixed Micellar Systems

The simplest model used by Lange,[64,65] Shinoda[66] and Clint[67] assumes ideal mixing of the constituents and this has been used successfully to predict c.m.c.'s in systems containing homologous surfactants. The expression for the c.m.c. is given in equation 2.2.1

$$\frac{1}{c_{mix}} = \frac{x}{c_1} + \frac{1-x}{c_2} \qquad \ldots. \; 2.2.1$$

where x is the mole fraction of component 1 in the total mixed solute, c_{mix} is the c.m.c. of the mixed system and c_1 and c_2 are the c.m.c.'s of the pure surfactants 1 and 2. The ideal mixing theory breaks down when the surfactants have dissimilar head groups. Moroi et al.[68] have extended the theory of Lange to include ionic/nonionic mixtures but experimental difficulties in measuring monomer concentrations in the mixed systems hinder rigorous testing of the theory. Rubingh[69] has suggested that regular solution theory can be used to calculate the activity coefficients, f of each component. Equations 2.2.2 and 2.2.3 give expressions for f.

$$f_1 = \exp(\beta^1(1-x)^2) \quad \ldots\ldots 2.2.2$$

$$f_2 = \exp(\beta^1 x^2) \quad \ldots\ldots 2.2.3$$

where β^1 is an interaction parameter related to the molecular interaction in the mixed micelle by equation 2.2.4

$$\beta^1 = (W_{11} + W_{22} - 2W_{12})/RT \quad \ldots\ldots 2.2.4$$

W_{11} and W_{22} are the energies of interaction between the molecules in the single component micelles and W_{12} is the interaction energy between the two species in the mixed micelle. R is the gas constant. Examples of the calculated values of β^1 are given in Table 2.2.1

Table 2.2.1. Values of the interaction parameter β^1 for several mixed systems

System	Reference	β^1
$C_{12}H_{25}OSO_3Na$/ $C_8H_{17}(OCH_2CH_2)_6OH$	65	-4.1
$C_{16}H_{33}N(CH_3)_3Cl$/ $C_{12}H_{25}(OCH_2CH_2)_5OH$	69	-2.4
$C_{10}(CH_3)_2PO$/ $C_{10}(CH_3)_2SO$	69	-0.84
$C_{10}H_{21}OSO_3Na$/ $C_{10}H_{21}N(CH_3)_3Br$	70	-18.5

The greater the magnitude of β^1 the greater the deviation from ideality and therefore as expected the $C_{10}(CH_3)_2PO$/ $C_{10}(CH_3)_2SO$ system has the lowest β^1 value.

The general shapes of the c.m.c. against mole fraction graphs are illustrated in figure 2.2.1. (see page 24) When the c.m.c. of the ionic component is much greater than that of the nonionic, curve type (A) is found. As nonionic is added to the ionic solution the c.m.c. drops rapidly and approaches x = 0 asymptotically. This initial drop is more marked for anionic/nonionic systems than cationic/nonionic ones

due to the interaction of anionic head groups with the ether oxygens of the polyoxyethylene chains[71]. When the c.m.c. of the ionic surfactant is similar to that of the nonionic, curve type (B) (vat form) is found.

2.2.2 Charge Studies in Mixed Micellar Systems

When a nonionic surfactant enters an ionic micelle in place of ionic monomers the electrostatic repulsion between ionic head groups nearby is reduced and bound counterions can be released thereby regulating the surface charge density. This qualitative effect has been observed by several authors but no satisfactory quantitative explanation yet exists. Corkill, Goodman and Tate[72] determined values of α for the system sodium dodecyl sulphonate/hexaoxyethylene dodecyl ether as a function of mole fraction by vapour pressure and electrochemical measurements. Above a critical concentration it was deduced that micelles of constant composition were formed which considerably simplified the analysis. The results from the two sets of data were in agreement qualitatively but not quantitatively, most likely due to errors in the analytical procedure. In general α rose slowly proceeding from $(1-x) = 0$ to $(1-x) = 0.6$ then rose dramatically. A similar set of experiments were performed by Tokiwa and Moriyama[73] who studied the system sodium dodecyl sulphate/polyoxyethylene dodecyl ether ($C_{12}E_n$) where the degree of polymerisation n took the values 5, 9, 15 and 30. Employing the same techniques of vapour pressure, conductance and sodium ion activity determination they obtained the values of α shown in table 2.2.2 as a function of x and n.

Table 2.2.2 Values of α determined by vapour pressure and electrochemical measurements for

A) SDS/$C_{12}E_9$ as a function of x

B) SDS/$C_{12}E_n$ for x = 0.5 and varying n

A

x	α_{VP}/313K	α_{pNa^+}/298K
1	.16	.18
.8	.25	.30
.5	.40	.47
.2	.65	.66

B

n	α_{VP}/313K	α_{pNa^+}/298K
5	.30	.36
9	.40	.47
15	.51	.58
30	.63	.64

Both the techniques give comparable values of α and show that as x decreases, α increases for a given value of n and that for constant x, as n increases, α increases. Schick and Manning[74] also showed this result for the system with values of n of 4, 7, 23 and 30.

The addition of a series of n-alcohols, ethanol to heptanol, to a 2% SDS solution was studied by Lawrence and Pearson[75] who deduced from conductance and sodium ion activity measurements that the longer chain alcohols had greater effect in producing a release of counterions from the micelle due to the greater penetration achieved. Hayase and Hayano[76] determined the c.m.c.'s of the SDS/butanol-heptanol system and using Moroi's method of analysis were able to predict c.m.c.'s theoretically. They also found a linear relationship between the slope of the c.m.c. decrease with alcohol concentration and the carbon number, in agreement with the data of Lawrence and Pearson.

CHAPTER THREE

THEORY

CHAPTER 3

THEORY

3.1 Interactions Between Charged Particles in Aqueous Solution

In describing the environment of an ion in solution two main types of interaction must be discussed.

A) ion-solvent interactions

B) ion-ion interactions.

3.1.1 Ion-solvent interactions

The structure of the solvent, water, is all important to the study of ion-solvent interactions but despite much effort devoted to this subject there is no entirely satisfactory model for liquid water. At best it can be compared to a slightly broken down form of the ice lattice[77] with short range tetrahedral bonding and free water molecules in interstitial regions. However, the situation is dynamic and an averaged view of molecular positions must be taken. When an ion enters water it can orientate the dipolar solvent molecules in its immediate vicinity and these become tightly bound.[78] When the ion moves the tightly bound molecules move with it forming a kinetic unit. Such a solvation shell for a simple ion commonly contains one to six water molecules. Between the tightly bound hydration shell and bulk water far from the ion exists an intermediate region where water molecules can be partially orientated but are not held strongly (see figure 3.1.1). An important consequence of hydration is

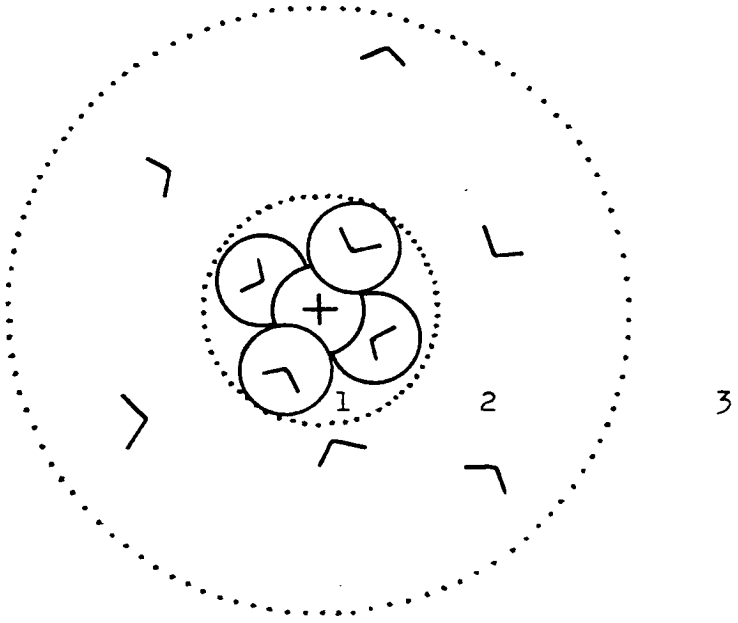

Figure 3.1.1 Hydration of a simple ion.

1. Primary solvation shell
2. Intermediate, secondary region
3. Bulk water

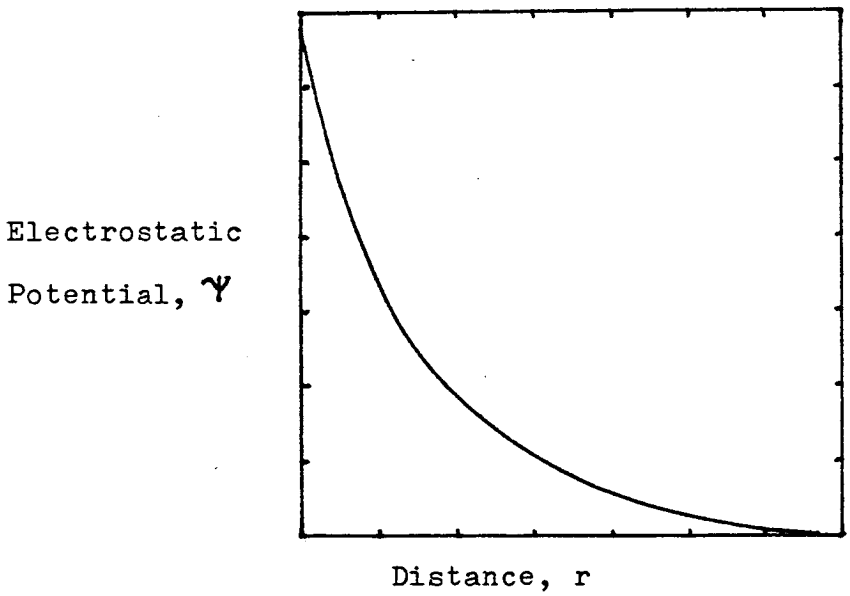

Figure 3.1.2 Electrostatic potential, Ψ as a function of distance, r from an ion in solution.

that ions in solution have solvated radii greater than their crystallographic radii, for example, the hydrodynamic radii of the alkali metal ions decrease in the order $Li^+ > Na^+ > K^+$, in the opposite direction to their crystallographic radii. This factor becomes important when the question of how close ions in solution can approach one another is considered.

3.1.2 Ion-ion interactions

Fundamental to the discussion of ion-ion interactions is a theory for predicting the distribution of ions around a central ion in solution. Debye and Hückel[79] analysed the problem using the following assumptions.

1) Ion-ion interactions are purely coulombic in origin. Short range interactions, for example dispersion forces are neglected.

2) Only one ion is treated as a discrete charge, the charge on the others being smeared out to give a continuous uniform charge density.

3) The role of the solvent is to provide a medium of constant permittivity ε for the operation of the interionic forces. For water ε takes the value 6.93×10^{-10} $CV^{-1}m^{-1}$.

The volume charge density ρ_r at a distance r form the reference ion is given by Poisson's equation of electrostatics

$$\frac{1}{r^2} \frac{d}{dr} \left(r^2 \frac{d\psi_r}{dr}\right) = - \frac{\rho_r}{\varepsilon} \qquad \ldots. 3.1.1$$

where ψ_r is the potential at distance r. Also ρ_r must be equal to the product of the total ion density and the charge.

$$\rho_r = \sum_i n_i z_i e \qquad \ldots. 3.1.2$$

where n_i is the concentration in moles per unit volume of the ith ion and z is the valency. The Boltzmann distribution law gives an expression for n_i

$$n_i = n_{io} \exp\left(\frac{-z_i e\psi_r}{kT}\right) \qquad \ldots. 3.1.3$$

where n_{io} is the concentration in the bulk solution far from the reference ion. Combining equations 3.1.2. and 3.1.3 gives equation 3.1.4

$$\rho_r = \sum_i n_{io} z_i e \exp\left(\frac{-z_i e\psi_r}{kT}\right) \qquad \ldots. 3.1.4$$

Debye and Hückel chose to consider only systems where the potential ψ was low

$$\text{i.e.} \quad z_i e\psi_r << kT \qquad \ldots. 3.1.5$$

Expansion of equation 3.1.4 in a Taylor series, neglecting all but the first two terms gives the linearised Boltzmann distribution

$$\rho_r = -\sum_i \frac{n_{io} z_i^2 e^2 \psi_r}{kT} \qquad \ldots. 3.1.6$$

Equating 3.1.6 with 3.1.1 gives the linearised Poisson-Boltzmann equation

$$\frac{1}{r^2}\frac{d}{dr}\left(r^2 \frac{d\psi_r}{dr}\right) = \frac{1}{\varepsilon kT} \sum_i n_{io} z_i^2 e^2 \psi_r \qquad \ldots. 3.1.7$$

Introducing the variable κ defined in equation 1.3.1, equation 3.1.7 reduces to

$$\frac{1}{r^2} \frac{d}{dr} \left(r^2 \frac{d\psi_r}{dr}\right) = \kappa^2 \psi_r \quad \ldots\ldots 3.1.8$$

The solution to equation 3.1.8 for the electrostatic potential at a distance r from the ion is for point sized ions

$$\psi_r = \frac{z_i e}{4\pi\varepsilon r} \cdot \exp[-\kappa r] \quad \ldots\ldots 3.1.9$$

Figure 3.1.2 illustrates the decay of potential with distance. The excess charge density distribution round the ion can now be calculated. From equations 3.1.1 and 3.1.8

$$\rho_r = - \varepsilon \kappa^2 \psi_r \quad \ldots\ldots 3.1.10$$

which combined with equation 3.1.9 gives

$$\rho_r = \frac{-z_i e}{4\pi} \frac{\kappa^2}{r} \exp[-\kappa r] \quad \ldots\ldots 3.1.11$$

Alternatively the assumption of point sized ions can be removed to give equations 3.1.12 and 3.1.13 in place of 3.1.9 and 3.1.11 for ions of finite size a.

$$\psi_r = \frac{z_i e}{4\pi\varepsilon} \frac{\exp[\kappa a]}{1+\kappa a} \frac{\exp[-\kappa r]}{r} \quad \ldots\ldots 3.1.12$$

$$\rho_r = \frac{-z_i e}{4\pi} \kappa^2 \frac{\exp[\kappa a]}{1+\kappa a} \frac{\exp[-\kappa r]}{r} \quad \ldots\ldots 3.1.13$$

The solutions for ψ_r above are based on the assumption of equation 3.1.5 that ψ_r is low but if this condition does not hold then the unlinearised Poisson-Boltzmann equation (3.1.14) must be solved.

$$\frac{1}{r^2}\ \frac{d}{dr}\ (r^2\ \frac{d\psi_r}{dr}\ )\ =\ -\ \frac{1}{\varepsilon}\ \sum_i z_i e n_{io}\ \exp[\frac{-z_i e\psi_r}{kT}] \qquad \ldots\ 3.1.14$$

For a symmetrical electrolyte, $z_+ = z_- = z$,

$$\sum_i z_i e n_{io}[\exp(\frac{-z_i e\psi_r}{kT})]\ =\ n_o ze\,[\exp(\frac{-z_i e\psi_r}{kT})\ -\ \exp(\frac{-z_i e\psi_r}{kT}) \qquad \ldots\ 3.1.15$$

and since $\exp(+x) - \exp(-x) = 2\sinh x$ 3.1.16

$$\rho_r\ =\ -2n_o ze\ \sinh(\frac{ze\psi_r}{kT}) \qquad \ldots\ 3.1.17$$

$$\text{or} \quad \frac{1}{r^2}\ \frac{d}{dr}(\frac{d\psi_r}{dr})\ =\ \frac{2n_o ze}{\varepsilon}\ \sinh(\frac{ze\psi_r}{kT}) \qquad \ldots\ 3.1.18$$

3.1.3 Consequences of ion-ion interactions

Before the mathematical treatment outlined in the previous section had been developed it had been noticed that experimentally many solutions did not obey the thermodynamic equation

$$\mu_i - \mu_{io}\ =\ RT\ln x_i \qquad \ldots\ 3.1.19$$

describing the change in chemical potential μ between solutions of concentration x_i, in mole fraction units, and unity and the concept of activity coefficient f_i was introduced to account for the deviation from ideality in empirical terms.

$$\text{Thus } RT\ln f_i = (\mu_i - \mu_{io}) - RT\ln x_i \qquad \ldots. 3.1.20$$

Debye and Hückel now gave an expression for the potential of an ion surrounded by an ion atmosphere.

$$\psi_{ion} = -\frac{z_i e\kappa}{4\pi\varepsilon} \qquad \ldots. 3.1.21$$

which enabled the calculation of the energy of interaction for the change in chemical potential, $\Delta\mu_{i-I}$ i.e. $\mu_{real} - \mu_{ideal}$

$$\Delta\mu_{i-I} = \frac{-Nz_i^2 e^2 \kappa}{8\pi\varepsilon} \qquad \ldots. 3.1.22$$

Equating 3.1.20 and 3.1.22 gives

$$RT\ln f_i = \frac{-Nz_i^2 e^2 \kappa}{8\pi\varepsilon} \qquad \ldots. 3.1.23$$

This expression was transformed into the Debye-Hückel limiting law for the ion activity coefficient.

$$\log f_{\pm} = \frac{-A(z_+ z_-) I^{\frac{1}{2}}}{1 + \beta a} \qquad \ldots. 3.1.24$$

where $A = \frac{1}{2.303} \frac{Ne^2B}{8\pi\varepsilon RT}$ and $B = (\frac{2Ne^2}{1000\varepsilon kT})^{\frac{1}{2}}$

This produced the theoretical result which had long been observed experimentally, that log $f_{\pm}$ was proportional to the square root of the ionic strength.

3.1.4 Ion Pair Formation

Bjerrum[80] suggested that if a pair of oppositely charged ions approached close enough to be trapped in each other's coulombic field then an ion pair might be formed. He calculated the probability P of finding an ion of one type of charge near one of opposite charge.

$$P = 4\pi n_{io} e^{\lambda/r} r^2 dr \qquad \ldots. 3.1.25$$

where

$$\lambda = \frac{z_i z_k e^2}{4\pi\varepsilon kT}$$

The fraction θ of ions associated into ion pairs is found by integrating over the limits a to q where a is the closest distance of approach and q is the distance at which a minimum in the graph of P against r is found (see figure 3.1.3 and equation 3.1.26).

$$\theta = \int_a^q 4\pi n_{io} e^{\lambda/r} r^2 dr \qquad \ldots. 3.1.26$$

Therefore ions which approach closer than the separation q are considered as an ion pair whereas those which remain

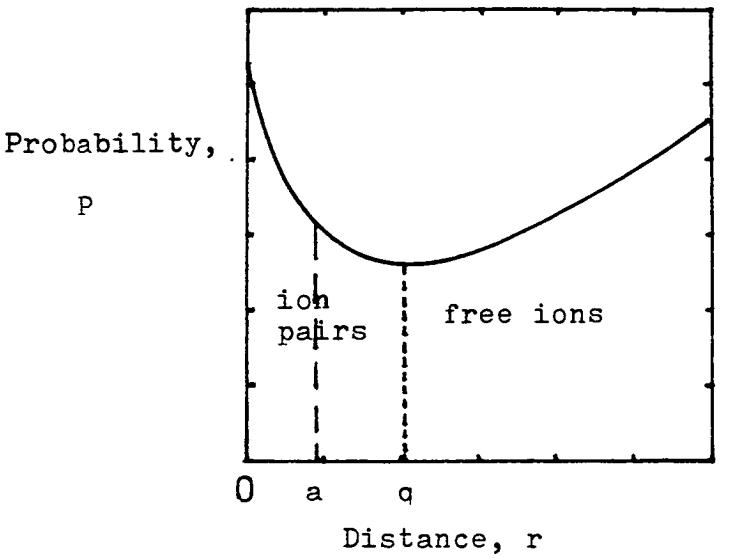

Figure 3.1.3 Probability, P of finding an ion of one type of charge near one of opposite charge as a function of distance, r.

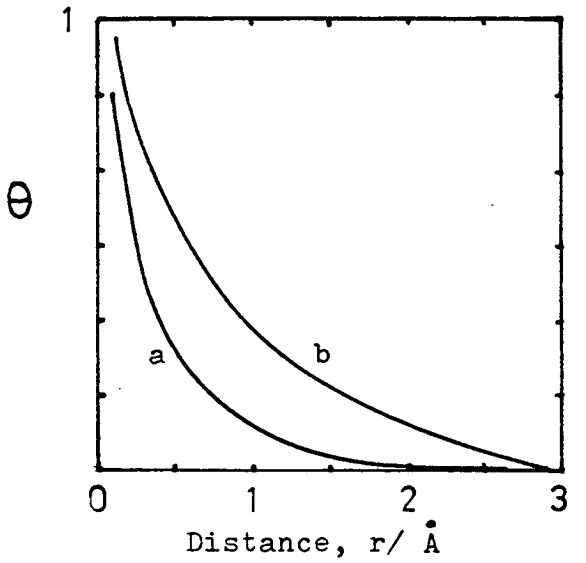

Figure 3.1.4 Fraction, θ of ions associated into ion pairs as a function of separation, r for various ionic strengths.

Salt concentration/mol.dm^{-3}.

a. 0.02 b. 0.2

further apart are considered free. Figure 3.1.4 shows θ as a function of ionic radius for several values of ionic strength.

3.1.5 Interactions in Colloidal Systems

The dispersed phase in a colloidal system normally consists of large molecules or small particles with at least one dimension in the range 1 nm - 1 μm but the distinction between some colloidal systems and ionic solutions containing large ions is not clear. Despite the fact that the ion cloud theory of ionic interactions is attributed to Debye and Hückel, Gouy[22] was the first to develop the model of an ion atmosphere in his treatment of the distribution of charges near a flat plate electrode as shown in figure 1.3.2.

Exactly the same results are produced as given in equations 3.1.1-3.1.18 giving the expression for the charge density at distance r from the plate

$$\rho_r = -2n_o ze \sinh\left(\frac{ze\psi_r}{kT}\right) \quad \ldots. \; 3.1.17$$

For a flat double layer equation 3.1.1 holds and the solution to 3.1.18 must be found.

Using the boundary conditions A) $\psi = \psi_o$ at $r = 0$

B) $\psi = 0$, $\frac{d\psi_r}{dr} = 0$ at $r = \alpha$

the solution of 3.1.18 is obtained.

$$\psi = \frac{2kT}{ze} \ln\left[\frac{1+\gamma\exp(-\kappa r)}{1-\gamma\exp(-\kappa r)}\right] \quad \ldots\ldots 3.1.27$$

$$\text{where } \gamma = \frac{\exp\left[\frac{ze\psi_o}{2kT}\right] - 1}{\exp\left[\frac{ze\psi_o}{2kT}\right] + 1} \quad \ldots\ldots 3.1.28$$

which for small ψ using the approximation of equation 3.1.5 reduces to

$$\psi = \psi_o \exp(-\kappa r) \quad \ldots\ldots 3.1.29$$

This predicts an exponentially decaying ψ as a function of distance as shown in figure 3.1.2.
It is to be noted that close to the surface where the Debye-Hückel approximation is inapplicable the potential decreases at a rate greater than that predicted by equation 3.1.29.

The charge density σ_o at the surface can also be found by integrating equation 3.1.17 with respect to r.

$$\sigma_o = -\int_o^\infty \rho_r \, dr \quad \ldots\ldots 3.1.30$$

$$\sigma_o = (8n_o \varepsilon kT)^{\frac{1}{2}} \sinh\left(\frac{ze\psi_o}{kT}\right) \quad \ldots\ldots 3.1.31$$

At low potentials this reduces to

$$\sigma_o = \varepsilon\kappa\psi_o \quad \ldots\ldots 3.1.32$$

For curved surfaces the Gouy-Chapman theory for a flat plate can only be used when the double layer is thin compared to a large particle radius so for spherical colloids of radius a, equation 3.1.29 must be modified to

$$\psi = \psi_o \frac{a}{r} \exp[\kappa(a-r)] \quad \ldots\ldots 3.1.33$$

Thus the potential at a distance r from the colloid depends on both the surface charge density and the nature of the electrolyte solution.

Gouy-Chapman theory considers only point sized ions comprising the double layer but it becomes necessary to introduce a finite ion size parameter to prevent predictions by equation 3.1.4 of ridiculously high ion concentrations close to the surface. Stern[24] modified the double layer model by considering the adsorption of ions onto the charged surface forming a layer of thickness δ. Within this layer the potential decays linearly and the outer limit is termed the Stern plane. Ions whose centres lie at a distance equal to δ from the particle surface are considered to be specifically adsorbed. Grahame[81] later made further modification subdividing the inner region of the double layer and defining an outer and inner Helmholtz plane, the former being equivalent to the Stern plane and indicating the closest distance of approach of hydrated ions in solution and the latter being the site of the centres of

specifically adsorbed ions which are therefore necessarily desolvated in the direction of the surface (see figure 3.1.5).

3.1.6 Micellar Systems

Micelles lie somewhere intermediate between typical colloids and simple ions in their properties and solution behaviour. Their dimensions are at the lower end of the colloidal range, typical radii being of the order of 20 to 30 Å, and have very high surface potentials even when considerable counterion binding is known to be present. As a result micellar systems are thermodynamically very stable lyophilic systems. It is perhaps therefore more appropriate to discuss micelles as large multivalent ions. However, theories of such systems are lacking. It is relatively easy now to describe theoretically a 1:1 electrolyte system and recent advances have improved the treatments of divalent and trivalent systems but micelles described in this manner would be, for example 20:1 electrolytes and good theoretical descriptions of the properties of such systems are not available. Therefore both approaches, from the colloidal and from the ionic view are required, and as already shown the basic principles involved do not differ, only the approximations made for exact solutions to the equations obtained in the analysis.

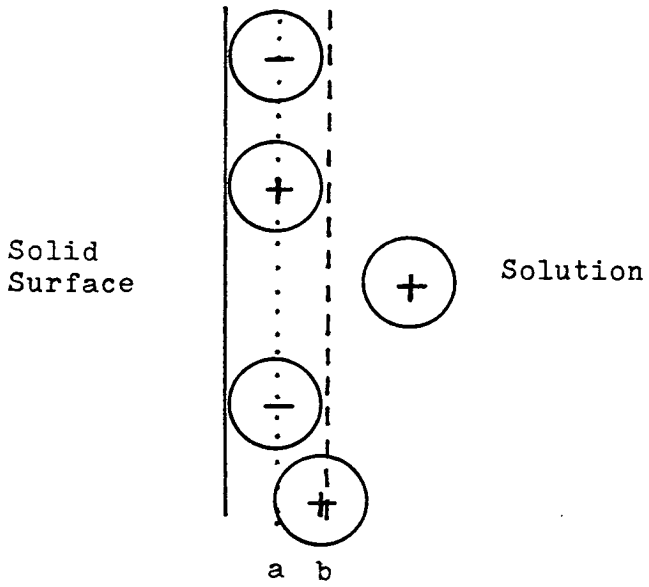

Figure 3.1.5 Electrical Double Layer (Grahame).

a. Inner Helmholtz Plane

b. Outer Helmholtz Plane

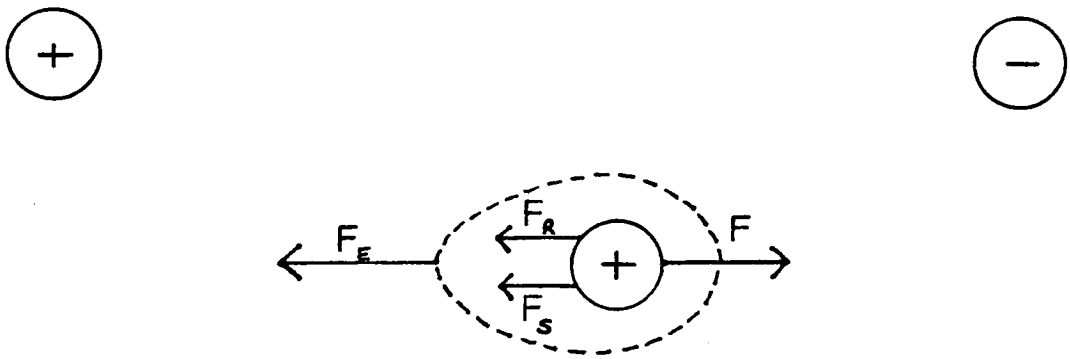

Figure 3.2.1 Model of a micelle in motion.

3.2 Transport in Micellar Solutions

Under the influence of an applied electric field the micelles and their bound counterions move in one direction while the free counterions move in the opposite direction carrying solvent along with them and causing it to flow. This phenomenon is known as electrophoresis and is one of the four electrokinetic phenomena described below.

(1) Electrophoresis: the movement of a charged surface relative to a stationary liquid by the application of an electric field.

(2) Electroosmosis: the movement of a liquid relative to a stationary charged surface by the application of an electric field.

(3) Streaming potential: the electric field which is created when a liquid is made to flow along a stationary charged surface.

(4) Sedimentation potential: the electric field which is created when charged particles move relative to a stationary liquid.

The measurement of the electrophoretic mobility is the most common technique used to study electrokinetic properties of colloidal systems. It yields information about the properties of the colloid at the 'surface of shear' between the inner and outer parts of the double layer. The electrical potential at this surface of shear is the zeta potential (ζ) but interpretation of data is made difficult by the uncertainty of the exact location of this surface. It cannot be clearly defined mathematically but is rather a region of rapidly changing viscosity and its position depends on the properties of the electrolyte solution surrounding the colloid. Thus the

motion of a micelle in aqueous solution must be described by consideration of the micelle properties, for example size and charge, and the solution properties, for example ionic strength and temperature, in conjunction with the Debye-Hückel theory of section 3.1.

The model considered for a micellar kinetic unit is shown in figure 3.2.1. Various forces acting on the micelle are identified. F is the force of the electric field acting on the micelle and is equal to QX where Q is the micellar charge and X is the field strength. F_S is the Stokes frictional force acting in the opposite direction to F when the micelle moves and it is given by

$$F_S = -6\pi\eta au \qquad \ldots. 3.2.1$$

η is the solvent viscosity and u is the mobility of the micelle. Two further sources of retardation must be considered

A) electrophoretic effect F_E

B) relaxation effect F_R

A) As the micelle moves in one direction, the free ions in its ion atmosphere, being oppositely charged, move in the opposite direction creating a local movement of liquid close to the micelle and causing a braking effect on the motion

B) Asymmetry of the ion atmosphere is created since it necessarily lags behind the central micelle in its path

towards the electrode. The centres of charge density of micelle and ion atmosphere therefore no longer coincide as they do in the system at rest and this electrical force slows the micelle.

The resultant force on the micelle, F^1, is given by

$$F^1 = F - (F_E + F_R + F_S) \quad \text{.... 3.2.2.}$$

This approach applies not only to colloidal systems but also to simple ions. Ion transport has been described by Debye and Hückel,[79] Onsager[82] and later Falkenhagen[83] Fuoss[84] and Pitts[85] by consideration of the various forces outlined above (see section 4.2). The colloidal aspects have been studied by Loeb, Wiersema and Overbeek[59] whose solution to the problem enables calculation of zeta potentials from electrophoretic mobility measurements and White and O'Brien[86] have recently extended the treatment.

CHAPTER FOUR

EXPERIMENTAL

CHAPTER 4

Experimental

4.1 Materials

4.1.1 Surfactants

A) Ionic surfactants

1) Sodium dodecyl sulphate (SDS; $C_{12}H_{25}OSO_3Na$)

Two samples of SDS supplied by (i) BDH, specially pure, and (ii) Cambrian Chemicals, were investigated. Quantities of each sample were recrystallised from 95% ethanol and the resulting four samples were compared by conductance and surface tension measurements. The form of a typical conductance against concentration and surface tension, γ, against ln concentration plots are shown in figure 4.1.1. The points of interest on each plot are the slope above and below the c.m.c. and the intersection of the lines at the c.m.c. In table 4.1.1 some literature values of c.m.c.'s are compared with present results and good agreement is found. In addition information can be gained from points very close to the c.m.c. on the surface tension plot. If an organic impurity is present it will tend to be concentrated in the first few micelles formed at the c.m.c.[95] and a minimum in surface tension is produced in this region.

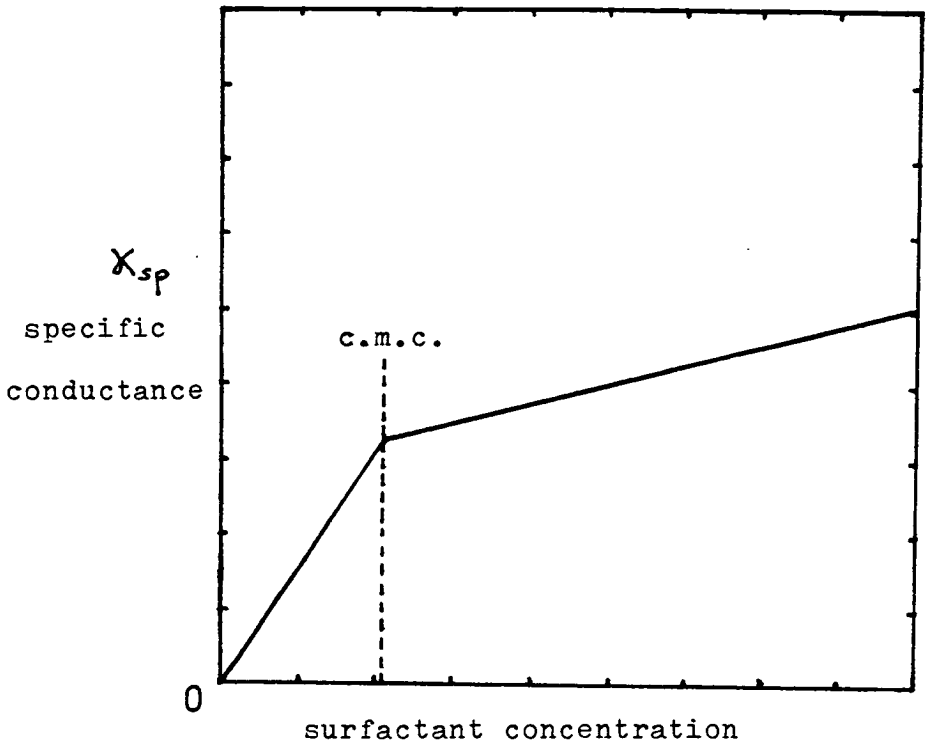

Figure 4.1.1. (A) Form of the typical specific conductance against concentration plot.

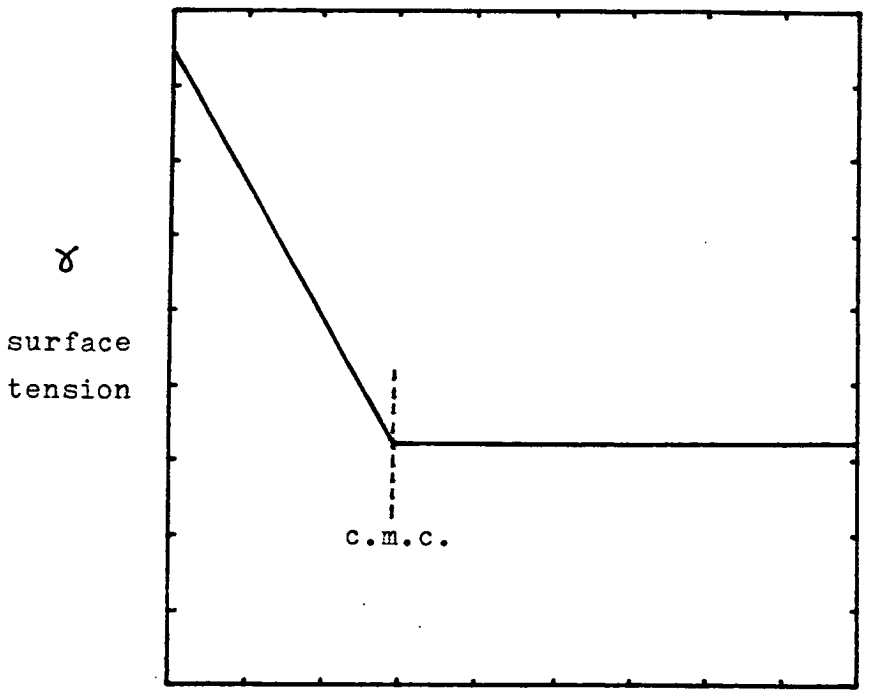

Figure 4.1.1. (B) Form of the typical surface tension against ln concentration plot.

Table 4.1.1 Experimental and comparable literature values of the c.m.c. of SDS and CTAB

Technique	Surfactant	T/K	c.m.c./ mol m^{-3}	reference
surface tension	SDS	291	8.65	experiment
conductance	SDS	298.15	8.33	experiment
surface tension	SDS	298	8.3	87
surface tension	SDS	298	8.2	88
conductance	SDS	298	8.16	89
conductance	SDS	298	8.27	90
conductance	SDS	298	8.4	88
surface tension	CTAB	298	0.90	experiment
conductance	CTAB	298.15	0.955	experiment
surface tension	CTAB	298	0.80	91
conductance	CTAB	298	0.920	92
conductance	CTAB	298	0.980	93
conductance	CTAB	298	0.90	94

Both BDH samples and the recrystallised Cambrian Chemicals portions gave identical conductance and surface tension values across the experimental concentration range but the untreated Cambrian Chemicals SDS had consistently higher conductance. The difference was of the order of 2% and may be attributed to the presence of approximately 1% Na_2SO_4 impurity. None of the surface tension against ln concentration plots showed a minimum at the c.m.c. indicating undetectable amounts of organic impurities were present.

Using the method of Barr, Oliver and Stubbings,[96] SDS concentration was estimated by titration of standard solutions. No difference between samples could be detected to within the precision of determining the end point of the titration.

2) Cetyl trimethylammonium bromide (CTAB; $C_{16}H_{33}N(CH_3)_3Br$) One sample supplied by BDH (laboratory reagent grade) was used and was recrystallised from a 10% acetone in water mixture. The recrystallised sample had the lower conductance although both samples yielded identical surface tension against ln concentration plots with no minimum at the c.m.c. C.m.c.'s as determined by both techniques are recorded in table 4.1.1.

B) Nonionic surfactants

1) Tetraethyleneglycol n-octylether (C_8E_4; $C_8H_{17}(OCH_2CH_2)_4OH$) was supplied by Unilever Research Laboratory, Port Sunlight, and was used without further purification.

2) Hexaethyleneglycol n-dodecylether ($C_{12}E_6$; $C_{12}H_{25}(OCH_2CH_2)_6OH$) was supplied by Nikko Chemical Co. Ltd., Tokyo and was claimed by the manufacturer to have a uniform polyoxyethylene chain length. A sample gas chromatograph is shown in figure 4.1.2. The chemical was stored in a freezer at 255 K under nitrogen in a well sealed flask to prevent oxidation.

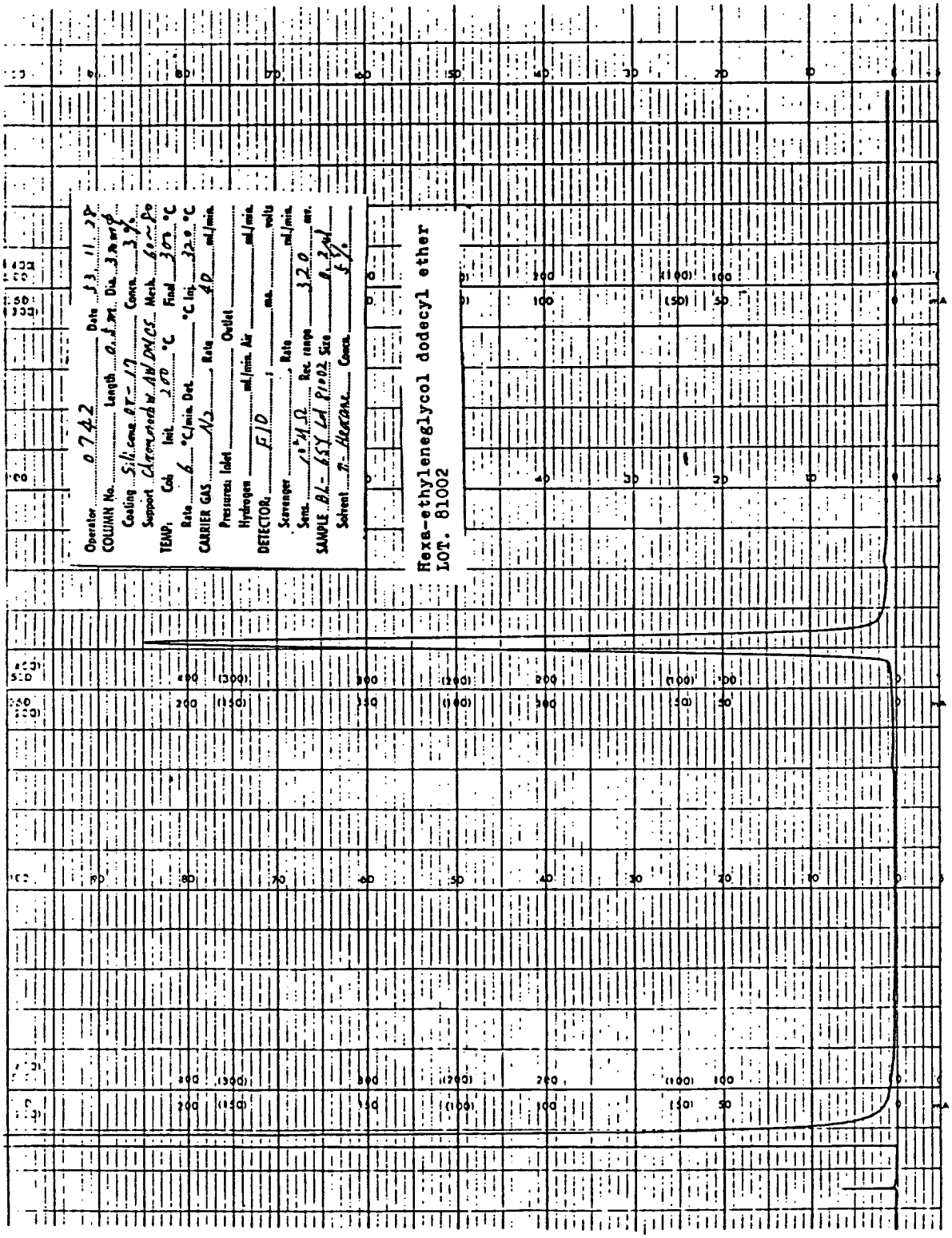

Figure 4.1.2 Gas chromatograph of $C_{12}E_6$.

4.1.2 Water

Triply distilled air equilibrated water was used in all experiments. The specific conductivity was less than $1.2 \times 10^{-6} cm^{-1} \Omega^{-1}$.

4.1.3. Other Reagents

A) electrolytes: NaBr, NaCl and KBr were AnalaR grade and were dried in an oven before use.

B) alcohols: laboratory reagent grade BDH samples were used without further purification.

C) dye: Sudan IV (BDH standard stain C.I. 26105) was used as received.

4.1.4 Preparation of Solutions

Surfactant solutions were prepared by weighing out the required amount of material and making up with solvent to a specific volume at 293 K. Alcohols were also added in this manner. Dye solutions were prepared by shaking a small amount of Sudan IV with surfactant solution and leaving overnight for the dye to be absorbed by the micelles. Excess dye was filtered off. All other solutions were prepared immediately prior to use to avoid the formation of significant amounts of oxidation or hydrolysis products.

4.2. Conductance

4.2.1 Theory

When a potential difference, ΔV, is established between two electrodes placed in an ionic solution and separated by a distance, l, the ions experience a force directing their motion towards the electrode of opposite charge. This force F_i is given by

$$F_i = QX \qquad .....4.2.1.$$

where Q is the ionic charge and X is the field gradient given by $\Delta V/l$. The flux, J, of ions passing through unit area per second is

$$J = BX + CX^2 + ... \qquad .....4.2.2$$

where B and C are constants. For small fields, however, terms above BX are negligible and the approximation can be made

$$J = BX \qquad .....4.2.3$$

The current density, i, is then

$$i = JzF = zFBX \qquad .....4.2.4$$

where z is the valency of the ion and F is the Faraday. The total current, I, is

$$I = i \times A \qquad .....4.2.5$$

where A is the area of the electrode. Two types of conductance unit can be defined,

1) specific conductivity, $\kappa_{sp} = zBF$ $/cm^{-1}\Omega^{-1}$

2) molar conductivity, $\Lambda = \kappa_{sp}/c = Fu$ $/cm^{2}\Omega^{-1}mol^{-1}$

where u is the mobility of the ion. For a cell constant, $a = 1/A$, substituting into Ohm's law, $V = IR$

$$\kappa_{sp} = a/R \qquad .....4.2.6$$

where R is the resistance of the solution. Combining the expressions for κ_{sp} and Λ with the law of independent migration of ions

$$\Lambda = \lambda_{+} + \lambda_{-} \qquad .....4.2.7$$

gives a new expression for κ_{sp}

$$\kappa_{sp} = \sum zFuc \qquad .....4.2.8$$

At first sight Λ might be expected to be constant over a range of electrolyte concentrations but is found by experiment to decrease with concentration. The empirical relationship, expressed in Kohlrausch's Law, which is obeyed by many ionic solutions at low concentrations

$$\Lambda = \Lambda^{o} - A\sqrt{c} \qquad .....4.2.9$$

where $\Lambda^{o} = \Lambda$ at infinite dilution and A is a constant, requires a theory of ion-ion interactions, as described in chapter 3, for explanation.

The simplest treatment by Debye, Huckel,[79] and Onsager[82] gives the limiting law for point sized ions

$$\Lambda = \Lambda^{o} - (B_1\Lambda^{o} + B_2)\sqrt{c} \qquad .....4.2.10$$

where B_1 and B_2 are parameters of the theory depending on charge, viscosity, permittivity and temperature. If an ion size parameter is included equation 4.2.10 is modified to

$$\Lambda = \Lambda^{o} - \frac{(B_1\Lambda^{o} + B_2)}{1 + \kappa a}\sqrt{c} \qquad .....4.2.11$$

Rearrangement of equation 4.2.10 gives

$$\Lambda^{o} = (\Lambda + B_2\sqrt{c})/(1 - B_1\sqrt{c}) \qquad .....4.2.12$$

The right hand side of which Shedlovsky[97] recognised was not a constant as predicted by Onsager but varied linearly with concentration. He therefore proposed the expression

$$\Lambda = \Lambda^{o} - (B_1\Lambda^{o} + B_2)\sqrt{c} + bc(1 - B_1\sqrt{c}) \qquad .....4.2.13$$

where b is a constant. Further development and refinement by Onsager, Fuoss,[84] Falkenhagen[83] and Pitts[85] has produced the general equation

$$\Lambda = \Lambda^{o} - Sc^{\frac{1}{2}} + E' c\ln c + J_1 c - J_2 c^{3/2} \qquad .....4.2.14$$

with slight variations in the coefficients S, E', J_1 and J_2 for each approach.

4.2.2 Conductance of Micellar Solutions

Below the c.m.c. most surfactants behave as typical 1:1 electrolytes and the simple Onsager equation 4.2.10 applies, but some, particularly those with longer alkyl chains show signs of dimerisation or even greater extents of aggregation below the c.m.c.[98,99] (see figure 4.2.1). The latter behaviour is difficult to detect in many cases and methods of analysis of data often give ambiguous results. For example from equation 4.2.8 the conductance of a monovalent surfactant solution below the c.m.c. is given by

$$\kappa_{sp} = F\sum ucz \qquad .....4.2.8$$

The monomer contribution to κ_{sp} is

$$\kappa_{spl} = Fu_1c_1z_1 \qquad .....4.2.15$$

and for $z_1 = 1$,

$$\kappa_{spl} = Fu_1c_1 \qquad .....4.2.16$$

The corresponding contribution of dimers in the same solution is

$$\kappa_{sp\ dimer} = Fu_{dimer}c_{dimer}z_{dimer} \qquad .....4.2.17$$

Since $z_{dimer} = 2$ and $c_{dimer} = \frac{1}{2}c_1$, and if u is proportional to z/r and r is the ionic radius (Stoke's Law) and r increases by up to a factor of 2 on dimerisation then $\kappa_{sp\ dimer}$ is only slightly greater than or equal to Fu_1c_1 and $\kappa_{spl} \doteqdot \kappa_{sp\ dimer}$ and little differentiation can be made between the two types of behaviour. Thus much controversy exists over the phenomenon of premicellar aggregation.

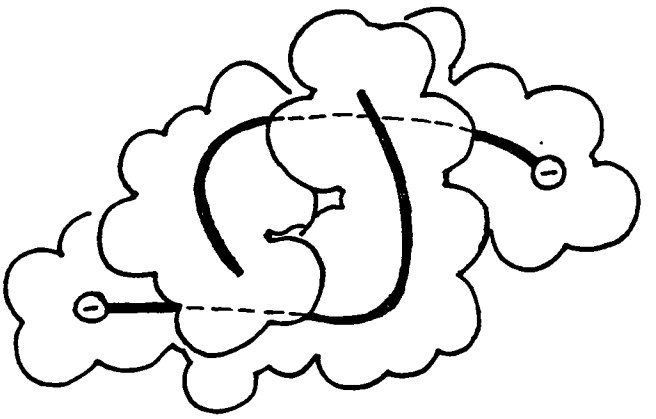

Figure 4.2.1 One of the possible structures of the dimer of lauryl sulphate ion. (reference 98)

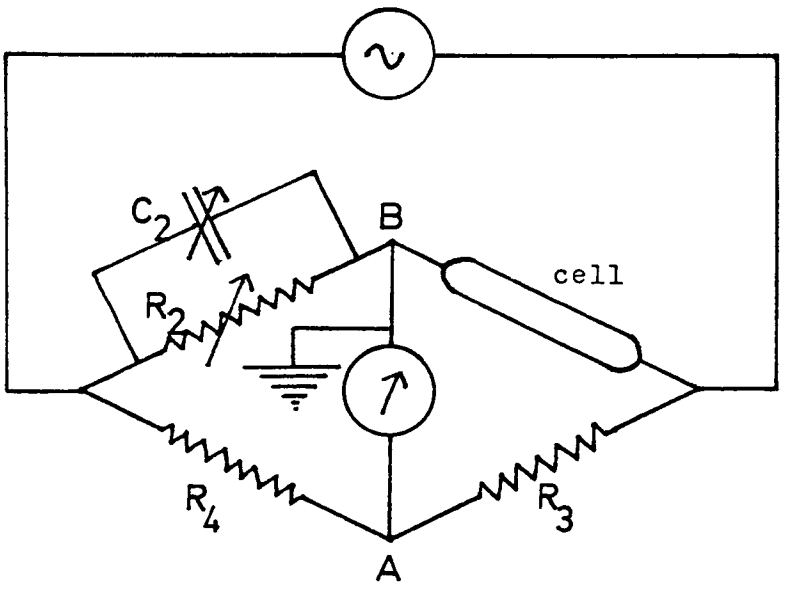

Figure 4.2.2 Wheatstone Bridge.

The conductivity against concentration plots show a discontinuity at the c.m.c. and were among the first measurements to give an indication that counterions bind to ionic micelles. McBain[5] pointed out that the specific conductance of a surfactant solution should increase if ions aggregated to form multivalent species. He argued that if m spherical ions of radius r aggregated to form a spherical micelle the minimum radius obtainable assuming close packing of ions would be $rm^{1/3}$. The resistance to motion as given by Stokes' Law would then be $rm^{1/3}/rm$ (i.e. $m^{-2/3}$) times its former value. The electrical force acting on the ions would be constant and so the velocity would increase by a factor of $m^{2/3}$ and the contribution to the specific conductivity would increase similarly. Experimental results proved the converse to be true for pure ionic systems and $d\kappa_{sp}/dc$ above the c.m.c. was less than $d\kappa_{sp}/dc$ below the c.m.c. The difference is attributable to counterion binding which considerably reduces the charge on the micelle.

From equation 4.2.8 the contributions from all species present are

$$\kappa_{sp}/F = c_1u_1z_1 + c_2u_2z_2 + c_{mic}u_{mic}z_{mic} \qquad .....4.2.18$$

where the subscript 1 refers to monomer
2 refers to counterions
mic refers to micelles

for $|z_1| = |z_2| = 1$ and $z_{mic} = \alpha n$
and $c_{mic} = \frac{c-c_1}{n}$ equation 4.2.18 becomes

$$\kappa_{sp}/F = c_1u_1 + c_2u_2 + \alpha(c-c_1)u_{mic} \qquad .....4.2.19$$

The analysis of the conductance behaviour of ionic micellar solutions above the c.m.c. therefore requires knowledge of the mobilities and concentrations of each species and all attempts to date to link these quantities in order to determine α have either resorted to oversimplification of the terms, for example the method described by equation 2.1.16 or the lengthy rigorous approaches of section 2.1.8.

4.2.3 Conductance Apparatus

The object of the conductance experiment is to measure the resistance of the solution between two electrodes so that the specific conductivity can be calculated from equation 4.2.6.

The use of direct current (d.c.) is unsuitable as the electrodes become polarised as a double layer builds up at each electrode surface. Gas can be liberated which opposes the passage of current, a counter E.M.F. is set up and the measured resistance increases. To reduce polarisation effects it therefore became normal practice to use alternating current (a.c.) for conductivity measurements since it was recognised that the polarising effect of equal and opposite pulses would neutralise each other. However, new problems were created. The electrode now acts as a condenser and the cell behaves as a resistance in series with a large capacitance C making the impedance Z the experimentally accessible parameter rather than resistance alone. Z is given by

$$Z^2 = R^2 + \frac{1}{C^2\omega^2} \qquad \ldots\ldots 4.2.20$$

where ω is the angular frequency of the sinusoidal a.c. In order to determine the resistance R the cell is placed in one arm of a Wheatstone Bridge as shown in figure 4.2.2. R_3 and R_4 are normally standard resistors of 10, 100, 1000 or 10000 ohms and R_2 and C_2 are varied to give minimum deflection on the meter which indicates the balance point. The condition for balance is

$$\frac{Z_1}{Z_2} = \frac{Z_3}{Z_4} = \frac{R_3}{R_4} \qquad \ldots\ldots 4.2.21$$

The values of R_3 and R_4 and their ratio R_3/R_4 are chosen to be of the same order as the resistive parts of Z_1, Z_2 and Z_1/Z_2 so that similar current flows through $Z_2 - Z_1$ and $R_4 - R_3$.

The full experimental conductivity bridge and circuitry are shown in figure 4.2.3 and comprise

1) electrolytic conductance bridge Type 4896 (H. Tinsley & Co. London)
2) tuned amplifier and null detector meter Type 1232A (General Radio Co. USA)
3) low frequency a.c. generator Type SG66 (Advance, England).

A Wagner earth is incorporated in the conductance bridge (R_6 and C_6) to ensure that points A and B are not only at the same potential but also at earth potential. Once the minimum

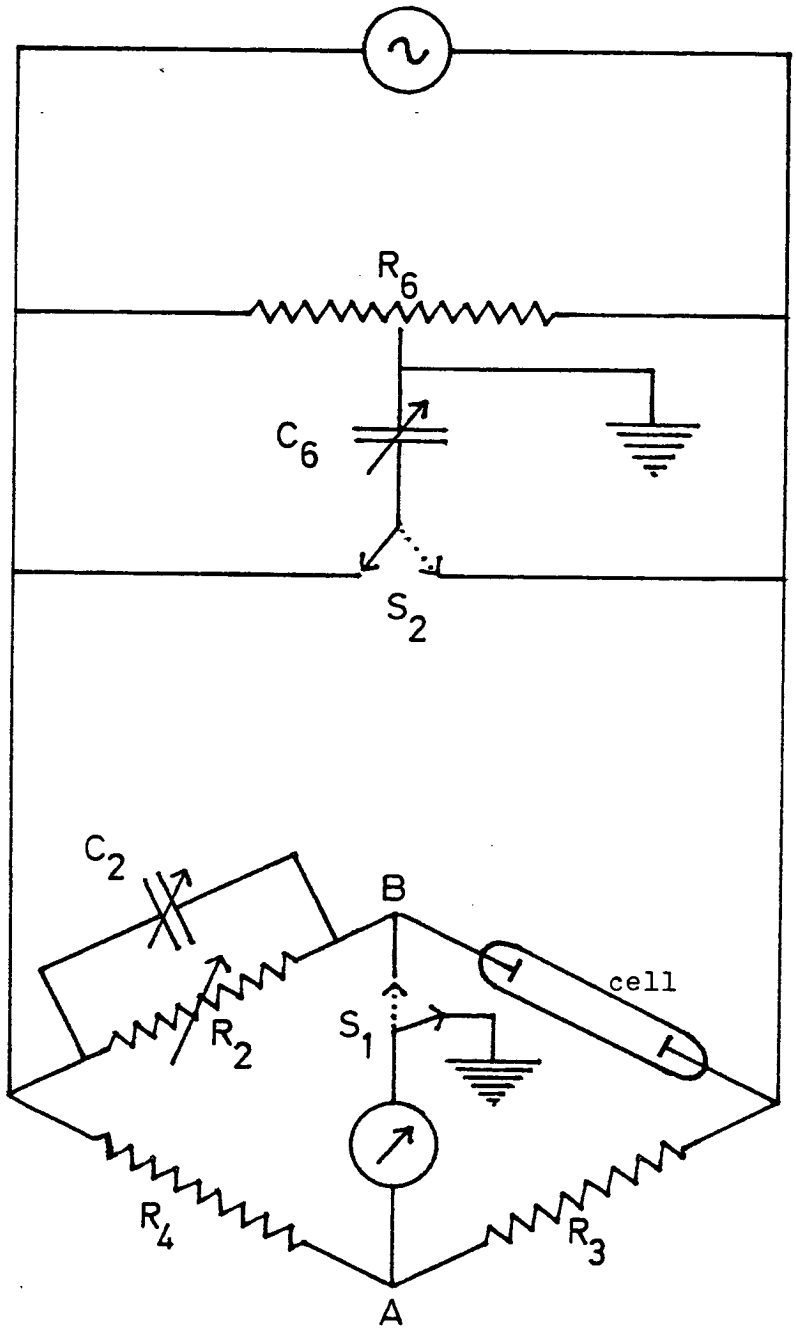

Figure 4.2.3 Conductivity Bridge.

deflection is obtained by varying R_2 and C_2 switch S_1 is connected to earth potential and with S_2 in each position R_6 and C_6 are varied to give minimum deflection.

Conductance Cell

Two cells with slightly different cell constants were used, one for cationic and the other for anionic systems to avoid contamination. The cell constants were determined by filling with standard NaCl and KCl solutions and are given below along with the masses of the dry empty cells in table 4.2.1.

Table 4.2.1 Cell constants and weights of conductance cells

cell number	cell constant/cm^{-1}	Mass of cell/g
1	1.472 ± 0.002	258.45
2	0.998 ± 0.001	273.85

Each cell (see figure 4.2.4) was constructed of Pyrex glass and had platinum disc electrodes, gold soldered onto stout platinum wire, which were coated with a fine layer of platinum black to reduce polarisation errors.[100] Only a very thin layer was applied as despite the advantage of reduced polarisation effects, thick layers may cause catalysis of electrode reactions or adsorption of significant amounts of electrolyte. The layer was applied by electrolysing

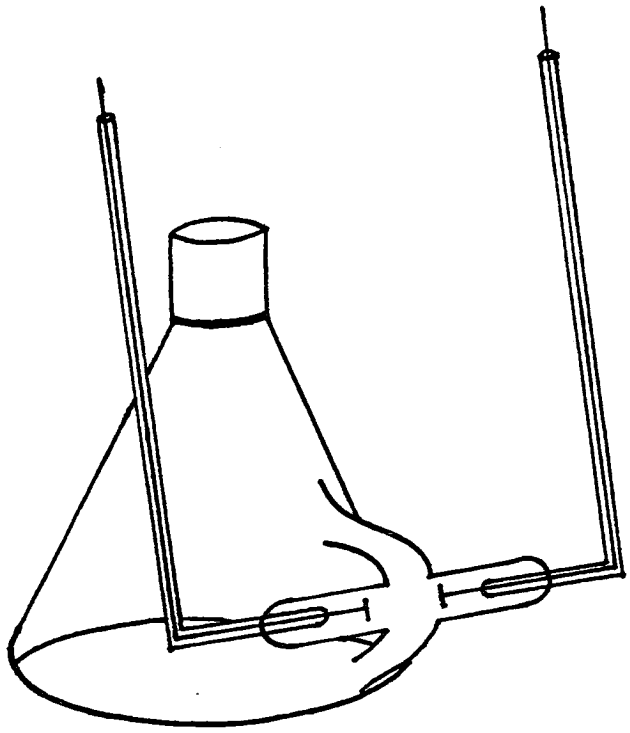

Figure 4.2.4 Experimental conductance cell.

a solution of 2 g platinic chloride and 0.02 g lead acetate in 100 cm^3 of water for five minutes, the current being reversed every 20 seconds and regulated such that a moderate stream of bubbles formed at the electrode. The platinising solution was then replaced by dilute sulphuric acid and current passed for half an hour in each direction to remove all traces of the original solution. The electrodes were well rinsed in triply distilled water for several days before silver leads were attached and the cell was assembled. The platinum wire required to be sealed into the structure via soda glass/Pyrex seals to prevent leakage of solution from the electrode compartment which may occur if other glass/platinum seals are used. The silver leads were spaced at a separation of 20 cm[101] to eliminate the Parker effect. This is an added capacitance effect which occurs when the leads pass close to the solution whose conductance is being measured. The volume of the electrode compartment was 30 cm^3 and the total volume 500 cm^3 so that substantial amounts of solvent could be added for dilution of the cell contents.

Thermostatting

Since the conductance of an ionic solution rises by over 2% per degree efficient thermostatting is required. The use of water as a thermostat liquid[102] was avoided where possible as this gives undesirable capacity effects across the cell walls, so measurements of conductivity were performed at

298.15 ± .05 K in a well stirred light oil bath, the temperature of which was measured with a platinum resistance thermometer. A few experiments were done at 288.15 and 308.15 K in water baths due to the difficulty in cooling the oil below room temperature and the fumes produced at higher temperatures.

The current must be relatively low to avoid heating since the amount of heat produced is proportional to current^2 (i.e. i^2) and hence an amplitude of total variation of 0.1 V was used for all measurements.

Use

Solvent was added by weight to the well rinsed cell which was then immersed in the thermostat bath. Additions of surfactant solution were made by volume. The cell was rocked to ensure good mixing then left for twenty minutes for temperature equilibration, rocked again briefly, and the cell resistance measured. In practice it is found that due to the capacitance of the cell the resistance measured is not independent of the a.c. frequency (see equation 4.2.20) and the normal practice of measuring the resistance at various frequencies, plotting R against ω^{-1} and extrapolating to infinite frequency was employed.[103] The values chosen were 1120, 1550, 2450 and 4600 Hz and over the range 1120 to 4600Hz the frequency dependence was of the order of 0.5%. At the end of each experiment when up to twelve individual additions of surfactant solution or solvent had been made, the cell exterior was cleaned, dried, and the cell was weighed to check that the expected weight did not deviate from the actual weight. Agreement was always of the order of 0.2%

and this being the major source of error in the experiment the overall precision of conductance values obtained was estimated at 0.3%.

4.3 Electrophoretic Mobility Measurement

The conductance of a micellar solution as described in the previous section (4.2) reflects the sum of contributions from every ionic species present in solution. In order to determine the micellar contribution it is necessary to measure the micellar mobility, u_{mic}, or the transport number, t, which is equal to $u_{mic}/\Sigma u_i$ where u_i is the mobility of a single ionic species.

If colloidal dimensions are sufficiently large for the particles to be microscopically visible the electrophoretic mobility is readily measured by observation of particle movement under the influence of an applied electric field. For smaller particles such as micelles different techniques must be sought to find u_{mic}. Classical methods of determining t include the Hittorf method[78] and the moving boundary method.[78]

A) Hittorf Method (1853)

The apparatus consists of an anode compartment, a cathode compartment and a third compartment between these two. Current, measured by a coulometer, is passed and the change in composition of each section determined analytically. Assuming that the composition of the central compartment does not change then the loss in either the anode or cathode compartment gives one of the transport numbers. Analytical limitations of this method make its use for measuring micellar mobility of little value.

B) Moving Boundary Method

The moving boundary technique developed by MacInnes[104] for ordinary electrolytes is in favourable cases applicable to micellar solutions. If a solution AR lies below one of AX where A is a common positive ion, a sharp boundary will move downward when negative current moves downward provided that the following conditions are satisfied

i) AR must be heavier than AX

ii) disturbing effects of convection, electrolysis products, hydrolysis and electroosmosis must be absent.

iii) the R ion must be more mobile than the X ion both in their respective solutions and in any mixture of the two which might form at the boundary.

Then $$t_R = \frac{t_X c_R}{c_X} \qquad \ldots\ldots 4.3.1$$

where c is the concentration of the ion.

Unfortunately when AR is a univalent surfactant whose mobility is relatively low it is usually impossible to find a compatible salt AX where the mobility of X satisfies condition (iii) above. Some work has been done with the more mobile divalent surfactants but this is by no means a general method of determining transport numbers of micelles.

The balanced boundary method[105] was devised by Hartley et al. by adaptation of the above method, whereby the transport number of AX was determined rather than AR but this has not been extensively used.

An alternative moving boundary apparatus was developed mainly by Tiselius[106] for the study of dissolved proteins. This consists of a U-tube of rectangular cross section divided into a number of sections built up on ground glass plates so that they can be moved sideways relative to each other to create sharp boundaries at the start of the experiment. Current is passed through the cell and the movement of the boundary followed by some optical technique which detects concentration changes by the accompanying variations in refractive index.

4.3.1 Tracer Electrophoresis

For all the moving boundary methods described above two chemically different solutions are required but if portions of surfactant solution can be labelled in some way which does not significantly alter the composition or properties of the solution then the technique can be simplified. In the tracer electrophoresis technique either radioactive labelling or mild dye-tagging of surfactant solutions can be used. Brady[107] described a tracer method whereby a central compartment containing dye-tagged surfactant was separated from compartments on either side containing untagged surfactant solution by fritted glass discs. Unfortunately when current was passed there was Joule heating at the membranes which caused convection currents in the central compartment. This upset the flow pattern and dye escaped from both ends of the apparatus. Systematic errors were also introduced

by surface effects at the glass discs. Hoyer, Stigter, Mysels and Dulin used a similar but open tube method[108] to determine both the micellar[41] and counterion[46] mobilities and this is described below.

Apparatus

The apparatus design is that of Hoyer, Stigter and Mysels[108] with some improvements as shown in figure 4.3.1. It contains five separate sections:

1 and 5: These are electrode compartments containing reversible Ag/AgBr electrodes of surface area 100 cm^2 in 0.1 mol dm^{-3} NaBr solution. A high surface area is required so that the current density is low and gassing is minimised.

3: This is the central tube which at the start of the experiment contains surfactant solution plus a small amount of dye.

2 and 4: These are connecting tubes containing the same surfactant solution as in (3) but without the dye.

Each section is separated from the next by a three way PTFE tap which eliminates the need for the troublesome grease required in the original work.

With all taps except B and D closed, a potential difference is applied across the cell, dye tagged surfactant moves out of the central compartment at one end and untagged solution enters at the other at a rate depending on the experimental conditions of surfactant concentration and composition, applied potential , and the cross sectional

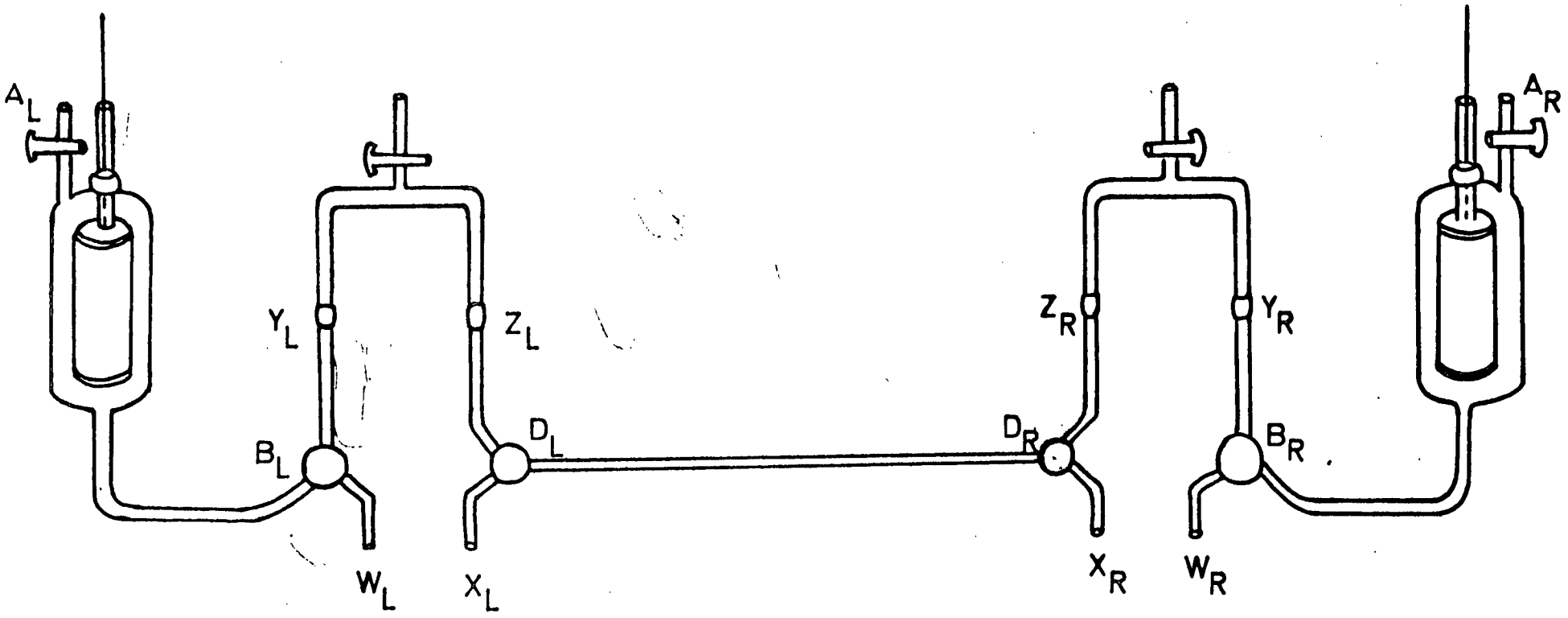

Figure 4.3.1 Tracer Electrophoresis Apparatus.

area of the tube (3). After some time the electric field is switched off and the contents of (3) are analysed to give the average change in dye content of the volume of solution contained between taps D_L and D_R. The electrophoretic mobility is calculated from

$$u = \frac{\kappa_{sp} v}{it} \left(\frac{c_o - c}{c_o}\right) \qquad \ldots\ldots 4.3.2$$

where v is the volume of the capillary/cm^3, i is the current/A, t is the time/s, c_o is the initial dye concentration and c is the final dye concentration.

A typical current against time profile is shown in figure 4.3.2. The current rises rapidly in the first 15 to 20 minutes then levels off. The extent of current rise with time after this initial period reflects a certain degree of heating in the capillary where most of the resistance is found. The mobility of an ionic species varies considerably with temperature, as mentioned in section 4.2.3. and so efficient thermostatting is vital. The capillary should have as small a diameter as possible so that excess heat can be efficiently dissipated and preferably the glass wall thickness should not be too great. The length of the tube is then limited by its strength. The central compartment was therefore constructed of Veridia glass of 7 mm diameter and 3.0 mm internal diameter and 50 cm in length. The volume between the taps was measured by repeated filling with mercury and was found to

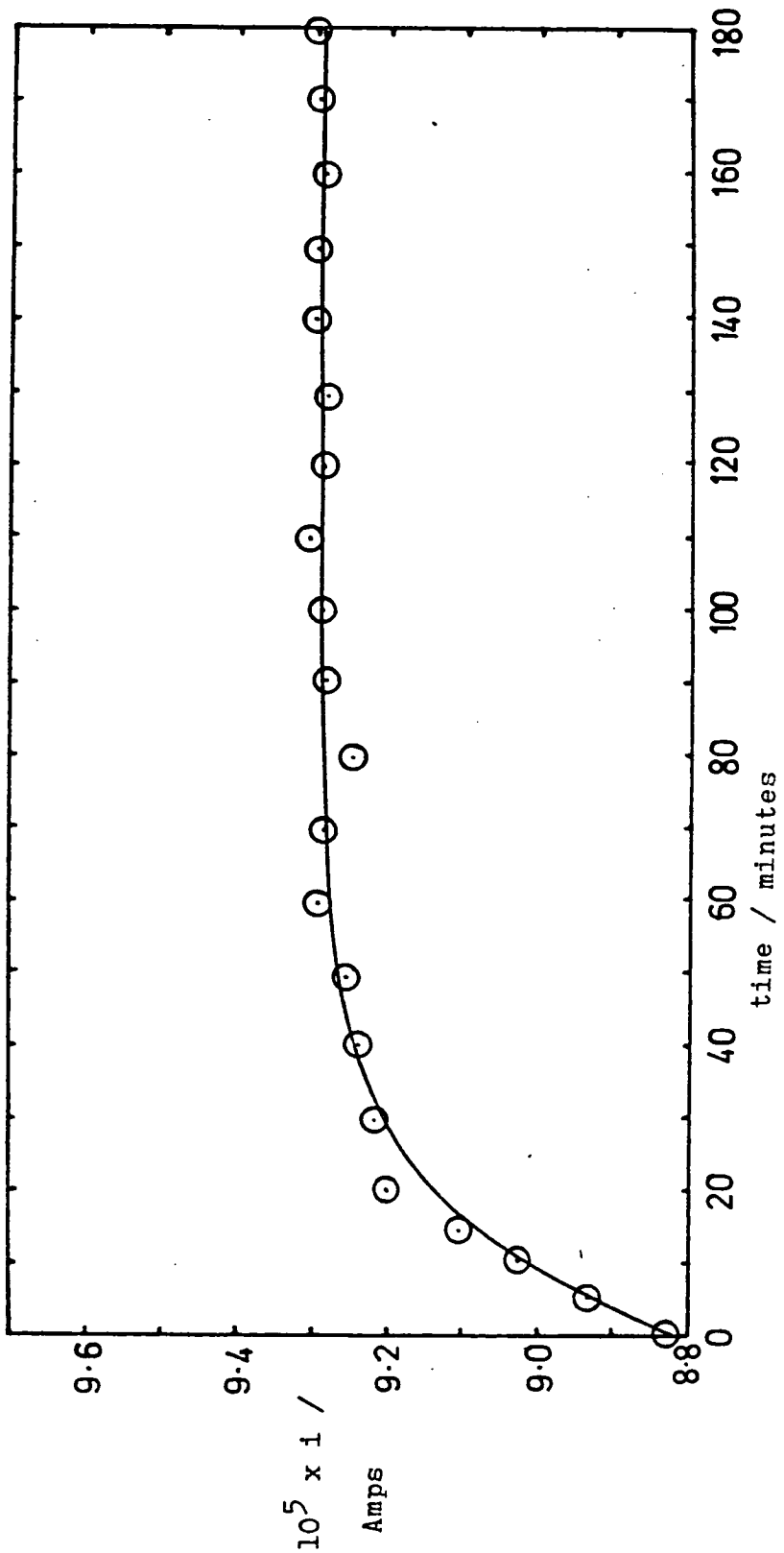

Figure 4.3.2 Typical current - time profile of the tracer electrophoresis experiment,

be 3.614 ± 0.007 cm^3. 3 cm^3 is the minimum volume suggested by Stigter et al. for the analytical technique to have better than 2% accuracy. The capillary had a surrounding water jacket through which water at 298.15 ±0.05 K was circulated. The entire apparatus was kept at 298 K in a thermostatted room.

The electrode compartments were filled with NaBr solution by applying suction at A with B immersed in electrolyte. The central compartment was filled by pouring dye solution gently down Z_R with tap D_L open to X_L. It was often necessary to tilt the cell to allow small bubbles to escape from the capillary at this stage. The apparatus was then assembled by means of the Quickfit joints Y and Z. Finally sections (2) and (4) were filled by suction at C with W and X immersed in surfactant solution. Thermal equilibrium did not take long to attain since all solutions were stored under the same conditions.

The applied voltage was switched on and the current noted at regular intervals by measuring the potential drop across a 10,000 ohm resistor connected in series with the cell. It was found that the surfactant solution containing dye was slightly denser than the untagged solution by observing the moving boundaries. The ascending boundary in (2) was always quite distinct and horizontal whereas the other moving along the central compartment was parabolic and became distorted after some time as shown in figure 4.3.3. At the end of the run the apparatus was dismantled and the contents of the central compartment were washed out with

Figure 4.3.3 Shape of the boundary in the tracer electrophoresis experiment.

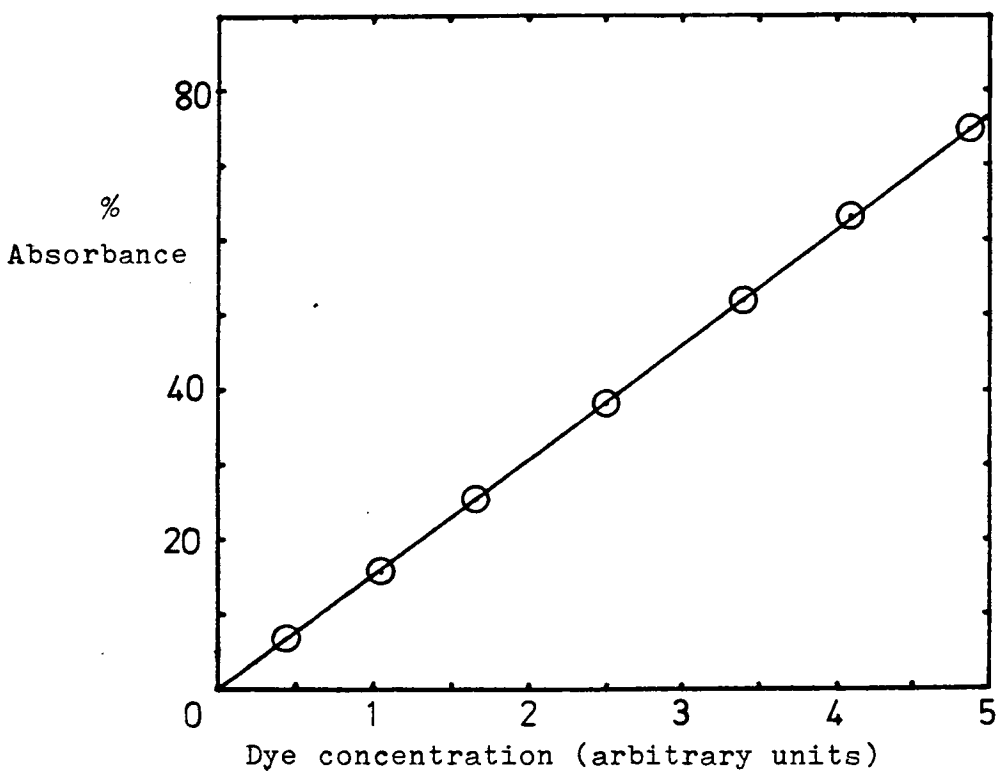

Figure 4.3.4 Plot of absorbance against dye concentration.

surfactant solution into a flask for weighing. The dye content was estimated using a Perkin-Elmer 402 ultraviolet/visible spectrophotometer and compared with the original dye concentration and several other prepared dilutions. A sample graph is shown in figure 4.3.4 demonstrating the linear relationship between absorbance and dye concentration. The uncertainty in the calculated % dye concentration is $\pm$ 1 to 2% and this is the major source of error in the experiment.

Conductance measurements of the dye containing solution confirmed that the addition of dye did not alter the specific conductivity and so the results obtained in section 4.2 were used to calculate the electrophoretic mobility of the micelles. This is in agreement with the observations of Mysels[109] who has shown that the presence of small amounts of dye does not significantly affect micellar properties.

Most mobility measurements were done in duplicate and several in triplicate with the electrode polarity reversed for alternate experiments and an average of u_{mic} taken.

Preliminary Experiments and Choice of Experimental Conditions

From the formula

$$u = \frac{\kappa_{sp} v}{it} \left(\frac{c_o - c}{c_o}\right) \qquad \ldots\ldots 4.3.2$$

it is seen that v is a constant and κ_{sp} is predetermined by the concentration and composition of each solution.

it is convenient to regulate the variables i (or V) and t so that $(c_o-c)/c_o$ is always in the range 0.4 to 0.5 for ease of observation in the capillary, ensuring that sufficient dye has left the central compartment while no untagged solution has passed the exit tap.

A) Variation of t

The results of two experiments (see figure 4.3.5) show no consistent relationship between calculated mobility and duration of the experiment when t is the only variable. However, for an experiment lasting less than two hours the initial period when the current rises rapidly is a significant part of the overall run and its inclusion in the calculation of the average current flowing may give significant errors. The error would be reduced in longer experiments when the current stabilises but diffusion and convection may become troublesome for very long running times. All runs were therefore chosen to last between two and five hours depending on the value of V and the mobility of the micelle being studied.

B) Variation of voltage V

Several experiments with V the only variable showed no dependence of mobility on V as required (see figure 4.3.6) substitution for

$$\kappa_{sp} = \frac{a}{R} \quad \text{and} \quad i = \frac{V}{R}$$

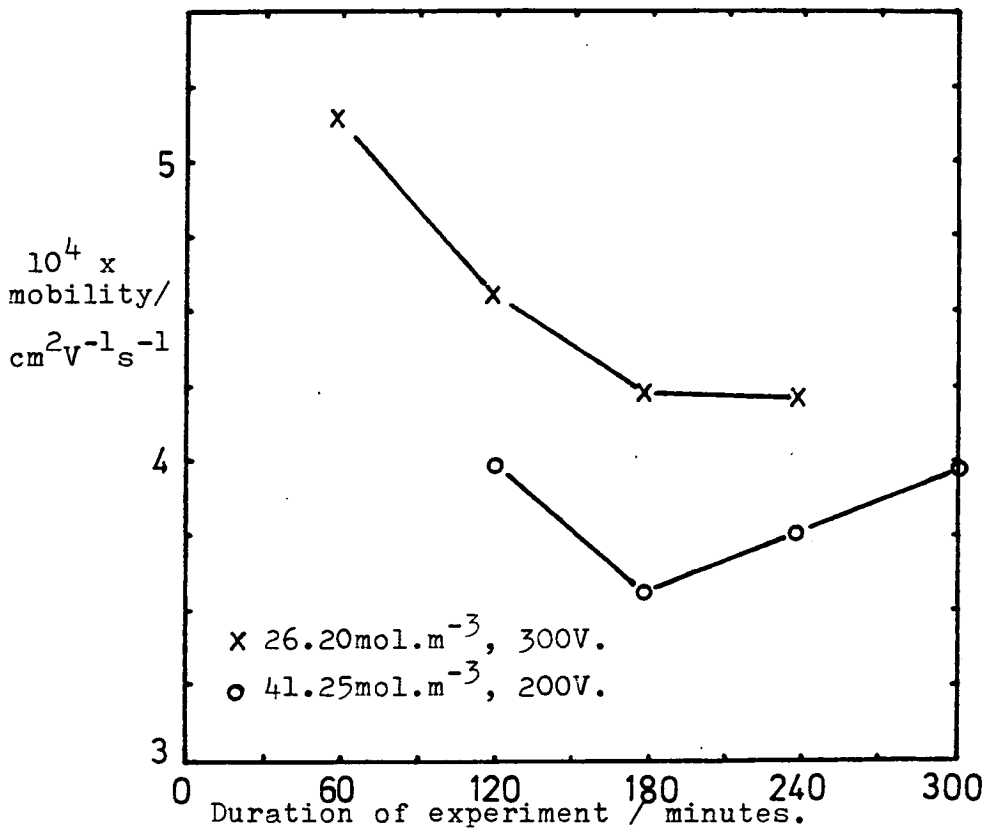

Figure 4.3.5 Plot of calculated micellar mobility against duration of experiment.

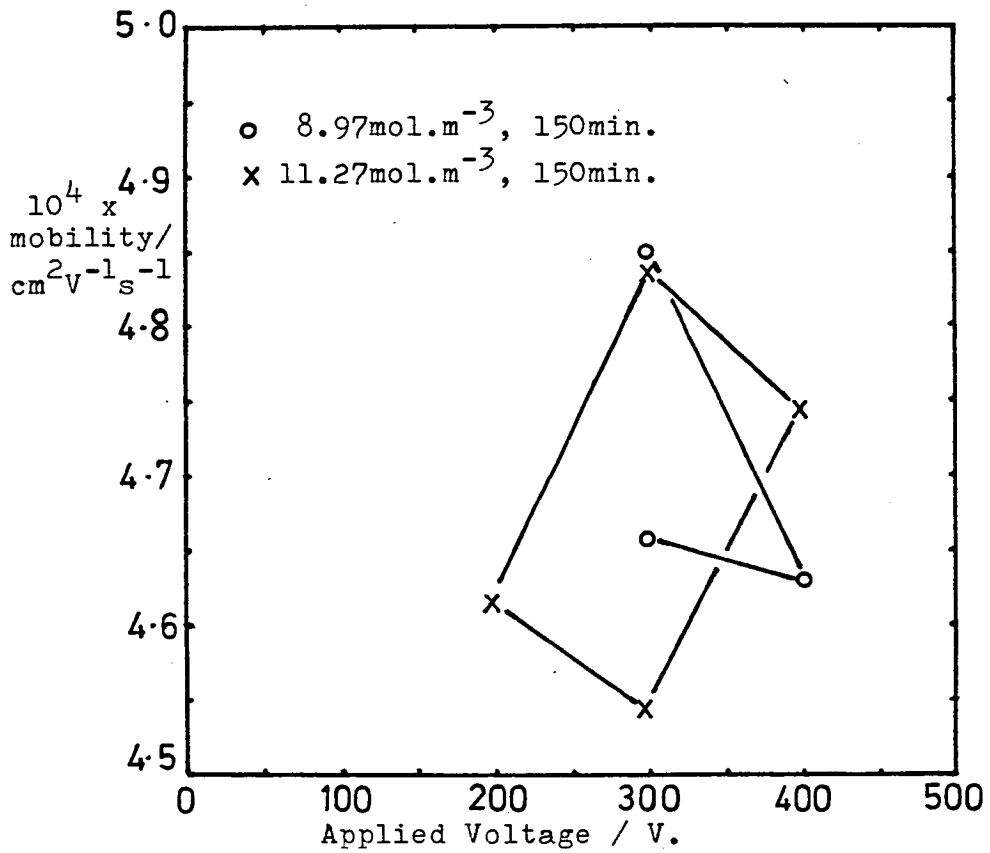

Figure 4.3.6 Plot of calculated micellar mobility against applied voltage.

where R is the resistance of the solution in equation 4.3.2 and taking $v(c_o-c)/c_o$ as constant gives for u_{mic}

$$u_{mic} = \text{constant} \times \frac{1}{Vt} \quad \ldots\ldots 4.3.3$$

V is varied on two counts

A) so that the current does not exceed 0.5 mA, to prevent heating

B) to keep the duration of the experiment in the range two to five hours.

4.4 Diffusion Coefficients

Colloidal particles, viewed under the microscope are seen to move about haphazardly and are said to be undergoing Brownian motion. This motion is not unique to particles of colloidal dimensions but occurs in any suspended system. Kinetic theory predicts that the translational kinetic energy of any particle is 3/2 kT or ½kT along any given axis and since the kinetic energy is equal to ½ mv^2 where m is the particle mass and v its velocity then

$$\tfrac{1}{2}\, mv^2 = \tfrac{1}{2}kT \quad \ldots\ldots 4.4.1$$

This shows that the average particle velocity depends only on the mass of the particle and the temperature.

Einstein[110] and Smoluchowski[111] deduced that the mean square distance, $\overline{x^2}$, travelled by a spherical uncharged particle of radius r in time, t, is

$$\overline{x^2} = 2t \frac{RT}{N} \frac{1}{6\pi\eta r} \quad \ldots\ldots 4.4.2$$

where R is the gas constant, N is Avodagro's number and η is the viscosity of the solvent. Also $\overline{x^2}$ is related to the diffusion coefficient, D, by the equation

$$\overline{x^2} = 2Dt \quad \ldots\ldots 4.4.3$$

Hence

$$D = \frac{kT}{6\pi\eta r} \quad \ldots\ldots 4.4.4$$

Thus for a system of noninteracting particles the diffusion coefficient is inversely proportional to the particle radius and measurement of D for micellar systems provides a measure of micellar size.

4.4.1 Photon Correlation Spectroscopy[112,113] (P.C.S.)

Conventional light scattering is a familiar technique for providing molecular weights and hence size of colloidal particles but the introduction of lasers as light sources has enabled more information to be obtained from the scattering pattern produced. Since a colloidal dispersion contains randomly placed particles free to diffuse in solution the

diffraction pattern of scattered light fluctuates with time, on a time scale proportional to the Brownian diffusion rate. When ordinary light which possesses a range of frequencies is used the fluctuation pattern cannot be easily interpreted but the use of monochromatic laser light produces an intensity trace which is characterised by a typical fluctuation time or correlation time. It is this correlation time, τ_c, which the P.C.S. experiment can provide and from it the diffusion coefficient of the particle can be found.

Theory

For a large number, N, of identical scatterers, the scattered field, E_s, at time, t, is given by

$$E_s(t) = \sum_{j=1}^{N} E_j(t)\exp[-i\underline{K}.\underline{r}_j(t)] \qquad \ldots\ldots 4.4.5$$

where E_j and $\underline{r}_j$ are the scattered field amplitude and position vector of the jth particle and $\underline{K}$ is the scattering vector (see figure 4.4.1). At a time $(t+\tau)$ later a similar expression gives

$$E_s(t+\tau) = \sum_{i=1}^{N} E_i(t+\tau)\exp[-i\underline{K}.\underline{r}_i(t+\tau)] \qquad \ldots\ldots 4.4.6$$

The autocorrelation function $g_1(\tau)$ is defined in terms of the scattered field

$$g_1(\tau) = \left\langle \frac{E(t)E^*(t+\tau)}{E(t)E^*(t)} \right\rangle \qquad \ldots\ldots 4.4.7$$

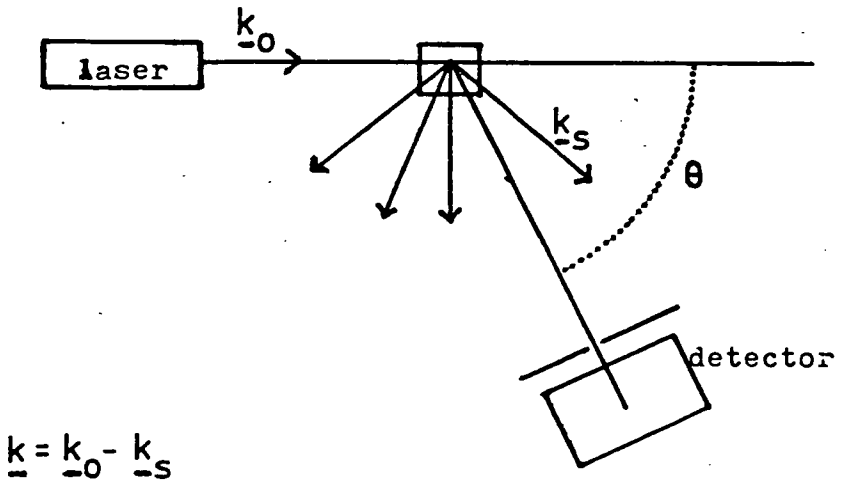

Figure 4.4.1 Schematic representation of the laser light scattering experiment.

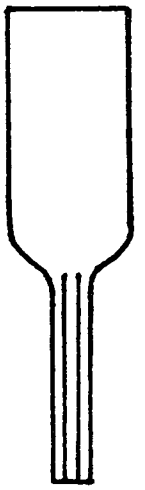

Figure 4.5.1 Diagram of the stalagmometer used for surface tension measurements.

where * denotes the complex conjugate

$$\frac{\sum_i^N \sum_j^N < E_i(t)E_j(t+\tau)\exp[i\underline{K}.(\underline{r}_i(t+\tau) - \underline{r}_j(t))] >}{\sum_i^N \sum_j^N < E_i(t)E_j(t)\exp[i\underline{K}.(\underline{r}_i(t) - \underline{r}_j(t))] >}$$

The expression for $g_1(\tau)$ can be shown to reduce to

$$g_1(\tau) = \exp(-DK^2\tau) \quad \ldots\ldots 4.4.8$$

The scattered light is detected by a photomultiplier and the normalised autocorrelation function $g_2(\tau)$ constructed by successive summation in the multichannel autocorrelator

$$g_2(\tau) = \frac{< n(t),\ n(t+\tau) >}{< n >^2} \quad \ldots\ldots 4.4.9$$

where n is the number of counts arriving in a given sample time and τ is the delay time.

$g_1(\tau)$ can be obtained using the relationship

$$g_2(\tau) = 1 + |g_1(\tau)|^2 \quad \ldots\ldots 4.4.10$$

Therefore $g_2(\tau) = 1 + c\exp[-2DK^2\tau]$ 4.4.11

where c is a constant.

Since the decay rate of the electric field Γ is the inverse of the correlation time τ_c and

$$\Gamma = DK^2 \quad \ldots\ldots 4.4.12$$

Therefore $$\frac{1}{\tau_c} = DK^2 \qquad \ldots\ldots 4.4.13$$

By substitution in equation 4.4.4 the particle radius is found.

If the function $g_2(\tau)$ cannot be described by a single exponential, for example for polydisperse systems then $g_2(\tau)$ must be modified to

$$g_2(\tau) = 1 + C[\int_0^\infty G(\Gamma)\exp(-\Gamma t)]^2 d\Gamma \qquad \ldots\ldots 4.4.14$$

where $G(\Gamma)$ is the light intensity scattered from the processes characterised by the correlation time Γ^{-1}. The distribution $G(\Gamma)$ is normalised to one. Then the correlation function can be expanded in a power series in time.

$$\ln(g_2(\tau)-1) = \ln C - 2\bar{\Gamma}t + Q_2(\bar{\Gamma}t)^2 - {}^1/_3 Q_3(\bar{\Gamma}t)^3 \qquad \ldots\ldots 4.4.15$$

where $$\bar{\Gamma} = \int_0^\infty \Gamma G(\Gamma) d\Gamma$$

and $$Q_i = \frac{1}{\bar{\Gamma}_i} \int_0^\infty (\Gamma-\bar{\Gamma})_i G(\Gamma) d\Gamma$$

and $\bar{\Gamma}$ is the average inverse correlation time.

Experimental

Surfactant solutions were prepared by dilution of stock solutions immediately prior to use and dust particles were removed by Millipore filtration in a dust free box. The solution was placed in a 1 by 1 cm cell and briefly irradiated in an ultrasonic bath before being mounted in a thermostatted water bath at 298.15 ± .1 K in the path of the laser beam. A green argon ion laser Spectra Physics model 165 of wavelength 5145 Å was used. Light scattered at 90° was detected by a Malvern Photon Correlation Spectrometer with a forty eight channel store. Data was analysed by computer (Hewlett Packard model 9815A) to obtain the least squares fit for Γ in the linearised form of equation 4.4.14 and in general a quadratic fit gave the most consistent values of D when data from the first 16, 32 and 48 channels were considered. Each experiment was performed three times and an average value of D taken for the calculation of the micellar radius.

4.5 Surface Tension

Molecules of surfactant adsorb at the solution/air interface and significantly reduce the surface tension of water as their concentration increases, but above the c.m.c. this surface tension drop ceases as excess surfactant micellises and two distinct regions in the surface tension, γ, against ln concentration plot are obtained. Extrapolation of lines drawn above and below this region intersect at the c.m.c.

Surface tension measurements were performed for two reasons

1) to determine the c.m.c. independently of conductance, particularly for the low concentration cationic/nonionic mixtures.

2) to check the purity of the surfactant samples as described in Section 4.1.

Technique

The drop weight method was used.[114] Drops form at the tip of a capillary, fall, and are collected for weighing. If perfectly spherical drops formed then the simple law

$$W = 2\pi r\gamma \qquad \ldots\ldots 4.5.1$$

where W is the drop weight, and r is the tip radius, would apply but in practice up to 40% of the drop may remain attached to the tip so a correction factor, f, is required for the drop shape. This factor as a function of r/L where L is the drop dimension has been tabulated by Harkins and Brown.[115] Thus the equation for γ is

$$\gamma = \frac{mg}{2\pi rf(r/L)} \qquad \ldots\ldots 4.5.2$$

where m is the mass of the drop and g is the force due to gravity.

The diameter of the tip of the stalagmometer used (see figure 4.5.1) was measured with a travelling microscope and was found to be 5.43 mm. At least five sets of twenty drops were collected for weighing for each concentration, the level of liquid in the tube being the same at the beginning of each collection.

It is to be noted that the drop weight method gives non-equilibrium values of surface tension as the technique suffers from kinetic effects as described by Tajima[150,151]. Consequently c.m.c. values quoted here may differ significantly from those in the literature obtained using alternative methods.

150. K. Tajima, M. Muramatsu, T. Sasaki, Bull. Chem. Soc. Japan, 1970, 43 1991 & 3063

151. K. Tajima, Bull. Chem. Soc. Japan, 1970, 43, 629

CHAPTER FIVE

RESULTS AND DISCUSSION

CHAPTER 5

RESULTS AND DISCUSSION

5.1 Results

5.1.1 Conductance

5.1.1 (A) Pure Ionic Systems

For a pure ionic surfactant in water the typical plot of specific conductance, κ_{sp} against concentration is shown in figure 4.1.1 (A) and figure 5.1.1. Well below and well above the c.m.c. the plot is linear and extrapolation of these straight line portions gives an intersection point which is defined as the c.m.c. It has been mentioned in the introduction in chapter one that there is no sharp transition from a solution containing entirely free monomers and counterions below the c.m.c. to a solution containing only micelles above the c.m.c. and the onset of micellisation is gradual over a narrow concentration range. Careful examination of the conductance points close to the c.m.c. demonstrates this fact as the points are seen to lie on a curve slightly below the extrapolated lines in this region. An alternative method of plotting results is shown in figure 5.1.2. The graph of molar conductivity, Λ against $c^{\frac{1}{2}}$ also shows a break point at the c.m.c. In this case the portions above and below the c.m.c. are linear over only a moderate concentration range close to the c.m.c. and extrapolation of these straight line portions to give an

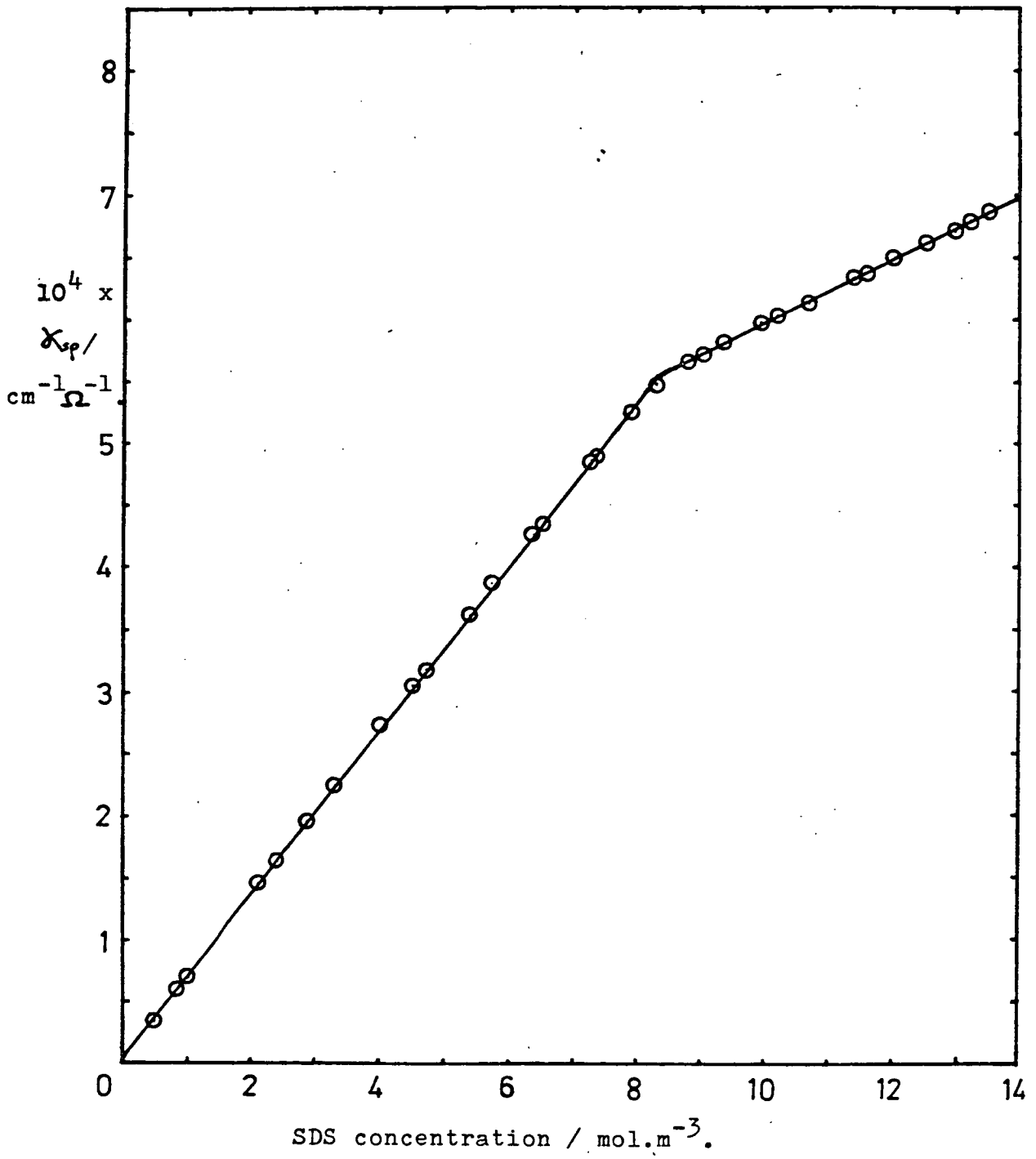

Figure 5.1.1 Plot of specific conductance against concentration for SDS in water at 298.15K.

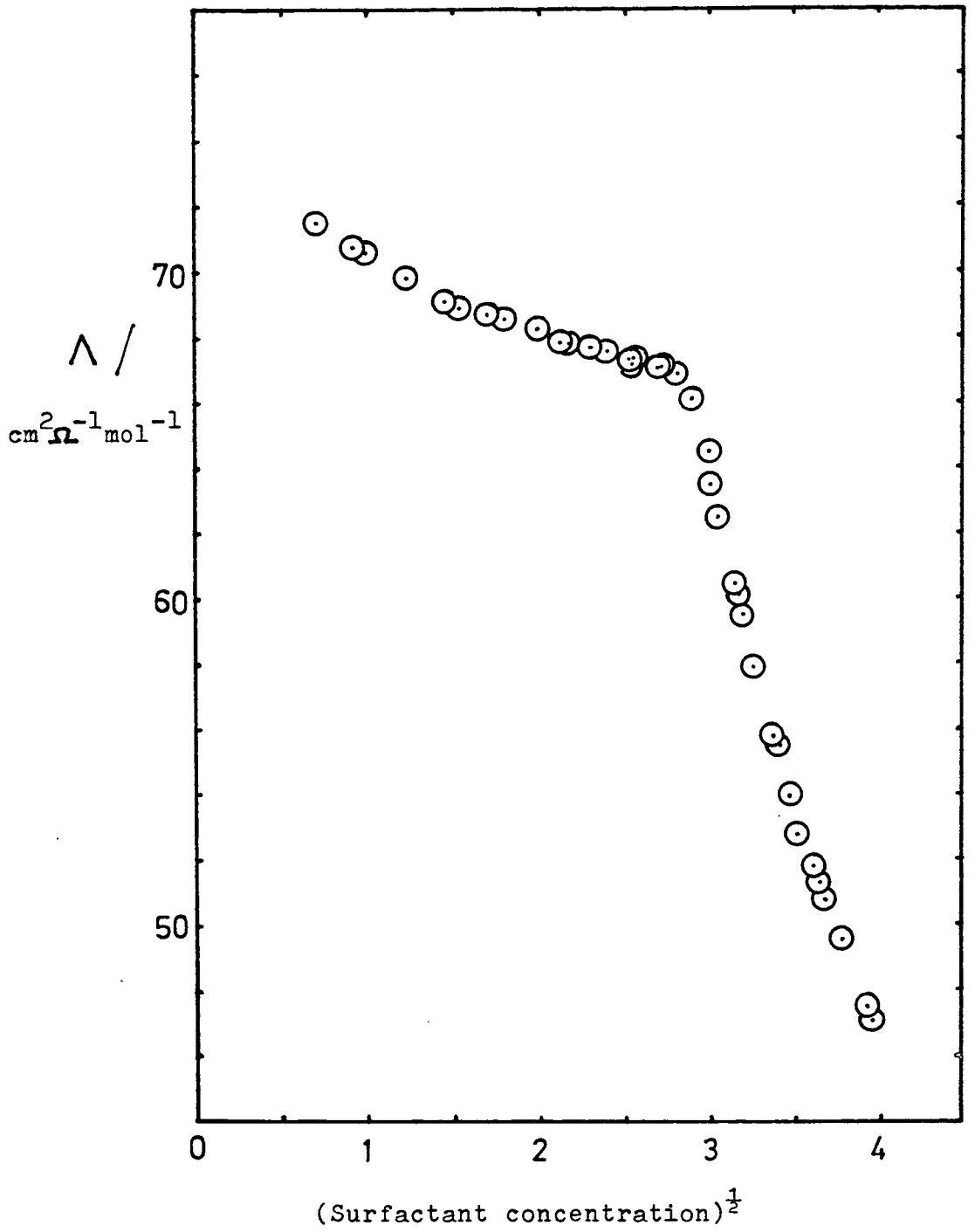

Figure 5.1.2 Plot of molar conductivity against concentration$^{\frac{1}{2}}$ for SDS at 298.15K.

intersection at the c.m.c. is not as straightforward as in the specific conductance against concentration case. There is invariably a discrepancy between c.m.c. values estimated by the two methods due to differences in extrapolating one plot which is linear in c and another which is linear in $c^{\frac{1}{2}}$. However, both methods are equally valid and the data obtained for SDS and CTAB by each method are presented in tables 5.1.1 and 5.1.2.

Table 5.1.1 Experimental Conductance Data for SDS and CTAB in water at 298.15 K

Surfactant	Average $d\kappa_{sp}/dc$ below c.m.c./ $cm^2\Omega^{-1}mol^{-1}$	Average $d\kappa_{sp}/dc$ above c.m.c./ $cm^2\Omega^{-1}mol^{-1}$	c.m.c. $(\kappa_{sp}vc)$/ $mol\ m^{-3}$	c.m.c. $(\Lambda vc^{\frac{1}{2}})$ / $mol\ m^{-3}$
SDS	66.54	24.79	8.303	8.12
CTAB	93.35	24.60	0.955	0.870

Table 5.1.2 Limiting Ionic Conductivities of Monomer and Counterions for SDS and CTAB in water at 298.15 K

Surfactant	λ_o monomer/ $cm^2\Omega^{-1}mol^{-1}$	λ_o counterion/ $cm^2\Omega^{-1}mol^{-1}$	$\Lambda_o/cm^2\ \Omega^{-1}mol^{-1}$
SDS	23.3	50.10	73.4 $\pm$ 0.5
CTAB	34.4	78.14	112.5 $\pm$ 5

More detailed lists of conductance data are tabulated in Appendix 1.

The Onsager slope for 1:1 electrolytes can be determined for each surfactant below the c.m.c. to test the assumption that there is no premicellar aggregation. Equation 5.1.1 is used where $B_1 = 0.2289\ mol^{-\frac{1}{2}}dm^{\frac{1}{2}}$ and $B_2 = 60.19\ cm^2\Omega^{-1}dm^{\frac{1}{2}}mol^{-3/2}$.

$$\Lambda = \Lambda_o - (B_1\Lambda_o + B_2)c^{\frac{1}{2}} \qquad \ldots\ldots 5.1.1$$

Thus for SDS $\Lambda = 73.4 - 76.99\ c^{\frac{1}{2}}$ 5.1.2

and for CTAB $\Lambda = 112.5 - 85.94\ c^{\frac{1}{2}}$ 5.1.3

The poor sensitivity of the conductance apparatus at very low concentrations, less than 2.5×10^{-4} mol dm^{-3}, makes it difficult to obtain accurate data for CTAB below the c.m.c. in order to determine the limiting ionic conductivity, Λ_o since the extrapolation of the Λ against $c^{\frac{1}{2}}$ plot must be done using points in a narrow concentration range (between $c^{\frac{1}{2}} = 0.015$ and $c^{\frac{1}{2}} = 0.027$). The value of Λ_o thus obtained is 112.5 $cm^2\Omega^{-1}mol^{-1}$ but is subject to an error of $\pm 5\ cm^2\Omega^{-1}mol^{-1}$ and therefore any calculated Onsager slope by the above method is likely to contain serious errors and little can be deduced from comparison with the experimental slope. Confining the treatment to the data for SDS it is found that the Onsager slope is greater than the experimental slope, that is the surfactant solution

conducts better than a 1:1 electrolyte (see figure 5.1.3). Mukerjee, Mysels and Dulin[98] also found this result and attributed it to the formation of dimers below the c.m.c. However, modifications to the Onsager treatment made since their study have provided improved conductivity equations and Parfitt and Smith[116] have shown that equation 5.1.4 due to Fuoss and Onsager[117,118] satisfies the condition that SDS behaves purely as a 1:1 electrolyte below the c.m.c.

$$\Lambda = \Lambda_o - Sc^{\frac{1}{2}} + Ec \log c + Jc \quad \ldots\ldots 5.1.4$$

S is the Onsager slope and E and J are parameters of the theory.

Variation of Salt Concentration

The effect of added salt on CTAB and SDS solutions is shown in figure 5.1.4 and the relevant data in table 5.1.3 and Appendix 1.

Table 5.1.3 Conductance Data for SDS and CTAB at 298.15 K as a function of added salt concentration

A) SDS with added NaCl solution

Added salt concentration/ mol m^{-3}	$d\kappa_{sp}/dc$ below c.m.c./ $cm^2\Omega^{-1}mol^{-1}$	$d\kappa_{sp}/dc$ above c.m.c./ $cm^2\Omega^{-1}mol^{-1}$	c.m.c./ mol m^{-3}
0	66.54	24.79	8.303
1	66.08	25.05	7.919
2.5	64.97	24.14	7.424
5	63.27	23.92	6.665
10	61.53	23.36	5.423

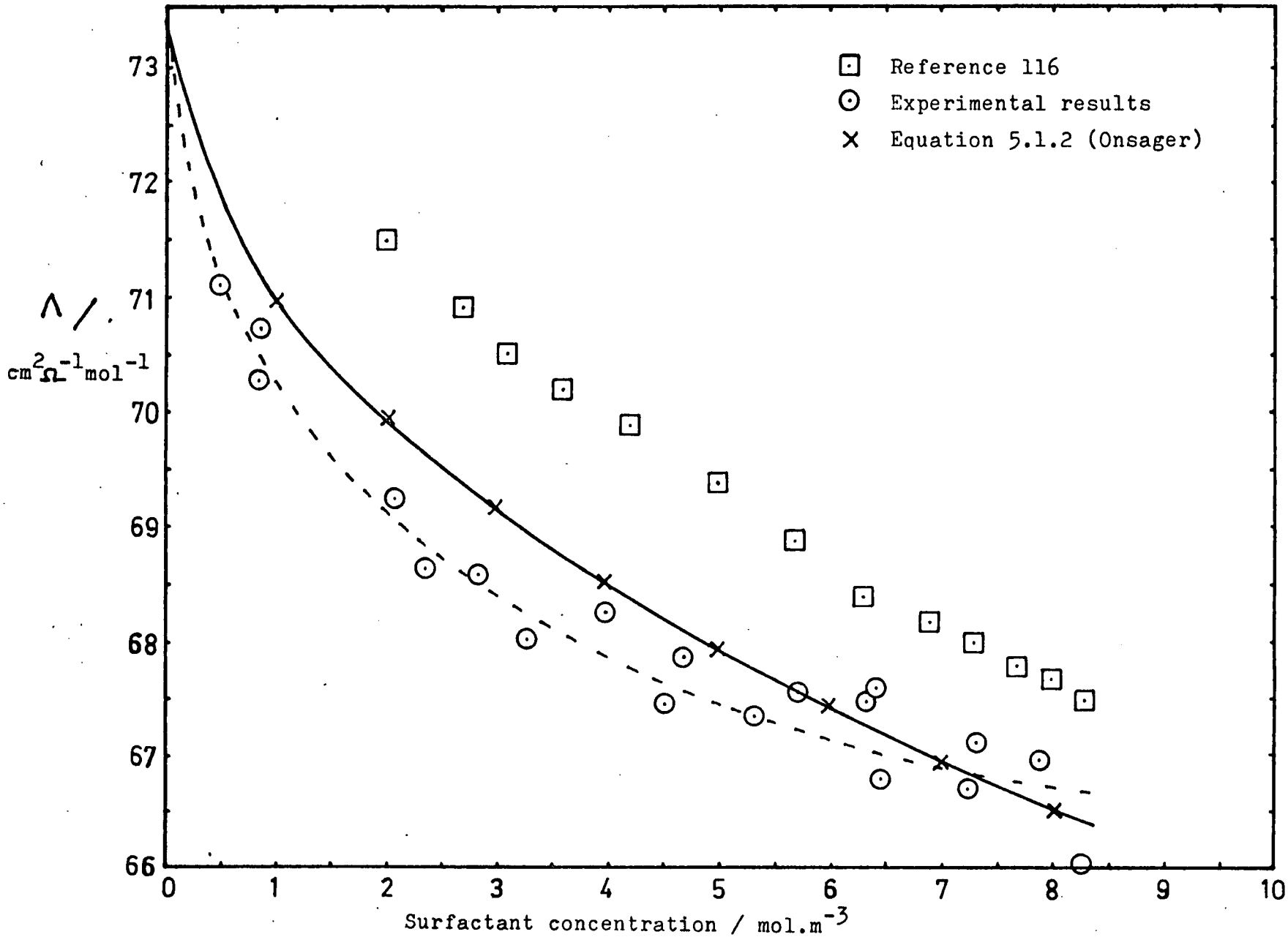

Figure 5.1.3 Molar conductivity of SDS as a function of concentration at 298.15K. (Onsager slope)

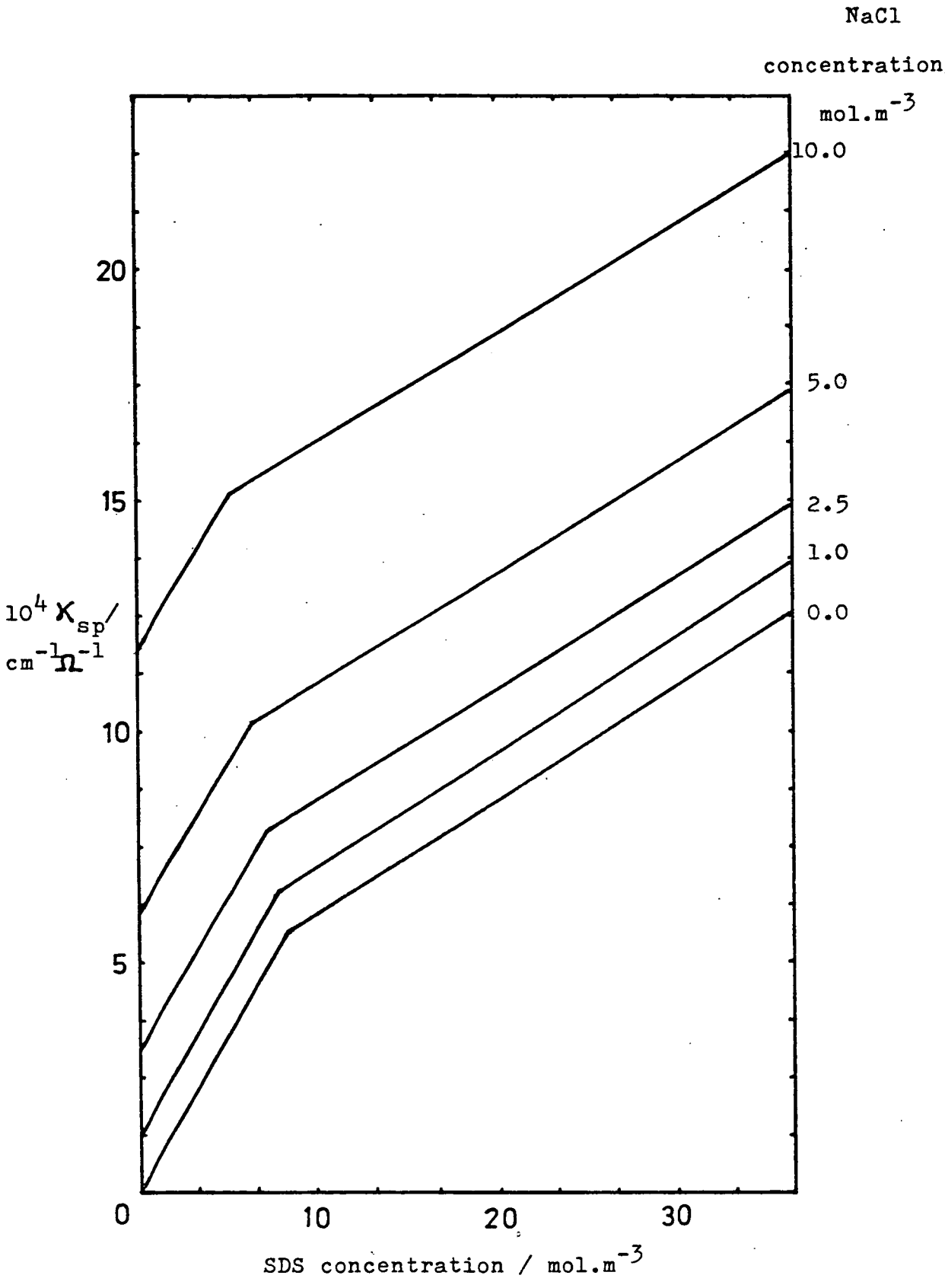

Figure 5.1.4 (A) Plots of specific conductivity against SDS concentration in NaCl solutions at 298.15K.

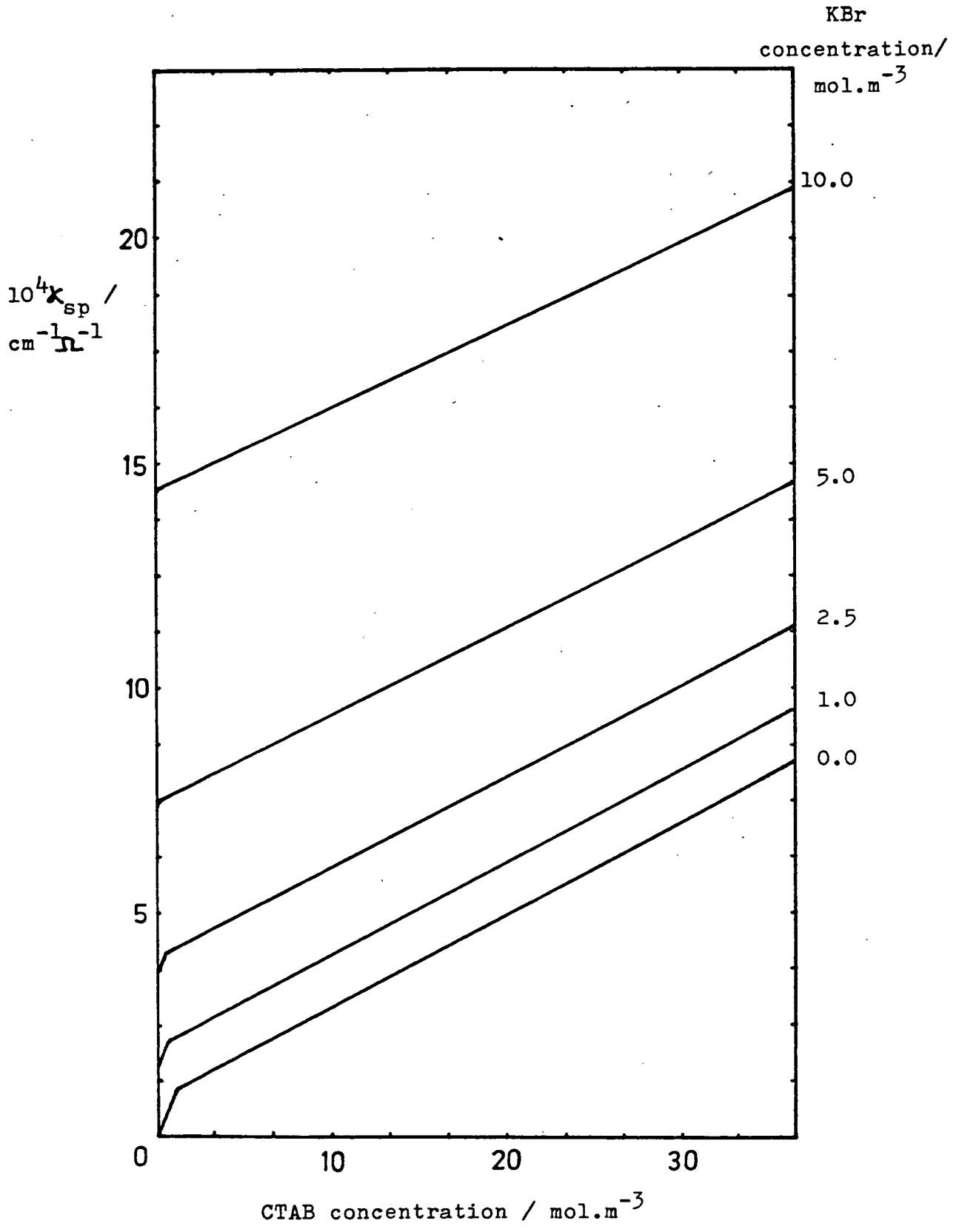

Figure 5.1.4 (B) Plots of specific conductivity against CTAB concentration in KBr solutions at 298.15K.

B) CTAB with added KBr solution

Added salt concentration/ mol m^{-3}	$d\kappa_{sp}/dc$ below c.m.c./ $cm^2\Omega^{-1}mol^{-1}$	$d\kappa_{sp}/dc$ above c.m.c./ $cm^2\Omega^{-1}mol^{-1}$	c.m.c./ mol m^{-3}
0	93.35	20.75	0.955
1	91.46	20.71	0.654
2.5	87.16	20.32	0.434
5	90.43	19.51	0.242
10	93.39	18.40	0.138

To a first approximation the conductances of the salt and surfactant are simply additive allowing for the reduction in c.m.c. as the salt concentration increases and the slopes above the c.m.c. do not vary significantly. Slight variations can be accounted for using Debye-Hückel theory which predicts a lower slope, $d\kappa_{sp}/dc$ for increasing salt content of the solution due to increased ion-ion interactions.

The variation of c.m.c. with salt concentration enables a plot of ln c.m.c. against ln I to be constructed as in figure 5.1.5 for SDS in NaCl solutions. Using the method described in section 2.1.2, α can be calculated and values thus obtained are given in table 5.1.4.

Table 5.1.4 Values of α calculated using the Mass Action Model (at 298.15 K)

Surfactant	Added salt	α
SDS	NaCl	0.314 $\pm$ 0.015
CTAB	KBr	0.172 $\pm$ 0.006

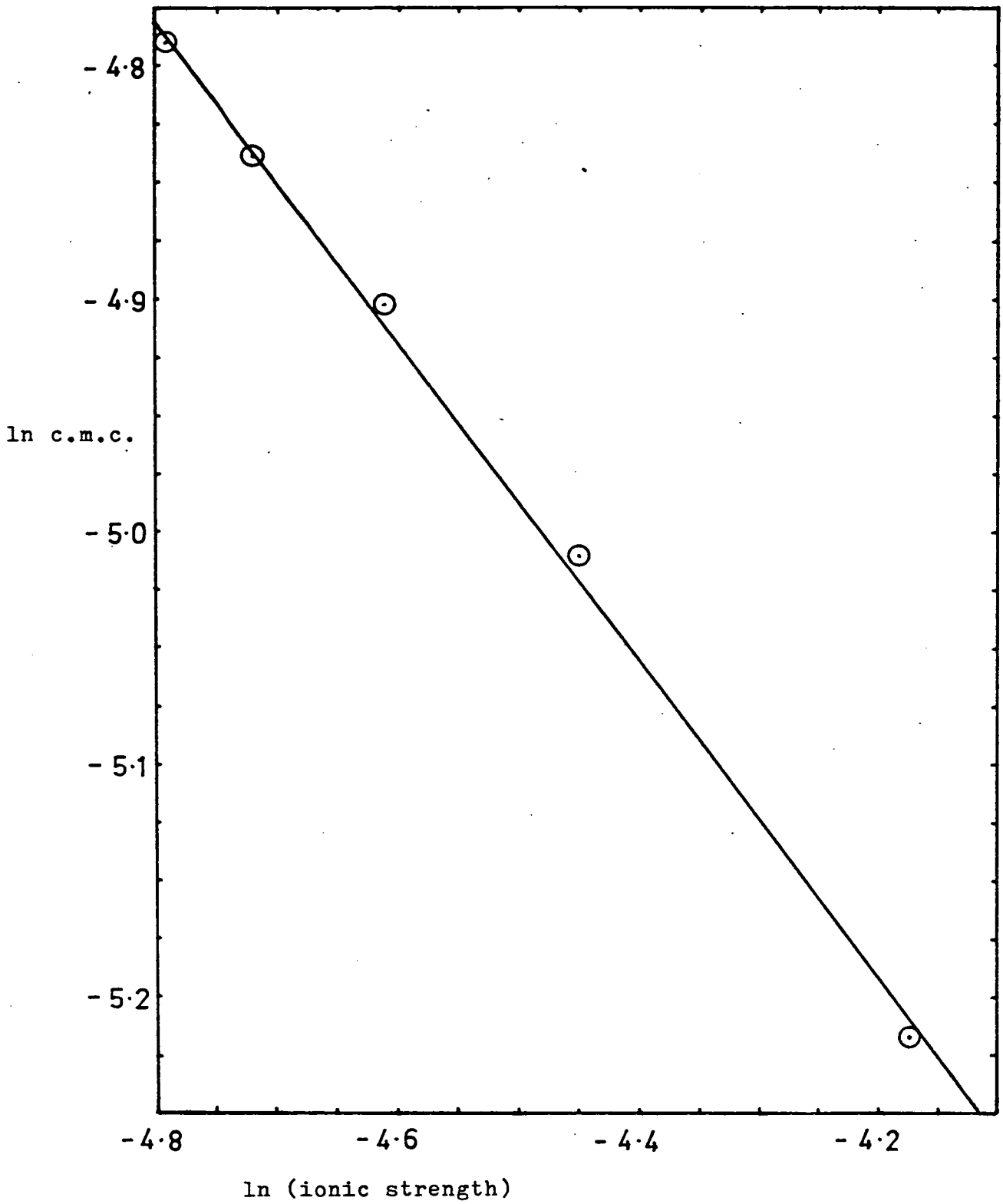

Figure 5.1.5 Plot of ln c.m.c. against ln (ionic strength) for SDS in NaCl solutions at 298.15K.

Variation of Temperature

In general the conductivity of an ionic solution rises by over 2% per degree so a change in temperature of 10 K produces considerable change in the specific conductance against concentration plot. For SDS, experiments were performed at three temperatures of 288, 298 and 308 K and results are shown in figure 5.1.6, table 5.1.5 and Appendix 1.

Table 5.1.5 The Conductivity of SDS solutions in water at 288.15, 298.15 and 308.15 K

Temperature/K	$d\kappa_{sp}/dc$ below c.m.c./$cm^2\Omega^{-1}mol^{-1}$	$d\kappa_{sp}/dc$ above c.m.c./$cm^2\Omega^{-1}mol^{-1}$	c.m.c./ mol m^{-3}
288.0	52.39	18.26	8.427
298.0	66.54	24.79	8.303
308.0	82.76	32.52	8.454

Two effects are noted. Firstly the change in temperature affects the slopes of the conductance plots below and above the c.m.c. as expected and secondly the c.m.c. changes. This effect of the change in c.m.c. with temperature has been observed and reported previously[119,120] for SDS and a minimum is obtained in the c.m.c. against temperature plot around 298 K (see figure 5.1.7). The same effect has been noted for other surfactants[121,122] in the range 288-313 K, and can be explained by considering the energy and entropy changes involved in micellisation. When micelles form the energy released must overcome electrostatic repulsion between head groups and balance

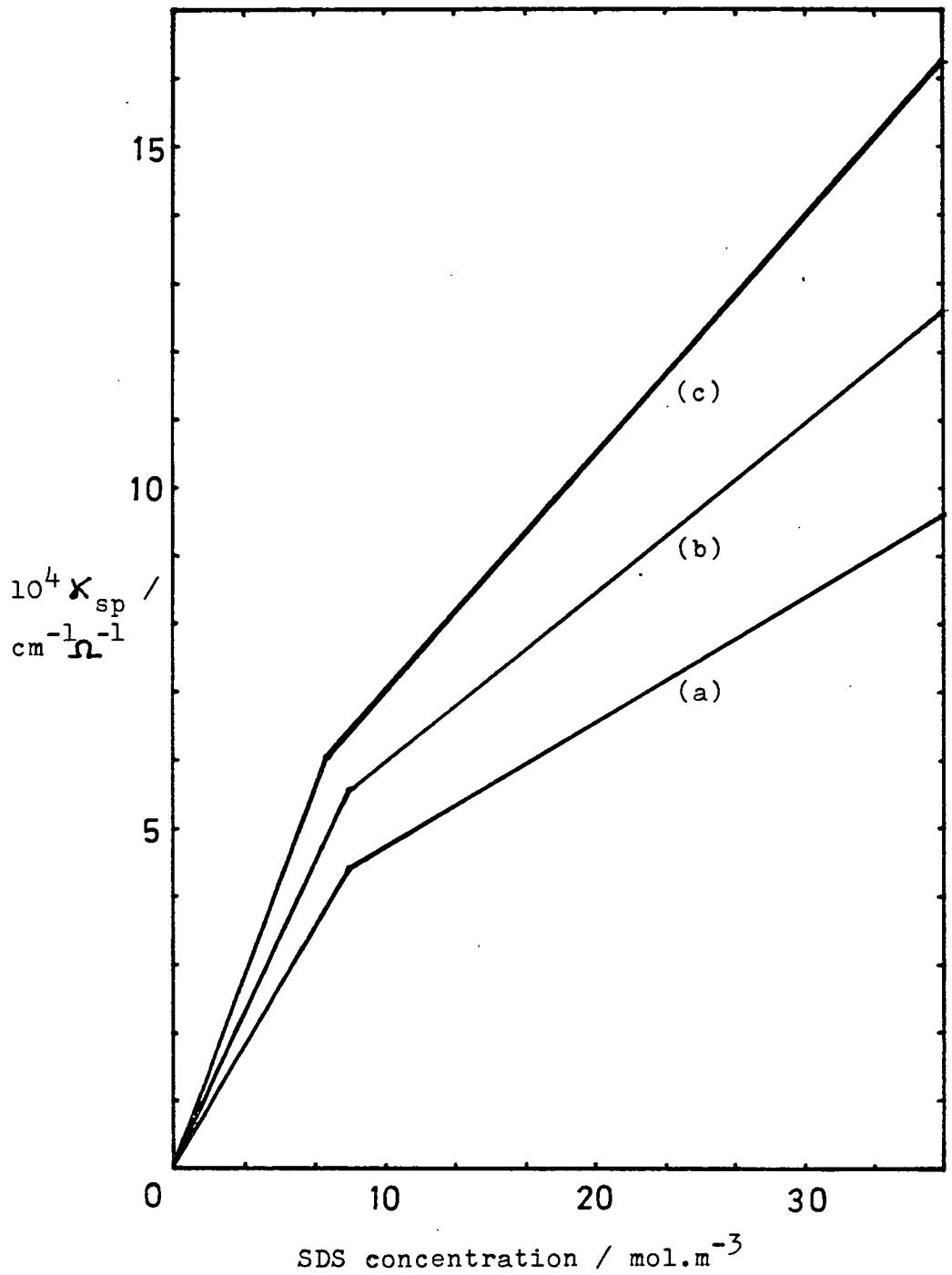

Figure 5.1.6 Plots of specific conductivity against SDS concentration at three temperatures; a) 288.15K
b) 298.15K
c) 308.15K

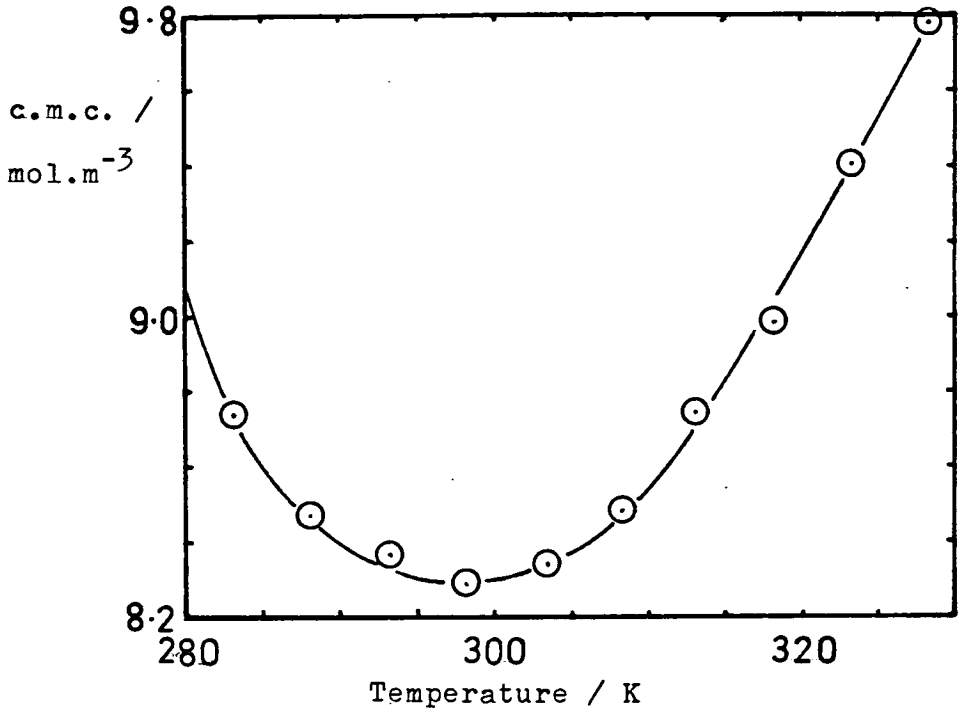

Figure 5.1.7 Plot of the c.m.c. of SDS as a function of temperature.

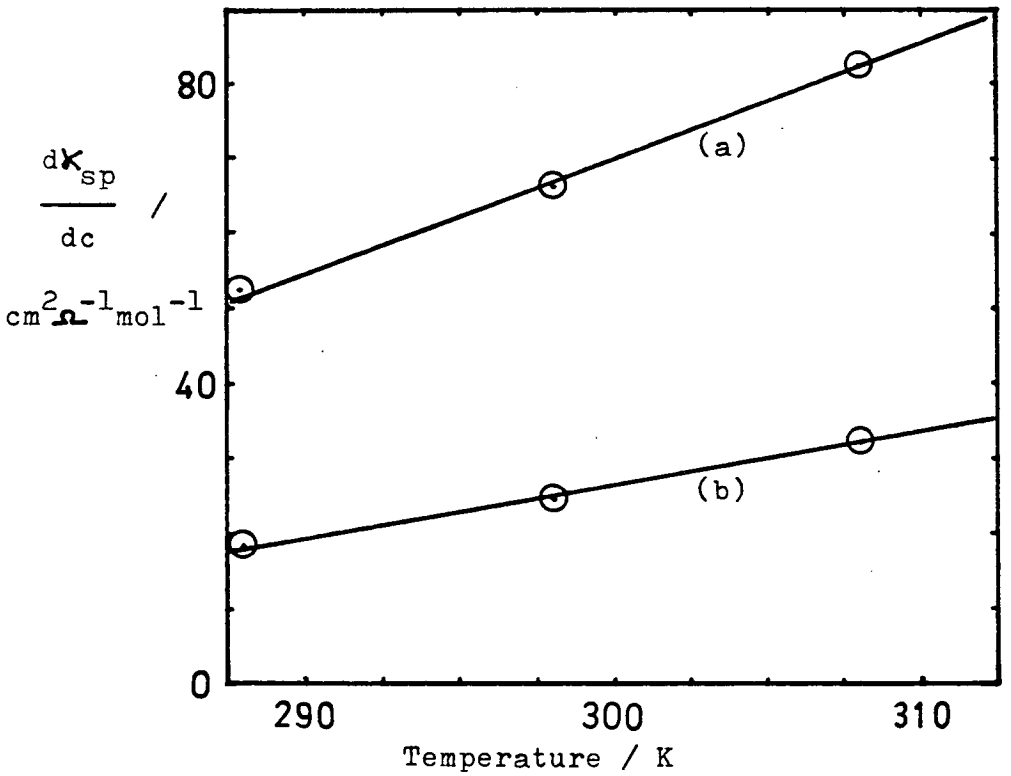

Figure 5.1.8 Plot of the slopes of the conductance curves of SDS in water as a function of temperature a) below c.m.c. b) above c.m.c.

the entropy decrease when the hydrocarbon chains aggregate. It is therefore expected that an increase in temperature would raise the c.m.c. since the free ions would have greater kinetic energy in the free state. However, the process is found to be dependent on changing entropy effects. At low temperatures the water in the immediate vicinity of the hydrocarbon chains has a very ordered structure (iceberg effect) and transfer of the hydrocarbon chain to the micelle interior produces a disordered water structure. Hence there is an entropy decrease rather than an increase on micellisation at low temperatures. As the temperature is raised the water structure breaks down and the entropy change on micellisation becomes negative as expected.

Further experiments at various added salt concentrations were performed to enable the calculation of α at each temperature by the method of section 2.1.2. Results are summarised in table 5.1.6.

Table 5.1.6 Calculated values of α for SDS/NaCl Solutions at 288.15, 298.15, and 308.15 K

Added salt concentration/ mol m^{-3}	c.m.c. (288.15 K)/ mol m^{-3}	c.m.c. (298.15 K)/ mol m^{-3}	c.m.c. (308.15 K)/ mol m^{-3}	Calculated α values
0	8.427	8.303	8.454	α 288.15 K =
1	8.037	7.919	8.134	0.308 $\pm$ 0.005
2.5	7.488	7.424	7.543	α 298.15 K =
5	6.729	6.665	6.804	0.314 $\pm$ 0.015
10	5.515	5.423	5.582	α 308.15 K =
				0.312 $\pm$ 0.014

Examination of the results reveals that within the limits of error of the determination of α, α is the same at each temperature and is equal to 0.311 $\pm$ 0.003. Since α appears constant over the temperature range studied and the mobilities of ions vary linearly with temperature then the slopes of the conductance plots below and above the c.m.c. should vary linearly with temperature.

Above the c.m.c. $$\left(\frac{d\kappa_{sp}}{dc}\right)_{T_1} = \alpha(\lambda_{ci,T_1} + \lambda_{mic,T_1}) \quad \ldots\ldots 5.1.5$$

and $$\left(\frac{d\kappa_{sp}}{dc}\right)_{T_2} = \alpha(\lambda_{ci,T_2} + \lambda_{mic,T_2}) \quad \ldots\ldots 5.1.6$$

$$\therefore \quad \Delta\left(\left(\frac{d\kappa_{sp}}{dc}\right)_{T_1} - \left(\frac{d\kappa_{sp}}{dc}\right)_{T_2}\right) = \alpha(\lambda_{ci,T_1} + \lambda_{mic,T_1} - \lambda_{ci,T_2} - \lambda_{mic,T_2}) \quad \ldots\ldots 5.1.7$$

Figure 5.1.8 illustrates the variation in slope of the conductance plot with temperature and the linearity of the plot confirms the constancy of α.

The data obtained above could be used in analysis of the thermodynamic properties of the micelle but since this is of little relevance in the present study this has not been pursued. The constancy of α must be explained therefore in qualitative terms considering the likely effects of change of temperature on micelle size

and electrostatic interactions. The small c.m.c. variation in the temperature range suggests little change in the micelles formed and indeed there is no reason to predict much change in electrostatic interactions or solvation of the ions present, hence α appears to be constant.

Variation of Counterion

If it were possible to take the same two surfactants but with different counterions, having different mobilities but binding to the micelles similarly, then α could be calculated from the conductances of each solution and their differences. The conductance of the surfactant with the first counterion above the c.m.c. is given by equation 5.1.8,

$$\kappa_{sp} = c_1(u_1 + u_2) + \alpha(c - c_1)(u_2 + u_{mic}) \quad \ldots\ldots 5.1.8$$

and that the surfactant with the second counterion is given by equation 5.1.9.

$$\kappa_{sp}' = c_1'(u_1 + u_2') + \alpha(c - c_1')(u_2' + u_{mic}') \quad \ldots\ldots 5.1.9$$

Also

$$\frac{d\kappa_{sp}}{dc} = \alpha(u_2 + u_{mic}) \quad \ldots\ldots 5.1.10$$

$$\frac{d\kappa_{sp}'}{dc} = \alpha(u_2' + u_{mic}') \quad \ldots\ldots 5.1.11$$

Assuming that the micellar mobility is the same in each case, which is reasonable if α is constant

$$u_{mic} = u_{mic}' \quad \ldots\ldots 5.1.12$$

Subtraction gives

$$\frac{d\kappa_{sp}}{dc} - \frac{d\kappa_{sp}'}{dc} = \alpha(u_2 - u_2') \quad \ldots\ldots 5.1.13$$

and

$$\alpha = \frac{\Delta\left(\frac{d\kappa_{sp}}{dc} - \frac{d\kappa_{sp}'}{dc}\right)}{u_2 - u_2'} \quad \ldots\ldots 5.1.14$$

The difficulty lies in finding two surfactants with counterions of sufficiently differing mobilities for the results to be meaningful and yet to be sure that the two counterions bind in the same manner to the micelles. The mobility of an ion depends on its charge and size and alteration of either is likely to change the mode and extent of binding.

The comparison of the conductance of SDS and LiDS is an example. Results are shown in figure 5.1.9, table 5.1.7 and Appendix 1.

Table 5.1.7 Conductances of SDS and LiDS at 298 K

Surfactant	$d\kappa_{sp}/dc$ below c.m.c./ $cm^2\Omega^{-1}mol^{-1}$	$d\kappa_{sp}/dc$ above c.m.c./ $cm^2\Omega^{-1}mol^{-1}$	c.m.c./ mol m^{-3}	λ_o counterion/ $cm^2\Omega^{-1}mol^{-1}$
SDS	66.54	24.79	8.303	50.10
LiDS	60.48	29.97	8.721	38.68

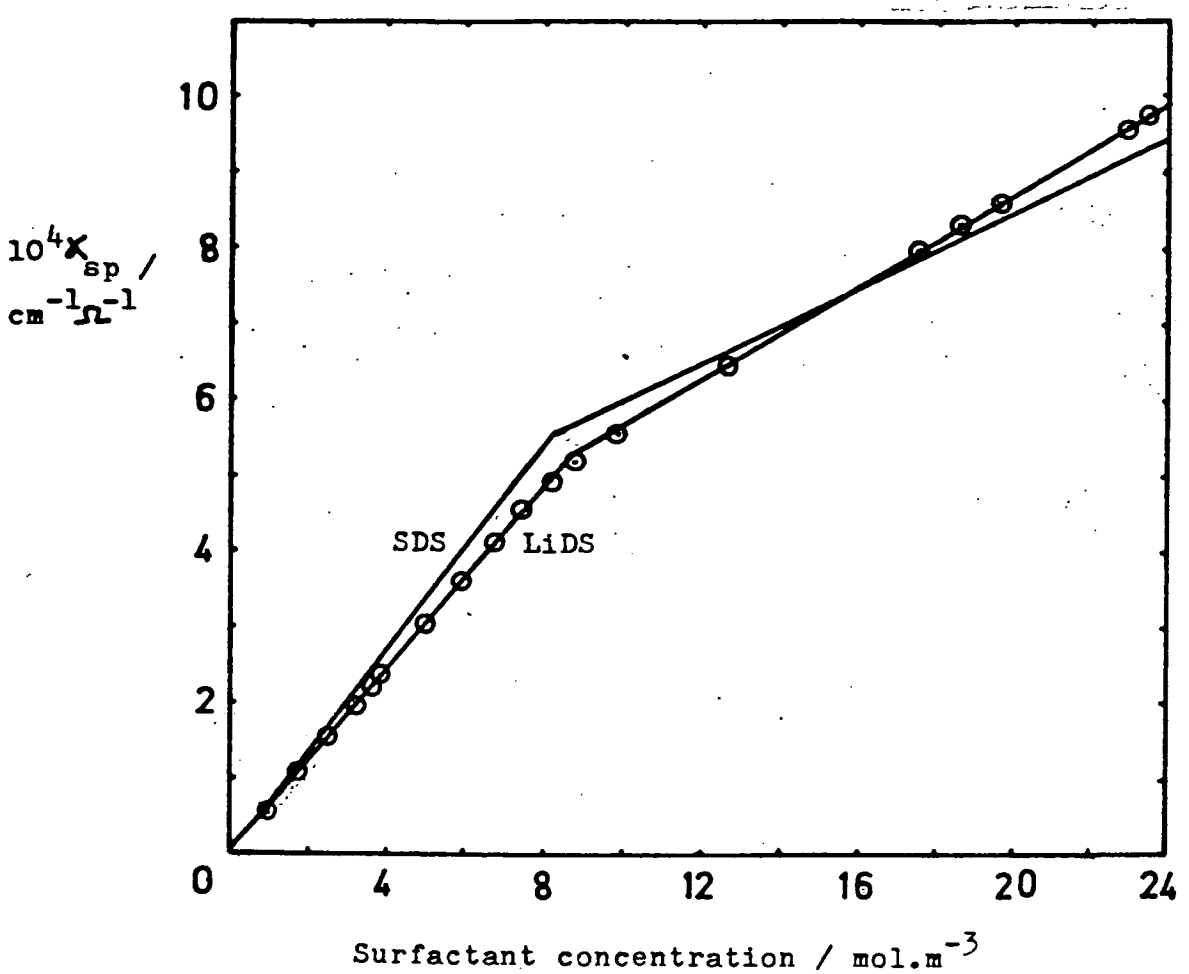

Figure 5.1.9 Plot of specific conductance against concentration of lithium dodecyl sulphate in water at 298.15K and that of SDS.

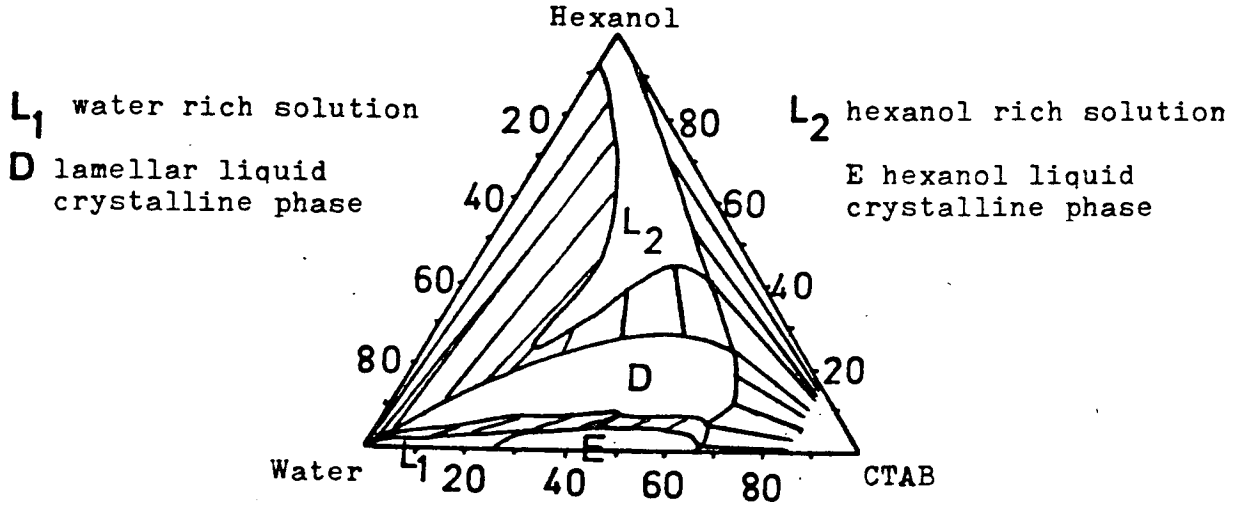

Figure 5.1.10 Phase diagram[128] for the system; CTAB-hexanol-water.

The molar conductivity of Li^+ is less than that of Na^+ so as predicted the slope of the LiDS curve below the c.m.c. is less than that of the SDS curve. However, above the c.m.c. the reverse is found and the LiDS solution is the more conducting one. Several conclusions can be made. Since the LiDS solution conducts better than predicted and the mobility of Li^+ must be nearly constant then either there must be more Li^+ free in solution than there are free Na^+ in the corresponding SDS solution, i.e. α has increased, or the micelles formed are more conducting due to a change in size or a change in α. The two effects are therefore inseparable and are rationalised by considering the ability of the Li^+ counterion to bind to DS^- micelles. In aqueous solution the counterions are hydrated and despite the larger ionic radius of Na^+ the hydrated radius of Li^+ is greater than that of Na^+. It is therefore more difficult to fit Li^+ ions around a DS^- micelle and α is higher. This suggests that geometric factors are important as well as electrostatic ones in counterion binding. A lyotropic series has been found[123,124] for a series of counterions binding to micelles formed from the same surfactant monomer. Binding increases in the order:

$$Cs^+ > K^+ > Na^+ > Li^+$$

$$\text{tetramethyl}^+ > \text{tetraethyl}^+ > \text{tetrapropyl}^+$$

and there is an obvious correlation between size of hydrated counterion and extent of counterion binding.

With regard to the variation of the counterion of hexadecyl trimethyl ammonium micelles substitution of the Br^- anion for Cl^- would be an obvious choice but it is well reported that CTAB and CTACl micelles adopt different shapes and hence have different properties in aqueous solution. Reiss-Husson and Luzzati[125] established that a transition from spherical to rodlike micelles occurs in the former but not the latter system. It was further discovered[126,127] that in solutions containing mixtures of CTAB and CTACl the two discrete micellar forms coexist and micelles with mixed counterions tend not to be formed.

5.1.1 (B) Mixed Micelles

Ionic Surfactant/Alcohol

The addition of alcohol to an ionic surfactant solution can produce one of several results depending on the nature of the alcohol and the location adopted in the solution. For short chain alcohols, methanol, ethanol, and propanol, the alcohol can remain in the aqueous phase and the conductance is affected mainly by the alteration of the permittivity, ε of the solvent. Larger alcohols are more hydrophobic and penetrate the micelle, their hydrocarbon tails being solubilised in the micelle interior and the alcohol, -OH, groups located somewhere near the micelle surface. For even larger, more water insoluble alcohols a separate phase

is formed containing alcohol, surfactant and water. An example of a phase diagram of such a system[128] is shown in figure 5.1.10. Not only is the position of the alcohol molecules uncertain but the amounts in each position may vary considerably as total composition varies. Thus when a solution of constant overall composition and concentration is diluted the partitioning of each component between the bulk and the micelles is constantly varying and different micelles are obtained.

SDS/Alcohol

The conductance plots of SDS/octanol systems of varying mole fraction are shown in figure 5.1.11 and certain specific trends can be identified. Below the c.m.c. the alcohol has no effect on the conductance of the SDS solution. As the alcohol content of the solution increases the c.m.c. decreases but becomes less distinct due to the curved nature of the plots in the region of the c.m.c. Similarly it is difficult to determine the slope of the conductance plots above the c.m.c. and the value depends on the concentration range chosen. The general trend can be noted that as the alcohol concentration increases the slope just above the c.m.c. increases indicating an increase in α but quantitative analysis is impossible without knowledge of the composition changes in the region.

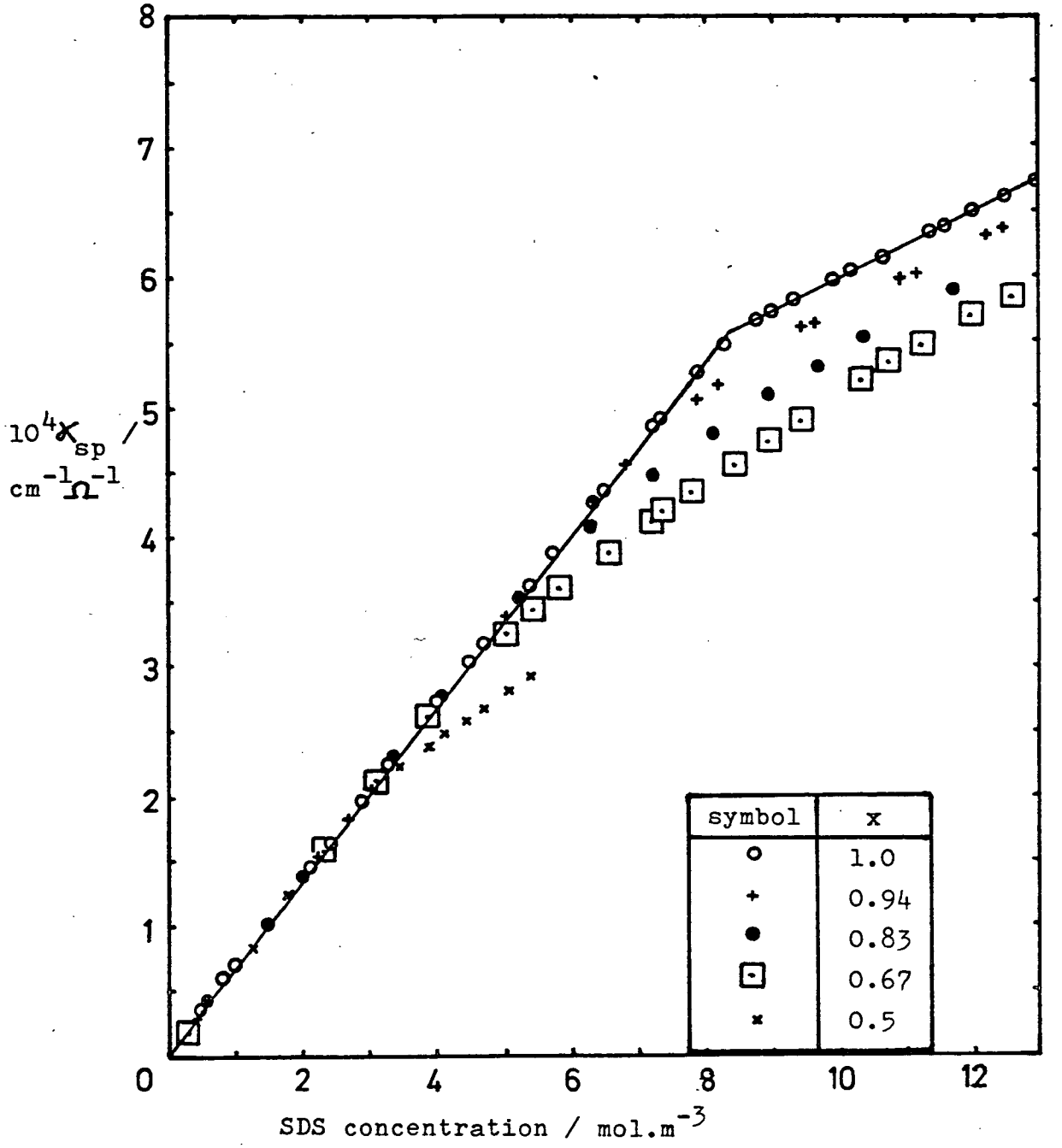

Figure 5.1.11 Plot of specific conductance against SDS concentration of SDS / octanol solutions in water at 298.15K.

CTAB/Alcohols

A range of straight chain alcohols from hexanol to dodecanol was added to CTAB solutions and results for various mole fractions were obtained. These are illustrated in figure 5.1.12. No change in conductance can be detected below the c.m.c. but above the c.m.c. a variety of curves is obtained. For low mole fraction, x with hexanol and octanol there is little change in conductance above the c.m.c. but dodecanol produces a reduction in specific conductance. For x = 0.5 the CTAB/hexanol plot is above that of pure CTAB indicating a significant increase in α, the CTAB/octanol plot is identical to that of pure CTAB, and the CTAB/dodecanol plot shows a dramatic decrease in specific conductance. This range of compositions and concentrations illustrates well the point that alcohols can have varying effects on surfactant solutions. The shorter chain alcohol penetrates the micelle and causes counterions to be released, increasing the conductance. The CTAB/dodecanol solution begins to look opaque at low concentrations and phase separation occurs, leaving the aqueous phase depleted of ionic surfactant and counterions and causing the conductance to decrease. Octanol is a borderline case.

A detailed study of surfactant/alcohol systems was considered too complex as a study of charged micelles due to the difficulty in precise determination of c.m.c.'s, composition, and the wide range of surfactant-alcohol interactions.

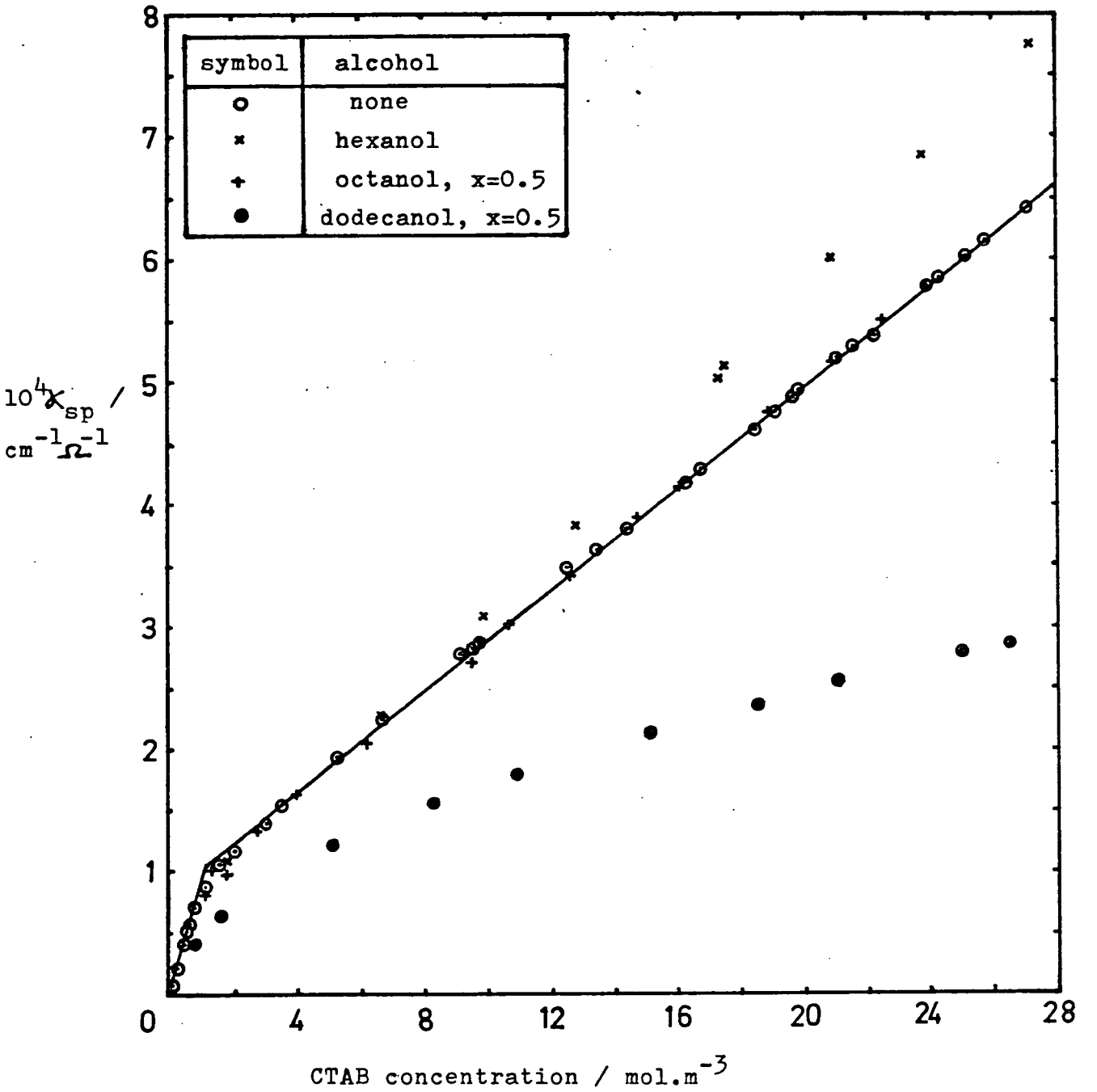

Figure 5.1.12 Plots of specific conductance against CTAB concentration of CTAB / alcohol solutions in water at 298.15K.

Cationic/Nonionic and Anionic/Nonionic Micelles

Two systems were chosen

1) SDS/C_8E_4

This system was chosen for several reasons. Pure SDS is readily available and there is good literature coverage of its properties. C_8E_4 has also been investigated not only in the pure state but also in mixed systems. The main reason, however, for this combination was the similarity of the c.m.c.'s which are given in table 5.1.8

Table 5.1.8 C.m.c.'s of Surfactants used in Mixed Systems at 298 K

Surfactant	c.m.c./mol m^{-3}	reference
SDS	8.30	Present study κ_{sp} against c
C_8E_4	8.0	65
CTAB	0.90	Present study γ against lnc
$C_{12}E_6$	0.071	manufacturer's estimate

It was hoped that since the c.m.c.'s were very close, forces operating would produce mixed micelles of approximately constant composition for a given mole fraction, well above the c.m.c. Figure 5.1.13(A) illustrates the variation of c.m.c. as determined from the specific conductance plots with mole fraction.

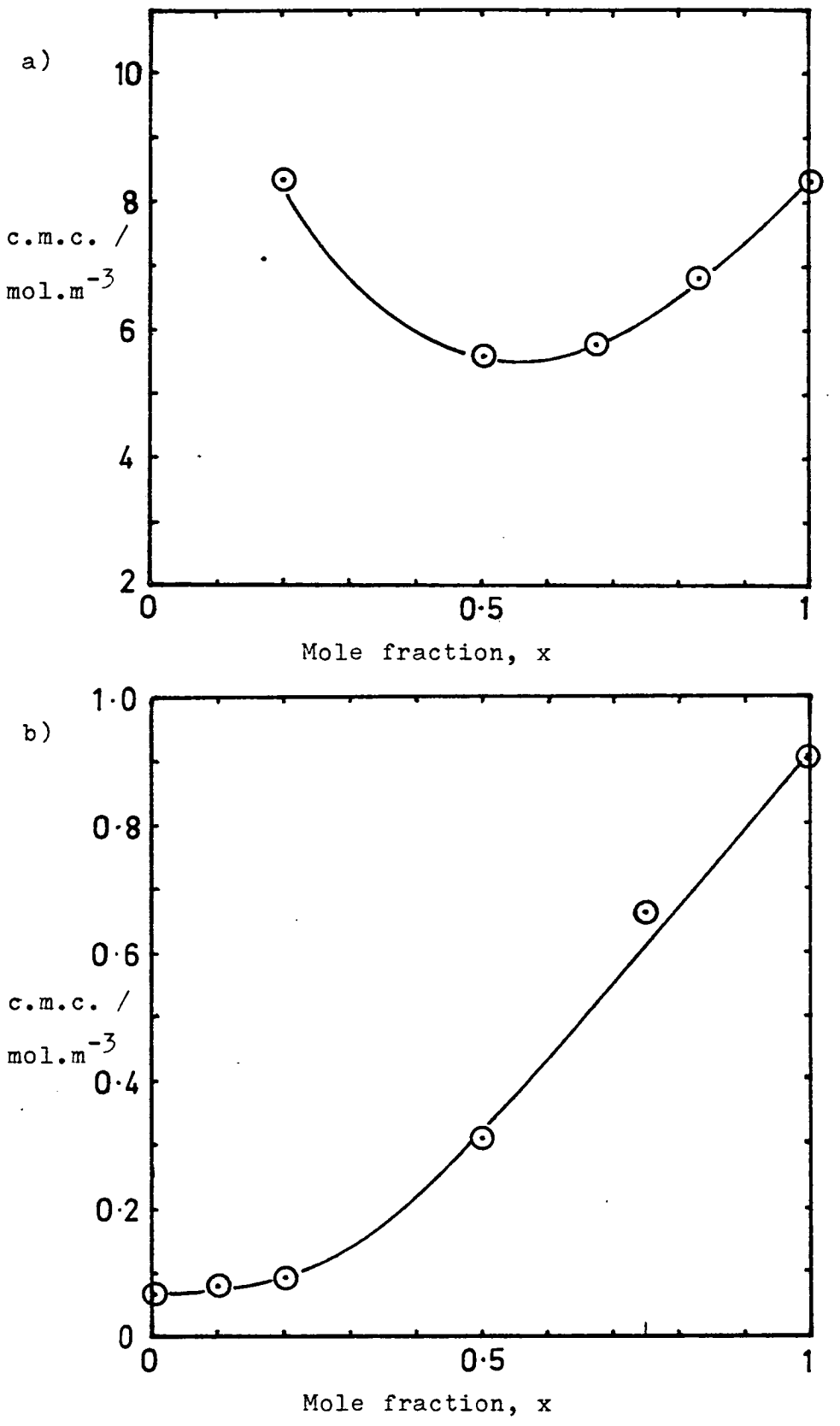

Figure 5.1.13 Plot of c.m.c. against mole fraction of ionic component of the systems a) SDS / C_8E_4

b) CTAB / $C_{12}E_6$

The conductance plots are shown in figure 5.1.14 and data in table 5.1.9 and appendix 1.

Table 5.1.9 Slopes of the Conductance Plots of Mixed Ionic/Nonionic Systems at 298.15 K

A) SDS/C_8E_4

x	$d\kappa_{sp}/dc$ above c.m.c/ $cm^2\Omega^{-1}mol^{-1}$
1.0	24.79
0.833	30.89
0.667	37.64
0.50	44.60
0.25	49.83

B) CTAB/$C_{12}E_6$

x	$d\kappa_{sp}/dc$ above c.m.c/ $cm^2\Omega^{-1}mol^{-1}$
1.0	20.75
0.833	26.91
0.75	29.61
0.50	39.06
0.20	52.60
0.10	61.60

2) CTAB/$C_{12}E_6$

This pair of surfactants was chosen for the very low c.m.c. of $C_{12}E_6$ and relatively low c.m.c. of CTAB, (see table 5.1.8). The c.m.c.'s of the mixtures are also very low so in the concentration range studied, i.e. up to 30 mol m^{-3}, the micelle composition is very nearly equal to the bulk composition.

The c.m.c.'s of the mixed systems at 298 K were determined by the surface tension method due to the insensitivity of the conductance technique at very low ionic concentrations of the order of the c.m.c. of the mixed system. These are presented in table 5.1.10 and the variation of c.m.c. with x is shown in figure 5.1.13(B).

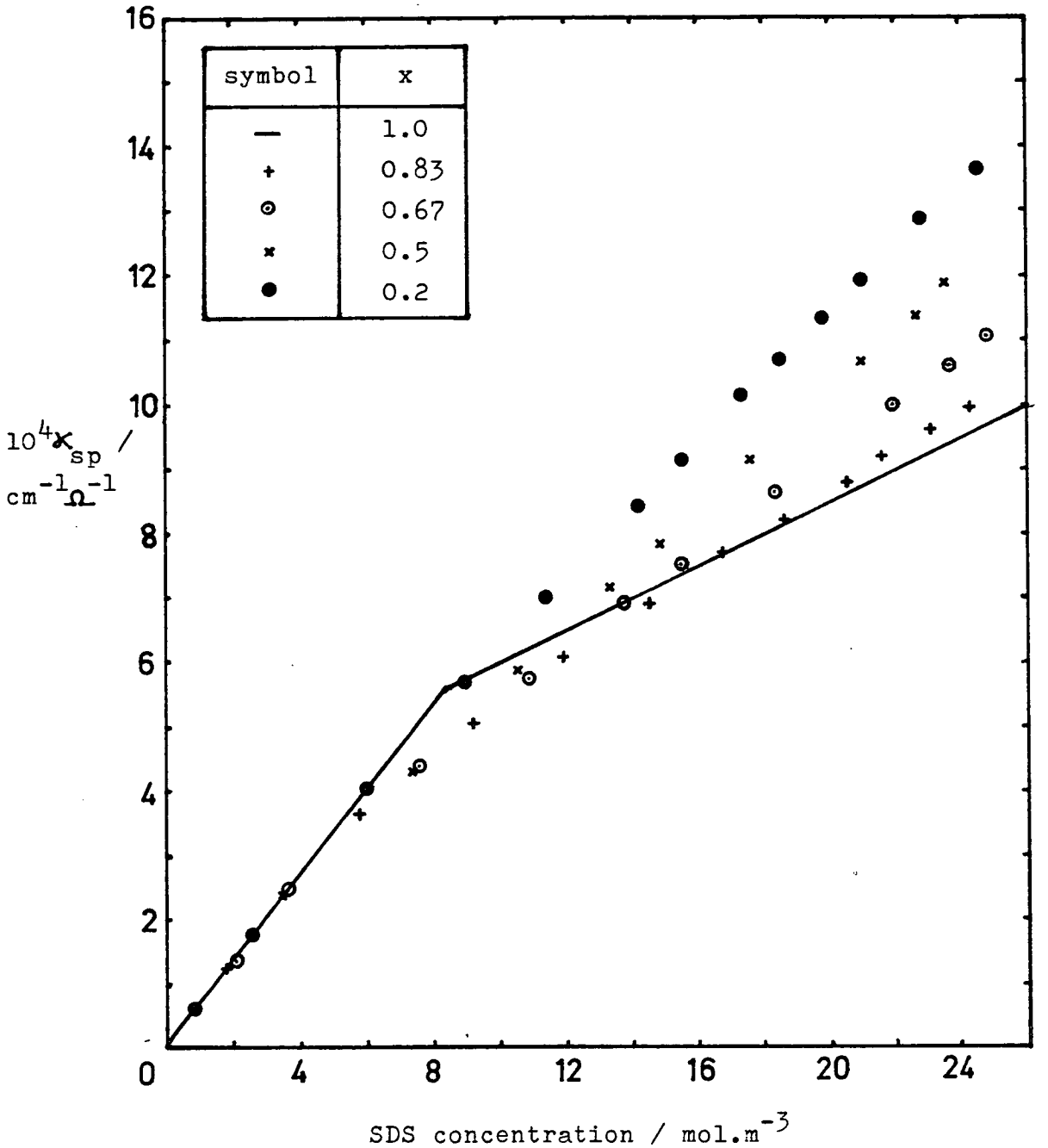

Figure 5.1.14 Plot of specific conductance against SDS concentration of SDS / C_8E_4 solutions in water at 298.15K.

Table 5.1.10 C.m.c.'s of CTAB/$C_{12}E_6$ Mixtures at 298 K as a function of x

x	c.m.c./ mol m^{-3}	reference
1.0	0.90	
0.75	0.66	Present study
0.50	0.31	(γ against lnc)
0.20	0.092	
0.10	0.081	
0.0	0.071	Manufacturer's estimate

Both systems have the same qualitative conductance behaviour. Below the c.m.c. the presence of the nonionic surfactant has no effect on the conductance but above the c.m.c., for increasing nonionic content of micelles, the slope of the conductance plot, and hence α, increases. A linear relationship between slope of the conductance plot above the c.m.c. and mole fraction is obtained from the data in table 5.1.9 and is illustrated in figure 5.1.15.

For SDS/C_8E_4 $d\kappa_{sp}/dc = -39.72x + 64.27$ 5.1.15

and for CTAB/$C_{12}E_6$ $d\kappa_{sp}/dc = -39.66x + 59.83$ ... 5.1.16

The linearity of the plots suggests a regularity in the variation of micelle properties with varying nonionic content. The equality of the slopes is probably coincidence as the interaction in the two different systems are most likely not to be comparable. In the SDS/C_8E_4 case the slope of the specific conductance plot increases with decreasing x and approaches the value of the slope of the plot below the

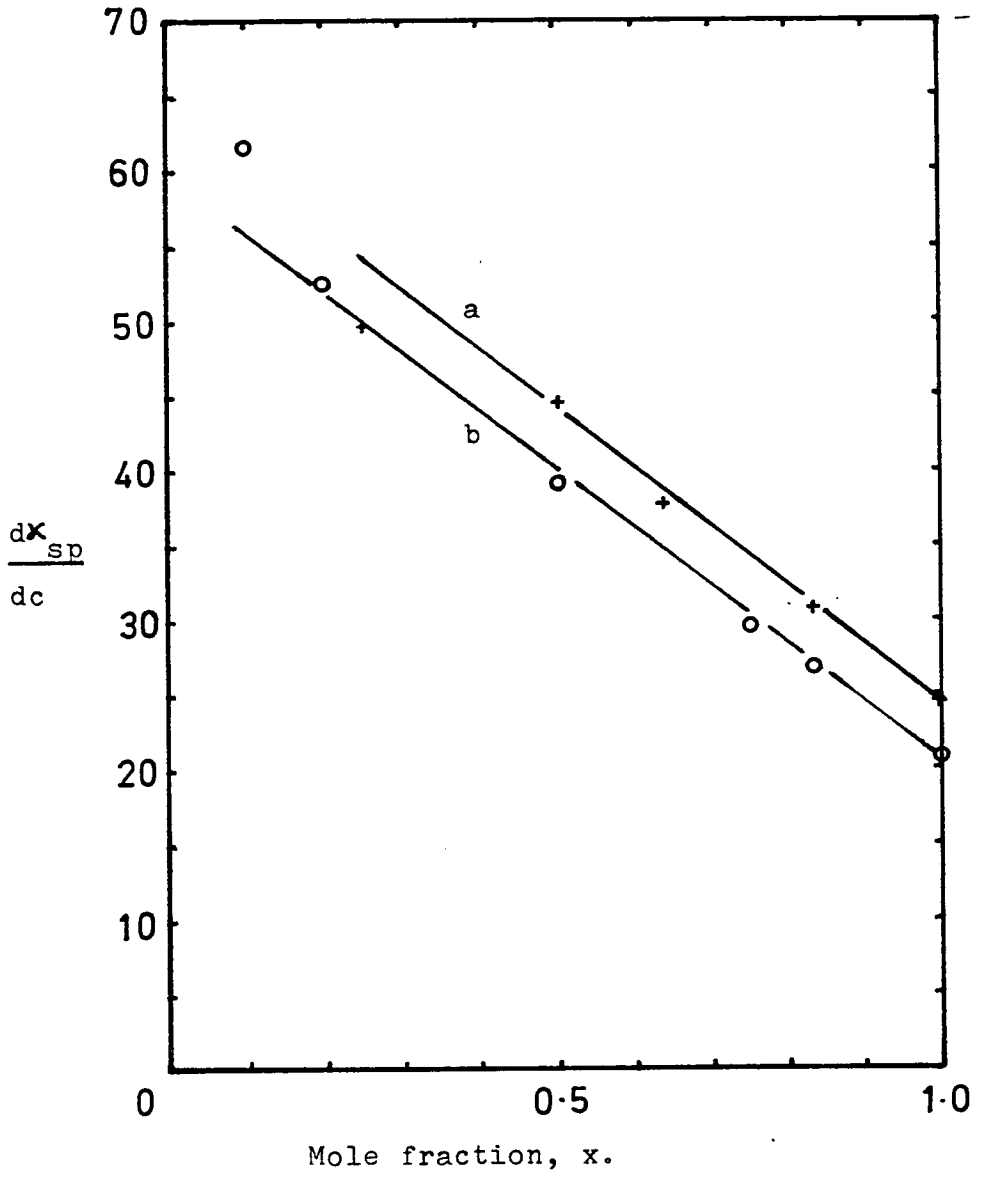

Figure 5.1.15 Plot of the slope of specific conductance against concentration curves above the c.m.c. against mole fraction of ionic component, x, for a) SDS / C_8E_4 b) CTAB / $C_{12}E_6$.

c.m.c. as x tends to zero. This corresponds to a situation in which α equals unity, i.e. all counterions are free in solution to conduct as in a simple electrolyte solution. In the CTAB/$C_{12}E_6$ case however, the slope below the c.m.c. is never approached even for very low x.

5.1.2 Photon Correlation Spectroscopy - Diffusion Coefficients

The diffusion coefficients of pure CTAB, pure $C_{12}E_6$ and mixed CTAB/$C_{12}E_6$ micelles in KBr solutions at 298 K were determined by photon correlation spectroscopy as described in section 4.4. A plot of diffusion coefficient, D against KBr concentration is shown in figure 5.1.16 and the corresponding data is given in table 5.1.11 and appendix 4. The apparent diffusion coefficients obtained at low ionic strength for micelles containing ionic surfactant are high, drop quite rapidly with increasing ionic strength and the plot levels off at high ionic strength. For low micellar concentrations, interactions between micelles are minimal because their charges are screened by counterions but long range Coulomb forces influence the diffusion rates of all ionic species present. These forces operate when the rapidly fluctuating concentration of counterions produces nonspherical charge

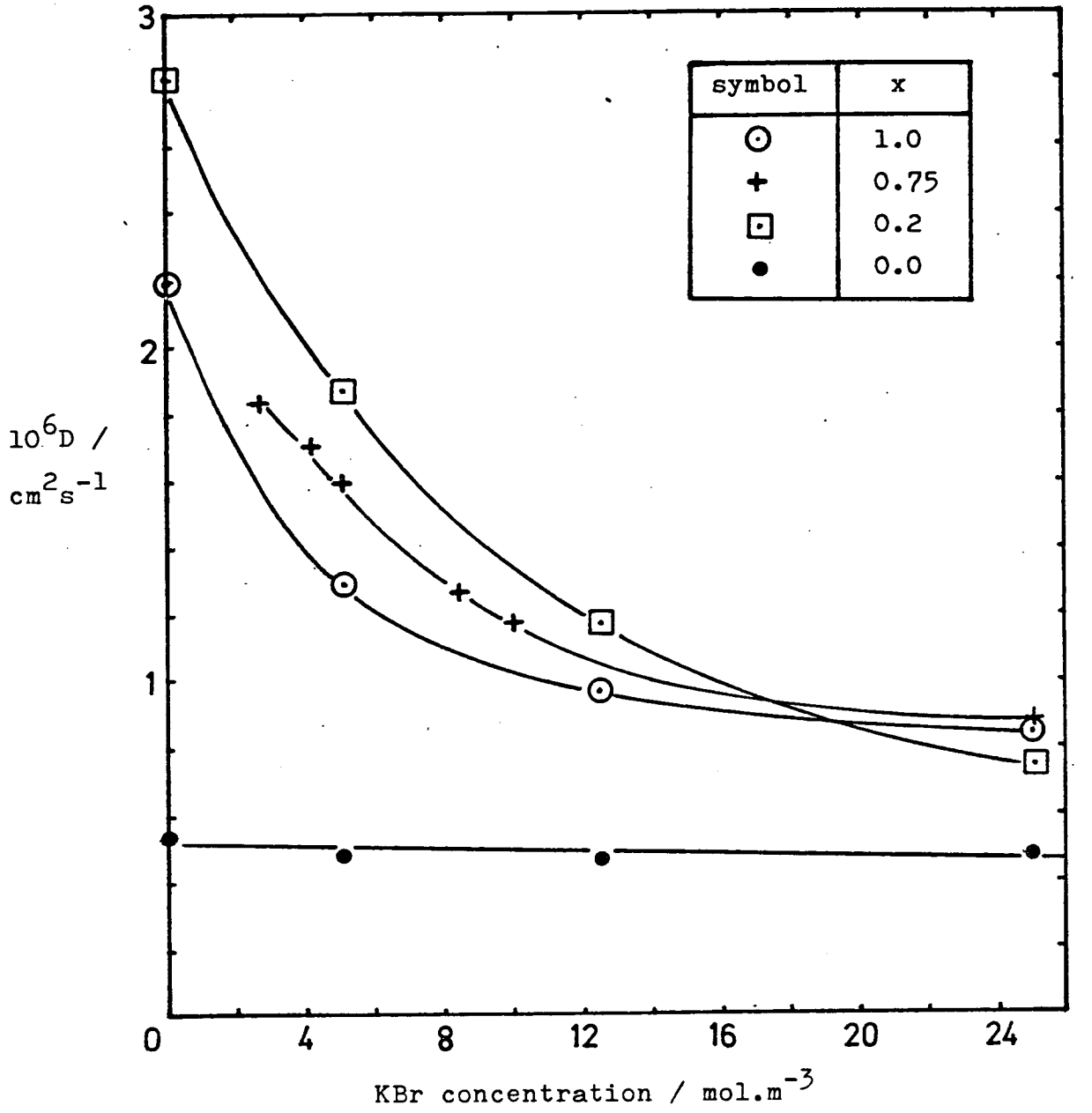

Figure 5.1.16 Plots of diffusion coefficient, D as a function of KBr concentration, of CTAB / $C_{12}E_6$ solutions in water at 298.15K.

Table 5.1.11 Diffusion Coefficients of CTAB/$C_{12}E_6$ micelles in KBr solutions at 298 K

x	Total surfactant concentration/ mol m^{-3}	KBr concentration mol m^{-3}	10^6 D/cm^2s^{-1}	10^6 error in D/cm^2s^{-1}
1.0	10.0	0.0	2.2	0.3
	10.0	5.0	1.30	0.07
	10.0	12.5	0.985	0.033
	10.0	25.0	0.851	0.018
0.75	13.33	2.67	1.84	0.35
	13.33	4.17	1.7	0.2
	13.33	5.00	1.6	0.05
	13.33	8.33	1.26	0.10
	13.33	10.00	1.18	0.05
	13.33	25.00	0.877	0.015
0.2	50.0	0.0	2.8	0.3
	50.0	5.0	1.86	0.09
	50.0	12.5	1.17	0.02
	50.0	25.0	0.734	0.014
0.0	10.0	0.0	0.540	0.002
	10.0	5.0	0.480	0.003
	10.0	12.5	0.463	0.004
	10.0	25.0	0.471	0.007

distributions around the micelles. The result is that at low ionic strength the micellar motion is accelerated while that of the counterions is retarded. At higher ionic strengths this effect is reduced until above a certain salt concentration, for example approximately 25 mol m^{-3} KBr for CTAB solutions, the effect is eliminated.

It is to be noted that the diffusion coefficient against KBr concentration plot for the pure nonionic surfactant shows no dependence on ionic strength and this is to be expected as the micelle carries no charge and hence charge effects are absent.

Stephen[129] obtained the expression shown in equation 5.1.17 for the diffusion coefficient of the micelle as a function of salt concentration by solving the Fokker-Planck equations for the motion of large ions in the presence of small coions and counterions in conjunction with the Poisson equation.

$$D = D_1\left(1 + \frac{q_1^2}{p^2 + \sum_{i=2}^{n} q_i^2}\right) \qquad \ldots\ldots 5.1.17$$

D_1 is the diffusion coefficient in the absence of electrostatic interactions, that is at high ionic strength and D is the experimentally determined diffusion coefficient. q_i is defined in equation 5.1.18 and p is the scattering vector.

$$q_i^2 = \frac{4\pi}{\varepsilon kT} z_i^2 c_i \qquad \ldots\ldots 5.1.18$$

Equation 5.1.17 illustrates that the measured diffusion coefficient increases with decreasing ionic strength.

Rohde and Sackmann[130] have devised a method of obtained α from the diffusion coefficients measured as a function of salt concentration using the formula of equation 5.1.19 derived from equation 5.1.17.

$$D = D_1\left(1 + \frac{n\alpha^2}{\dfrac{2\ c.m.c. + 2c_{salt}}{c - c.m.c.} + \alpha}\right) \qquad \ldots\ldots 5.1.19$$

Values of α obtained by this method are much lower than values obtained using many other techniques. Rohde and Sackmann calculated that for SDS α = 0.19 at zero added salt concentration, falling to α = 0.06 at 100 mol m^{-3} NaCl concentration compared to the average literature value of around 0.3 (see chapter 2).

Application of equation 5.1.19 to the results for CTAB in table 5.1.11 with n = 180 and D_1 = 0.75 x 10^{-6} $cm^2 s^{-1}$ produces the values of α shown in table 5.1.12

Table 5.1.12 Values of α calculated using equation 5.1.19 for CTAB in KBr solutions at 298 K

Added salt concentration/ mol m^{-3}	α
0	0.052
5	0.068
12.5	0.068
25	0.062

Again, these results are much lower than those obtained using other techniques and this casts serious doubts on the validity of the method. The discrepancies undoubtedly arise from the use of Stephen's theory which was developed with the assumptions of low macromolecular charge and mobility and which probably does not adequately account for coulombic interactions in micellar systems in which the diffusing micelles have a realtively high charge and mobility.

Another empirical method of Pusey[131] can be used to rationalise the variation of diffusion coefficient with salt concentration. He postulates two types of measurable radii, an effective hard sphere radius R_{eff}, and the true hydrodynamic radius R_H, which may differ considerably from R_{eff} depending on the bulk solution composition. A variable x and function h(x) are defined

$$x = \frac{R_{eff}}{R_H} - 1 \qquad \ldots\ldots 5.1.20$$

$$h(x) = 1/2 + 2(1 + x)^2(1 + 4x) - 15/8(1 + x)^{-1} \qquad \ldots\ldots 5.1.21$$

D is expressed in terms of the diffusion coefficient in the absence of electrostatic interactions D_1, h(x), and the volume fraction of micelles, ϕ.

$$D = D_1(1 + h(x)\phi + \ldots\ldots) \qquad \ldots\ldots 5.1.22$$

It is expected that the difference $\Delta R = (R_{eff} - R_H)$ will be related to the double layer thickness $1/\kappa$. An attempt was made to correlated ΔR with $1/\kappa$ by taking the values of α calculated from conductivity and mobility data (see section 5.2.1(c)) and calculating the various parameters in the theory. Examples of two such calculations for CTAB/$C_{12}E_6$ are shown in table 5.1.13 for mole fractions $x = 1$ and $x = 0.2$.

Table 5.1.13 Examples of use of equations 5.1.20 to 5.1.22 (Pusey's Method) for CTAB/$C_{12}E_6$

A) CTAB; 10 mol m^{-3} in KBr solutions: $C_1 = 0.75 \times 10^{-6} cm^2 s^{-1}$ $\alpha = 0.167$

Added salt concentration/ mol m^{-3}	$10^6 D/cm^2 s^{-1}$	$10^3 \phi$	x	R_{eff}/Å	$1/\kappa$/Å	R_H/Å	$R_{eff}-R_H$/ Å
0	2.2	3.96	3.205	132.0	61.9	31.4	100.6
5	1.30	4.24	2.055	95.9	36.6	31.4	64.5
12.5	0.985	4.30	1.383	74.8	25.4	31.4	43.4
25	0.851	4.35	0.880	59.0	18.6	31.4	27.6

B) CTAB/$C_{12}E_6$; CTAB concentration = 10 mol m^{-3} in KBr solutions, $x = 0.2$, $D_1 = 0.7 \times 10^{-6}$ cm^2 s^{-1}, $\alpha = 0.519$

Added salt concentration/ mol m^{-3}	$10^6 D/cm^2 s^{-1}$	$10^3 \phi$	x	R_{eff}/Å	$1/\kappa$/Å	R_H/Å	$R_{eff}-R_H$/ Å
0	2.8	21.8	1.855	89.7	42.0	31.4	58.3
5	1.86	21.8	1.408	75.6	30.1	31.4	44.2
12.5	1.17	21.8	0.88	59.0	22.8	31.4	27.6
25	0.734	21.8	0.10	34.5	17.5	31.4	3.1

In each case there is qualitative agreement between the trends in $R_{eff} - R_H$ and $1/\kappa$ as the ionic strength varies but no quantitative agreement can be found. Pusey has performed such calculations for the spherical virus R17 which has a radius of 140 Å and in 15 mol m^{-3} NaCl solution he calculated a value of R_{eff} which was 70 Å greater than the true sphere radius. $1/\kappa$ for this system is 25 Å and Pusey comments that these figures are of the same order and appears to be content with this degree of agreement considering the empirical nature of the method. On this basis the results of the calculations for CTAB/ $C_{12}E_6$ in table 5.1.13 do not seem to give unreasonable figures. It must be noted that a relatively small change in α and hence in the ionic strength, since $I = \alpha(c\text{-}c.m.c.) + c.m.c.$, produces a significant change in $1/\kappa$. For example a reduction in α from 0.167 to 0.10 increases $1/\kappa$ from 61.9 Å to 71.4 Å. Also the value of R_{eff} calculated for each salt concentration depends heavily on the value of D_1 and perhaps it would be advantageous to obtain data at even higher KBr concentrations to ensure that D does not decrease further in this range.

There are two more effects which must be considered concerning the addition of salt to surfactant solutions. Firstly the c.m.c. of the surfactant solution is lowered (see section 1.2.1) and this must be taken into account when calculating the micellar concentration and ionic strength. The second effect is that the size of the

micelle may be seriously affected as ionic micelles are known to grow larger with increasing salt concentration.[132,133] This happens because the extra counterions can shield the charge on the ionic head groups to a greater extent, thereby reducing the repulsions between head groups and allowing more monomers into a micelle. This size change has been noted for both SDS and CTAB and some examples are given in table 5.1.14.

Table 5.1.14 The Effect of Increasing Ionic Strength on the Size of SDS and CTAB Micelles

A) SDS/NaCl solutions

NaCl concentration/ mol dm^{-3}	n	r/Å	reference
0.00	62		50
0.03	72		
0.20	101		
0.50	142		
0.15	~ 60	25.3	132
0.30	~ 80	29.8	
0.45	~200	43.1	
0.55	~600	88.5	
0.60		120.8	

B) CTAB/NABr solutions

NaBr concentration/ mol dm^{-3}	n	r/Å	reference
0.00	99	21.8	133
0.0031	120	24.3	
0.0062	150	27.3	
0.0125	165	28.3	
0.025	181	29.9	
0.050	182	30.1	
0.075	180	30.1	
0.100	221	33.3	

The data for CTAB micelles suggests that the aggregation number doubles when the ionic strength is increased from zero to 25 mol m^{-3} and the radius increases by 40%. The effect on SDS micelles is much less at moderate ionic strengths.

Therefore, although it is necessary in order to reduce electrostatic interactions in the micellar solution to work at moderate or high ionic strength, it must be remembered that the system under study may well be so perturbed by the addition of salt that the data obtained refer to a different system from the one intended for study. For the remaining experiments, moderate ionic strengths were employed, namely 25 mol m^{-3} KBr for CTAB/$C_{12}E_6$ systems and 100 mol m^{-3} NaCl for SDS/C_8E_4 systems. The results of these studies are presented in table 5.1.15 and figure 5.1.17.

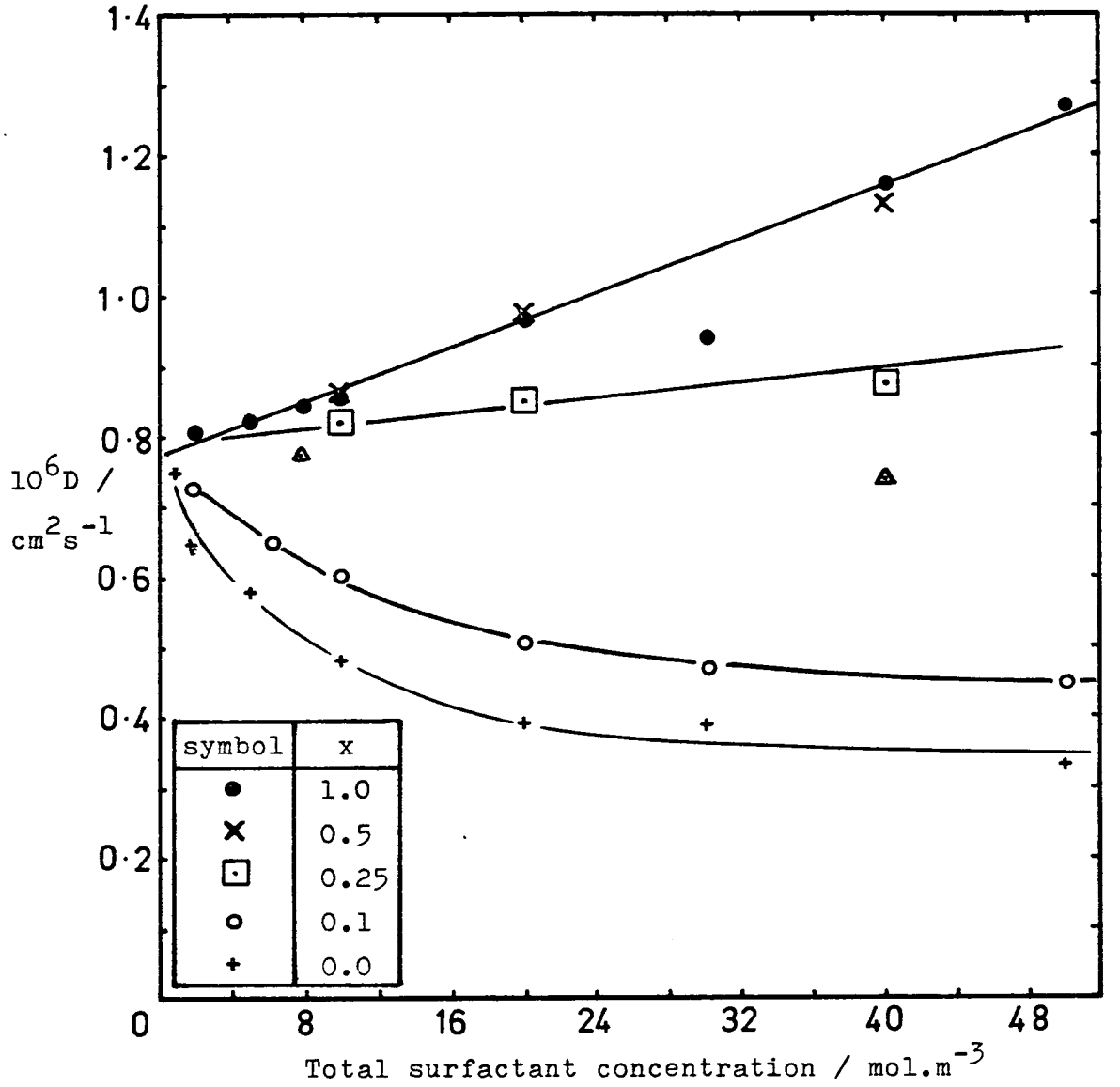

Figure 5.1.17 (A) Plots of diffusion coefficient against total surfactant concentration for CTAB / $C_{12}E_6$ and $C_{12}E_8$ ▲ in 25.0 $mol.m^{-3}$ KBr solution at 298.15K.

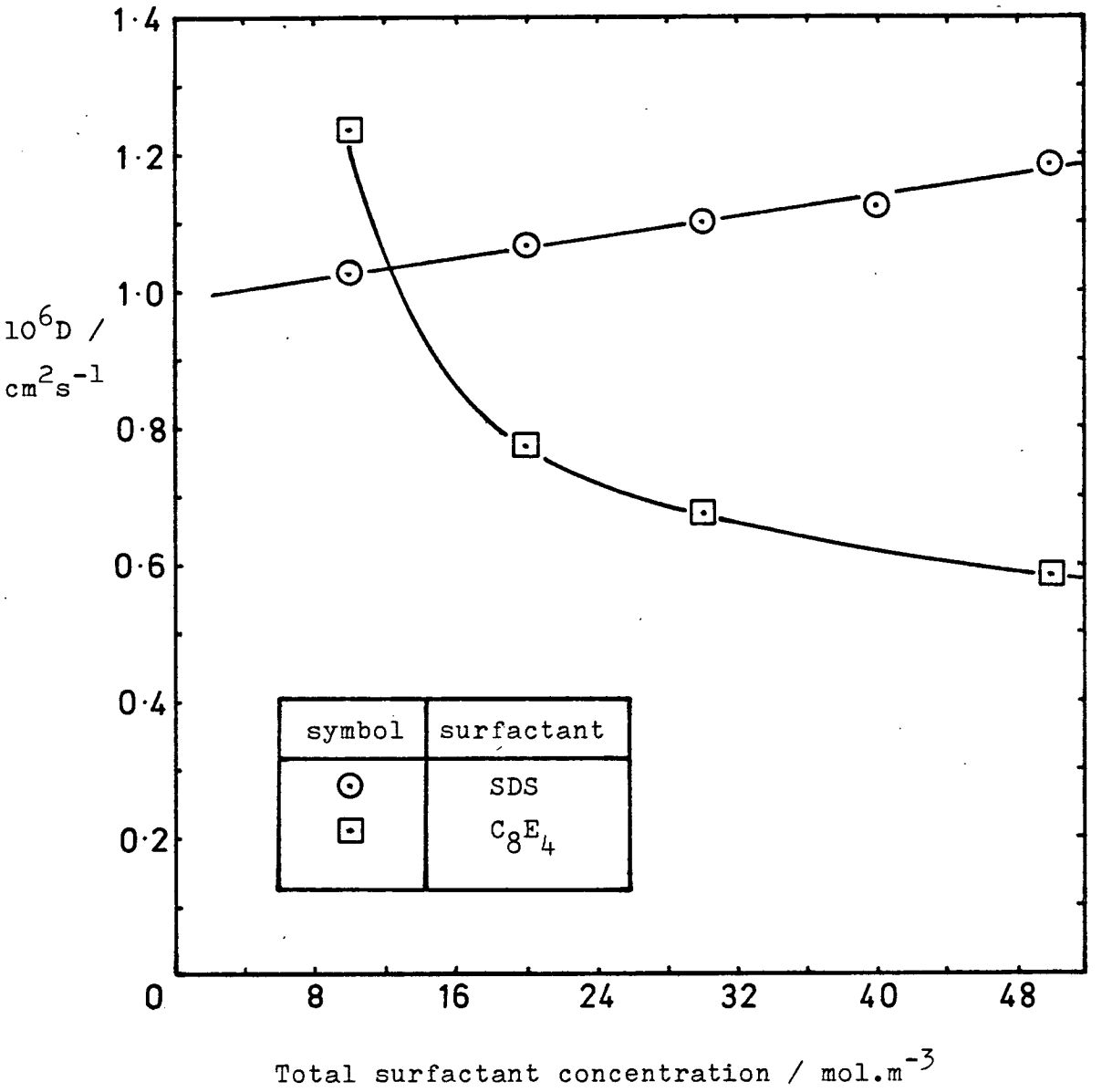

Figure 5.1.17 (B) Plots of diffusion coefficient against total surfactant concentration for SDS and C_8E_4 in 100.0 $mol.m^{-3}$ NaCl solution at 298.15K.

Table 5.1.15 Diffusion Coefficients of Pure and Mixed Systems at 298 K

A) CTAB/$C_{12}E_6$ in 25 mol m^{-3} KBr solutions

x_I	Total surfactant concentration/mol m^{-3}	$10^6 D/cm^2 s^{-1}$	10^6error/$cm^2 s^{-1}$
1	2.008	0.811	0.012
	4.987	0.823	0.005
	8.001	0.845	0.008
	10.00	0.856	0.016
	19.994	0.966	0.007
	30.00	0.938	0.009
	40.011	1.16	0.01
	50.00	1.273	0.006
0.75	10.00	0.818	0.017
	20.00	0.980	0.005
	40.00	1.163	0.005
0.5	10.00	0.861	0.005
	20.00	0.974	0.010
	40.00	1.127	0.007
0.25	10.00	0.816	0.008
	20.00	0.845	0.006
	40.00	0.873	0.003
0.1245	32.14	0.526	0.004
0.10	2.028	0.725	0.007
	6.572	0.644	0.005
	10.00	0.601	0.004
	20.00	0.504	0.002
	30.00	0.466	0.002
	50.00	0.447	0.002
0.0	0.990	0.755	0.028
	2.396	0.645	0.009
	5.035	0.576	0.009
	10.075	0.481	0.003
	19.98	0.391	0.003
	30.00	0.387	0.004
	50.00	0.330	0.002

B) SDS and C_8E_4 in 100 mol m^{-3} NaCl solutions

x_I	Total surfactant concentration/mol m^{-3}	$10^6 D/cm^2 s^{-1}$	10^6error/$cm^2 s^{-1}$
1	10.013	1.023	0.012
	20.028	1.064	0.013
	30.008	1.100	0.008
	39.991	1.121	0.014
	50.00	1.179	0.008
0	10.04	1.23	0.09
	20.01	0.770	0.011
	30.08	0.671	0.004
	50.06	0.582	0.001

It is evident from the study of figure 5.1.17 that for all systems the diffusion coefficient shows a marked dependence on micellar concentration. This is because although coulombic interactions have been eliminated by the addition of salt, micelle-micelle interactions are operative. These are both static and hydrodynamic in nature and affect the osmotic pressure and mobility respectively.

For a system of non-interacting particles at infinite dilution the osmotic pressure Π_o is given by the Van't Hoff equation

$$\Pi_o = nkT \qquad \ldots\ldots 5.1.23$$

where n is the number density of the particles.

Under the same circumstances the mobility of a spherical particle is given by the Stokes equation

$$u = \frac{1}{6\pi\eta r} \qquad \ldots\ldots 5.1.24$$

where r is the particle radius. The expression for the diffusion coefficient, D for a spherical particle is then

$$D = \frac{kT}{6\pi\eta r} \qquad \ldots\ldots 5.1.25$$

However at finite concentrations the expressions for Π and u must be modified on account of the particle interactions. Thus

$$\Pi = kT(n + B_2n^2 + \ldots) \qquad \ldots\ldots 5.1.26$$

$$u = \frac{1}{6\pi\eta r}(1 + \lambda\phi + \ldots) \qquad \ldots\ldots 5.1.27$$

B_2 is the second osmotic virial coefficient and can be related to the potential of mean force, W_{12} between two micelles. λ is a complex function also depending on W_{12} and ϕ is the volume fraction of micelles. Equation 5.1.25 is then modified to

$$D = \frac{kT}{6\pi\eta r}(n + B_2n^2)(1 + \lambda\phi) \qquad \ldots\ldots 5.1.28$$

B_2 can be determined experimentally by conventional light scattering. It is given by the slope of the Debye plot of the reciprocal intensity of scattered light against concentration. The variation in D with concentration can be expressed by

$$D = D_o(1 + K_D c) \quad \ldots\ldots 5.1.29$$

where D_o is the diffusion coefficient at infinite dilution and K_D is given by

$$K_D = 2B_2M_2 - K_s - \phi \quad \ldots\ldots 5.1.30$$

where M_2 is the micellar molecular weight and K_s describes the concentration dependence of the sedimentation coefficient, s with concentration

$$s = s_o(1 + K_s c)^{-1} \quad \ldots\ldots 5.1.31$$

Thus measurement of the sedimentation coefficient and light scattering of the micellar solution provides the information necessary to predict the slope of the diffusion coefficient against concentration plot. Corti and Degiorgio[134] have done this for CTAB and SDS solutions and find good agreement between the experimental slope and that predicted by the combination of results from the other techniques. The experimental slopes found in this study and Corti and Degiorgio's data are given in table 5.1.16 for comparison.

Table 5.1.16 Slopes of the Diffusion Coefficient against Concentration Plots for CTAB and SDS

System	10^3xslope of plot/ $cm^5\ mol^{-1}\ s^{-1}$	reference	10^6y-intercept/ $cm^2\ s^{-1}$
SDS/0.1 mol dm^{-3} NaCl	4.20	134	0.945
SDS/0.1 mol dm^{-3} NaCl	3.69	Present study	0.987
CTAB/0.025 mol dm^{-3} KBr	7.11	134	0.797
CTAB/0.025 mol dm^{-3} KBr	7.54	Present study	0.798

It is not possible in this study to perform such detailed analysis of the data, due to the lack of extra information required as outlined above and since the data from the present study for the pure ionic systems agree well with that of Corti and Degiorgio it can be assumed that their conclusions apply to the results obtained here.

The general trends are worth comment. The positive slopes of the pure ionic and some mixed systems indicate repulsive micelle-micelle interaction but below x = 0.2 for CTAB/$C_{12}E_6$ the repulsive force is no longer apparent and at x = 0.1 the slope is negative indicating an attractive micelle-micelle interaction, whereby micelles can approach each other but still maintain their individual identity. The marked negative slope of the x = 0.1 and x = 0 systems could alternatively be due to a secondary aggregation process of micelles forming larger micelles as has been

suggested by Tanford.[135] For comparison, two diffusion coefficient determinations were made using $C_{12}E_8$ which Tanford deduces does not undergo this aggregation process and the results are shown in figure 5.1.17. It is seen that the diffusion coefficient of $C_{12}E_8$ hardly changes at all across the concentration range, as might be predicted for a nonionic system. It may therefore be concluded that the shape of the curve for $C_{12}E_6$ and other $C_{12}E_6$ rich systems is more likely to be due to the aggregation process described above, than strong attractive forces between micelles.

The question remains, therefore, of what values of diffusion coefficient should be taken in order to calculate the hydrodynamic radius of the micelles using the Stokes-Einstein relationship (equation 5.1.25). There is only one point on each curve which satisfies equation 5.1.25 with modification, and that is the c.m.c. or point of infinite dilution. Each set of data was extrapolated to the c.m.c. and the results are shown in table 5.1.17.

Table 5.1.17 Values of Diffusion Coefficient extrapolated to the c.m.c. at 298 K

Surfactant	$10^6 D$ c.m.c./$cm^2 s^{-1}$	c.m.c./mol m^{-3}	r/Å (eqn.5.1.25)
SDS	0.988	0.16	24.8
C_8E_4	0.98	-	25.0
CTAB	0.78	0.07	31.4
$C_{12}E_6$	0.78	0.07	31.4
CTAB/$C_{12}E_6$	0.78	-	31.4
$C_{12}E_8$	0.78	-	31.4

Aggregation Numbers

Methods of determining micelle aggregation numbers are generally indirect and there are no standard accepted methods in the literature. Invariably, use of a model of the micelle is required and the question of whether or not to include counterions and hydration layers in the micelle arises, for example light scattering data give the molecular weight of the micelle but the choice of the molecular weight of the monomer unit is not always obvious. Photon correlation spectroscopy gives the hydrodynamic radius r_H and again similar problems are present concerning the choice of micellar density, molecular weight and extent of hydration.

The simplest possible approach considers a spherical micelle of radius r and density d' so that the aggregation number n is given by

$$n = \frac{4\pi r^3 d' N}{3M} \qquad \ldots\ldots 5.1.32$$

More realistic results may be obtained by making the following modification suggested by Stigter.
The head group dimension r_{HG} is subtracted from r_H and the remaining volume is considered to be the spherical hydrocarbon core of density d

$$n = \frac{4\pi (r_H - r_{HG})^3 dN}{3M} \qquad \ldots\ldots 5.1.33$$

Aggregation numbers calculated by these methods for SDS and CTAB with $d = d' = 0.8\ gcm^{-3}$ are shown in table 5.1.18 and are seen to vary by just under 10%.

Table 5.1.18 Aggregation Numbers of SDS and CTAB calculated from r_H by simple methods

Surfactant	$r_H/\mathring{A}$	$r_{HG}/\mathring{A}$	n_{simple}	$n_{Stigter}$
SDS	24.8	4.6	107	98
CTAB	31.4	4.0	171	185

Greater problems are encountered in the calculation of aggregation numbers of nonionic micelles due to the possible variations in configuration of the polyoxyethylene chains. Two such configurations[136] are illustrated in figure 5.1.18. In addition it is likely that the chains will be heavily hydrated. In theory they can lie anywhere between flat on the micelle surface subject to geometric constraints, and perpendicular to the surface, and in mixed micelles the possibility of specific interactions with the ionic monomers may favour one or the other form. For example it is found experimentally that the ether oxygens in the polyoxyethylene chains bind strongly to anionic surfactants[137] but hardly at all to cationic surfactants.[71] In practice some situation between these two extremes is expected.

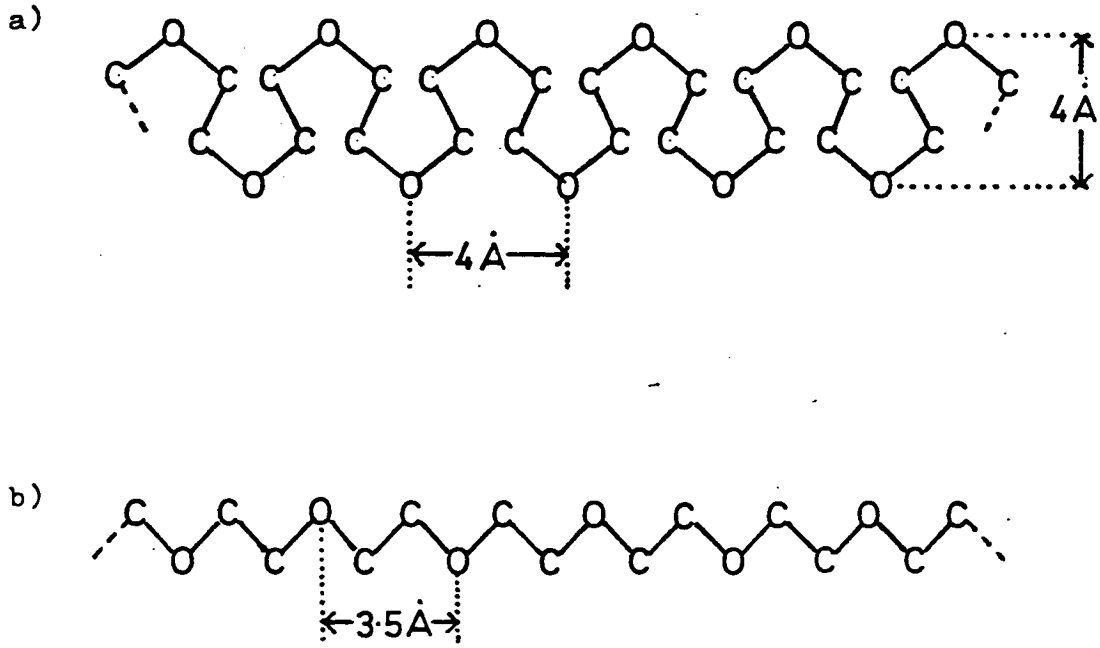

Figure 5.1.18 Two possible conformations of the polyoxyethylene chain in nonionic surfactants.

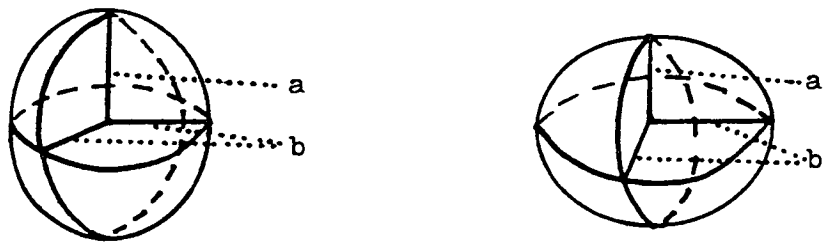

Prolate Oblate

Figure 5.1.19 Possible ellipsoidal micelle structures.

In table 5.1.19 some calculated aggregation numbers of nonionic micelles are given for different polyoxyethylene chain configurations. n_{simple} corresponds to the situation where the polyoxyethylene chains are condensed at the micelle surface.

Table 5.1.19 Aggregation Numbers of Nonionic Surfactants

Surfactant	$r_H/\mathring{A}$	n_{simple}	$r_{HG}/\mathring{A}$ maximum extension	$n_{maximum\ extension}$	$r_{HG}/\mathring{A}$ staggered conformation	$n_{staggered\ conformation}$
C_8E_4	24.8	101	14	23	8	85
$C_{12}E_6$	31.4	139	21	14	12	87

A most probable aggregation number range can be defined for each surfactant and the values are for

A) C_8E_4 : $85 < n < 100$

B) $C_{12}E_6$: $85 < n < 140$

Aggregation numbers used in future calculations for ionic, nonionic and mixed micelles are based on the simple approach of equation 5.1.32 in most cases due to the uncertainty in r_{HG} values.

Some literature values of n are shown in table 5.1.20 for comparison with the present study.

Table 5.1.20 Calculated Aggregation Numbers of SDS and CTAB

Surfactant	Salt concentration/ mol m^{-3}	T/K	reference	Technique	n
SDS	100	298	50	Light scattering	86
	0	298	138	Light scattering	64.4
	100	298	138	Light scattering	88.3
	100	298	139	Light scattering	91.4
	100	298	140	Membrane osmometry	88.5
	100	298	37	Sedimentation equilibrium	93
CTAB	25	298	134	Photon correlation spectroscopy	195
	25	303	141	Light scattering	270
	25	303	142	Membrane Osmometry	288
	25	298	143	Membrane Osmometry	274
	25	303	143	Membrane Osmometry	250

Micellar Shape

It should be mentioned that although the aggregation numbers calculated above from the experimental data of table 5.1.17 assume a spherical shape for the micelle, it is likely that none of the systems studied contain spherical micelles but rather ellipsoid structures. Controversy exists over the exact shapes and dimensions adopted but certain restrictions make the limits of the dimensions calculable. For example it was pointed out in section 1.1 that one dimension of the micelle cannot exceed twice the extended

length of the surfactant molecule. In table 5.1.21 data for SDS, CTAB and $C_{12}E_6$ are presented giving the maximum permissible smallest dimensions.

Table 5.1.21 Dimensions of Surfactant Molecules

Surfactant	Hydrocarbon chain	Extended length of hydrocarbon chain/Å	Hydrated head group dimension/ Å	Maximum radius/Å
SDS	$n\text{-}C_{12}H_{25}$	15.1	4.6	19.7
CTAB	$n\text{-}C_{16}H_{33}$	20.2	4.0	24.2
$C_{12}E_6$	$n\text{-}C_{12}H_{25}$	15.1	<21(see fig. 5.1.18A & B) <12	36.1 27.1

Recalling that the hydrodynamic radii of SDS and CTAB/$C_{12}E_6$ micelles calculated using equation 5.1.25 are 24.8Å and 31.4Å respectively it is clear that the ionic micelles cannot be spherical and therefore must be ellipsoids. Two types are postulated, the oblate and the prolate and are illustrated in figure 5.1.19. Equation 5.1.25 can be rewritten as

$$D = \frac{kT}{f} \qquad \ldots\ldots 5.1.34$$

where f is the friction coefficient and in the case of spherical micelles is equal to $6\pi\eta r$. For ellipsoids the friction coefficient which must be used in equation 5.1.34 is given by

$$\frac{f}{f_o} = \frac{[(a^2/b^2) - 1]^{\frac{1}{2}}}{(a/b)^{2/3} \tan^{-1}[(a^2/b^2)-1]^{\frac{1}{2}}} \qquad \ldots\ldots 5.1.35$$

for oblate ellipsoids, and for prolate ellipsoids

$$\frac{f}{f_o} = \frac{[1-(b^2/a^2)]^{\frac{1}{2}}}{(b/a)^{2/3} \ln \frac{1+(1-(b^2/a^2))^{\frac{1}{2}}}{b/a}} \quad \ldots\ldots 5.1.36$$

f is the friction coefficient for the ellipsoid and f_o is the friction coefficient for the sphere, b is the minor half axis and a is the major half axis. Assuming the the three shapes have the same volume then the values of a and b can be calculated and compared. Results are given in table 5.1.22.

Table 5.1.22 Calculated Aggregation Numbers for Three Micellar Shapes for CTAB Micelles

Shape	Volume of micelle = $1.297 \times 10^{-25} m^3$	b/Å	a/Å	Volume of hydrocarbon core $\times 10^{26} m^3$	n
Sphere	$4/3\ \pi r^3$			8.617	185
Oblate ellipsoid	$4/3\ \pi a^2 b$	24.2	35.8	8.557	183
Prolate ellipsoid	$4/3\ \pi a b^2$	24.2	52.9	8.358	179

The volume of hydrocarbon core is calculated from the formulae in column 2 of the table after the head group dimension has been subtracted from a, b and r. A core density of 0.8 g cm^{-3} is assumed and the aggregation number calculated using

equation 5.1.33. It is seen that there is not much variation in the calculated aggregation numbers and in future calculation the value of n = 180 is chosen for simplicity.

Corresponding calculations of aggregation numbers have been carried out for SDS and are given in table 5.1.23.

Table 5.1.23 Calculated Aggregation Numbers of SDS Micelles for Three Micellar Shapes

Shape	Volume of micelle = $6.389 \times 10^{-26} m^3$	b/Å	a/Å	Volume of hydrocarbon core/ $\times 10^{26} m^3$	n
Sphere	$4/3\ \pi r^3$			3.453	98
Oblate ellipsoid	$4/3\ \pi a^2 b$	19.7	27.8	3.404	97
Prolate ellipsoid	$4/3\ \pi a b^2$	19.7	39.3	3.314	95

No such deductions have been made about the nonionic micelles because of the complex nature of the head group and the topic is discussed in section 5.2.

5.1.3 Electrophoretic Mobility

The electrophoretic mobility of pure CTAB and mixed CTAB/$C_{12}E_6$ micelles in water at 298 K was determined by the dye tracer technique described in section 4.3 as a function of composition and surfactant concentration.

For each value of x the plot of mobility against concentration is a straight line (see figure 5.1.20) and the slopes and intercepts are given in table 5.1.24 and a full set of data is included in appendix 3.

Table 5.1.24 Electrophoretic Mobility Data for CTAB/$C_{12}E_6$ in Water at 298 K

x	Slope du/dc/ $cm^5V^{-1}s^{-1}mol^{-1}$	10^4 intercept/ $cm^2V^{-1}s^{-1}$	c.m.c./ mol m^{-3}	10^4u c.m.c./ $cm^2V^{-1}s^{-1}$
1.0	-2.860	5.002	0.90	4.976
0.75	-1.723	4.416	0.66	4.401
0.5	-2.073	4.129	0.31	4.116
0.2	-0.761	2.452	0.092	2.449
0.1	-0.425	1.692	0.081	1.689

Figure 5.1.21 illustrates the relationship between the mobility at the c.m.c. and x. As the mobility depends on the ionic content of the micelle it is expected that at high values of x the mobility will be high and at low values of x the mobility will be low and this behaviour is found. For each micellar composition the mobility decreases with increasing surfactant concentration and if suitable coefficients B_1 and B_2 could be theoretically predicted the Debye-Hückel - Onsager relationship of equation 5.1.34 could be tested.

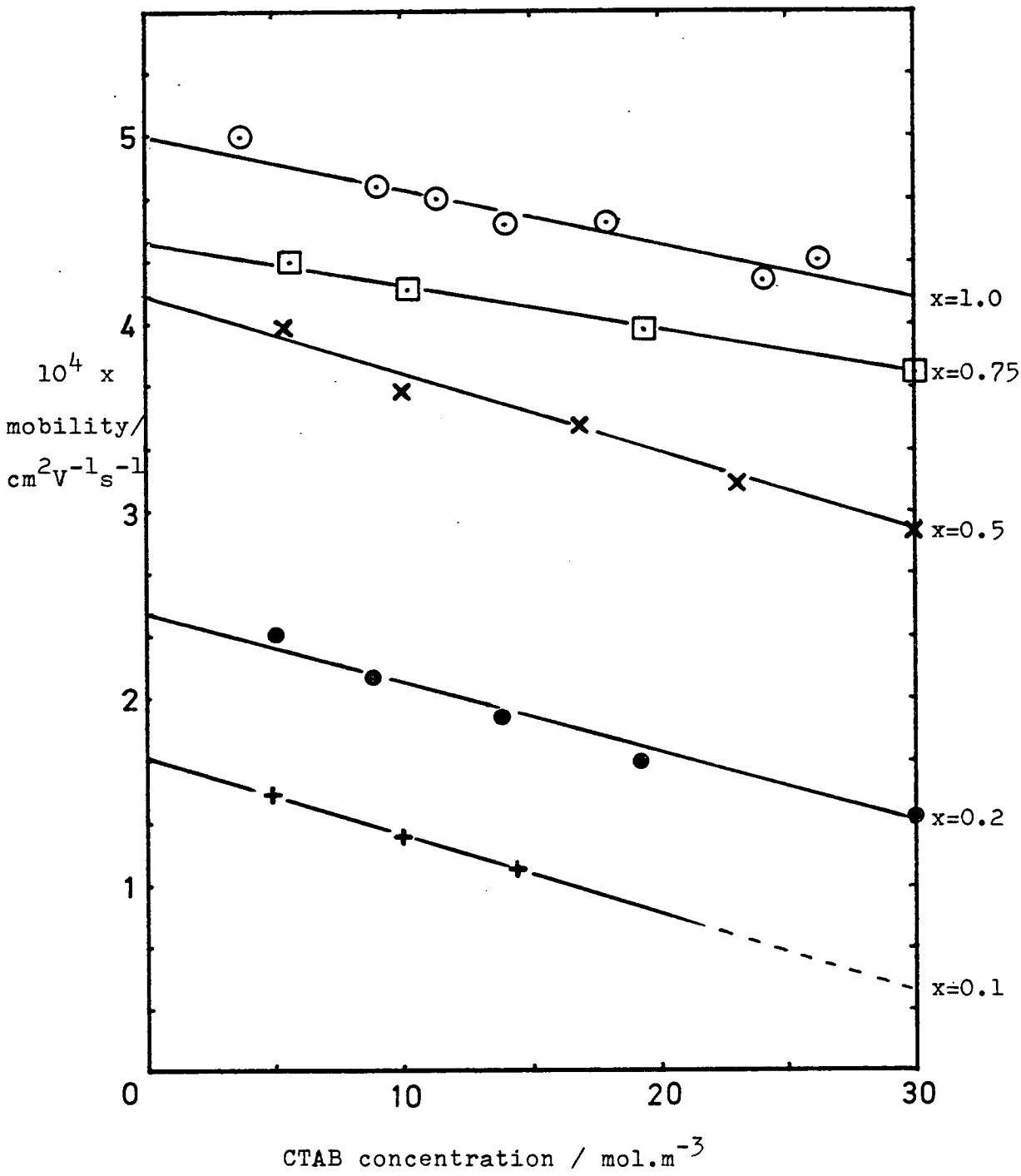

Figure 5.1.20 Electrophoretic mobility of CTAB / $C_{12}E_6$ micelles in water at 298.15K as a function of CTAB concentration.

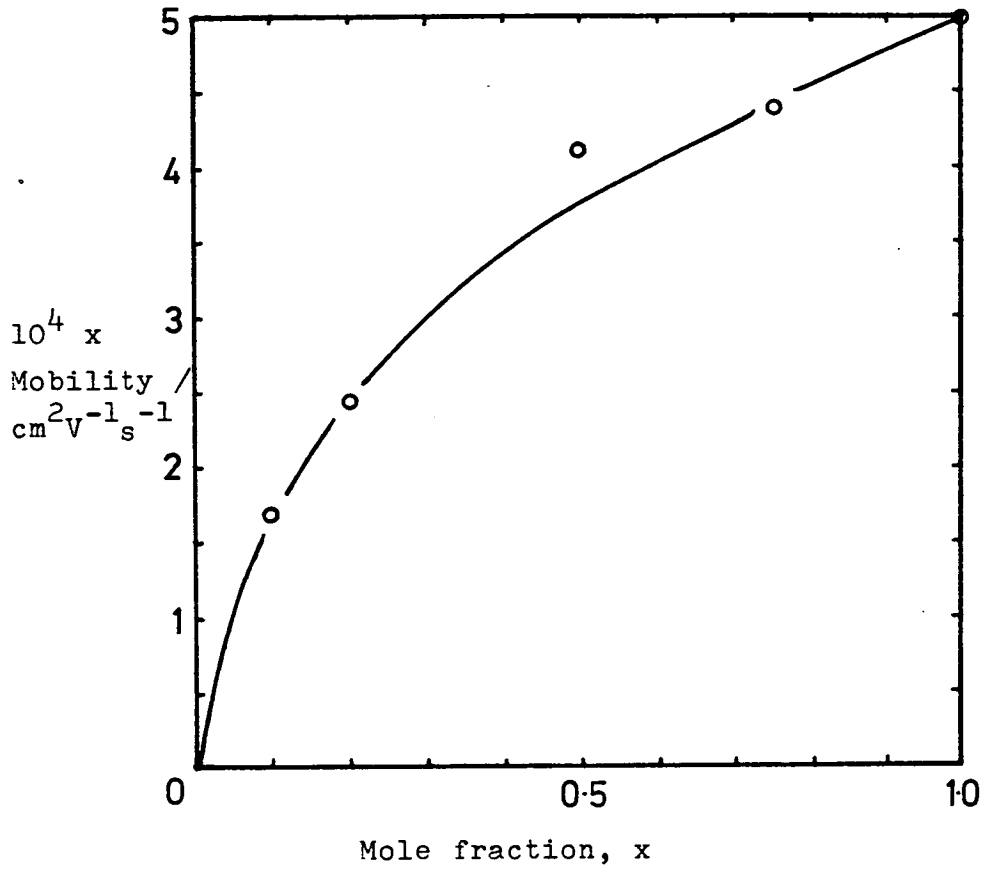

Figure 5.1.21 Plot of electrophoretic mobility of CTAB / $C_{12}E_6$ micelles at the c.m.c. in water at 298.15K against mole fraction

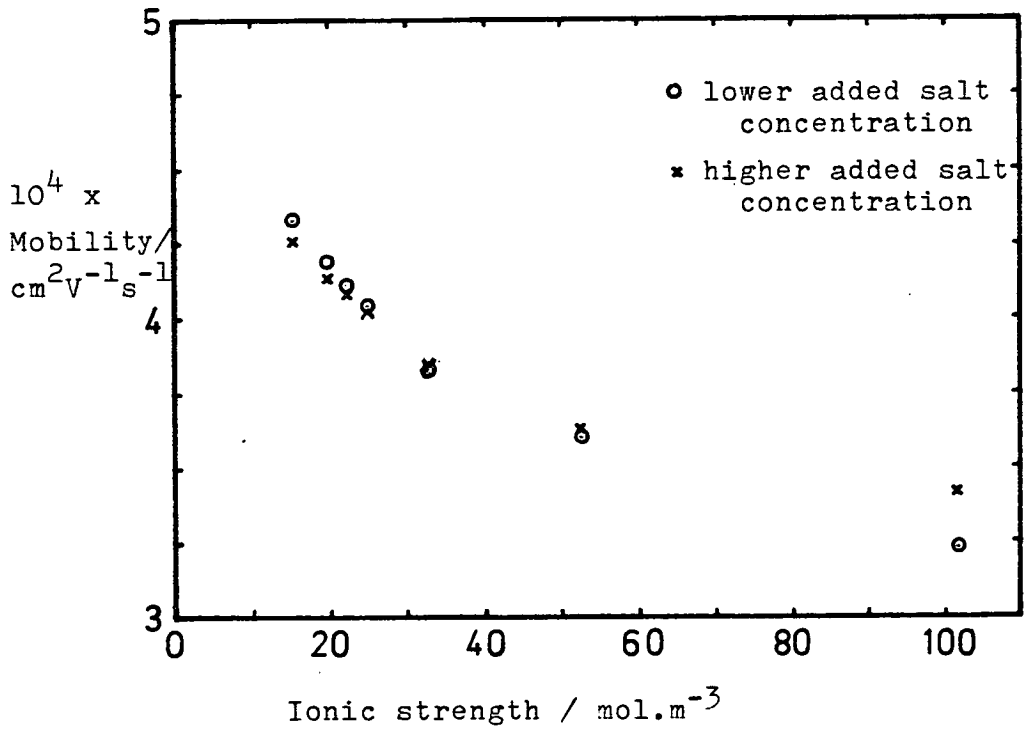

Figure 5.1.22 Plot of electrophoretic mobility of SDS micelles at 298.15K as a function of ionic strength.

$$\bar{u} = u_o - (B_1 u_o + B_2) c^{\frac{1}{2}} \qquad \ldots\ldots 5.1.34$$

However, at present qualitative agreement between experiment and equation 5.1.34 must suffice. Two factors may contribute to the decrease in mobility. Firstly, as the surfactant concentration increases, any micelle-micelle interactions will increase and retard the micelle motion, and secondly, as the ionic strength of the solution which is approximately equal to [c.m.c. + α(c-c.m.c.)] increases, ion-ion interactions will increase. The two effects are separable by performing experiments either as a function of concentration at constant ionic strength, or as a function of ionic strength at constant surfactant concentration. This has not been attempted here but a comparable analysis can be carried out on the data of Stigter and Mysels who determined the electrophoretic mobility of SDS micelles as a function of added salt concentration and concentration. Table 5.1.25 shows data extracted from their work.

Table 5.1.25. Mobility of SDS Micelles in NaCl Solutions at 298 K, due to Stigter and Mysels[41]

Added salt concentration/ mol dm^{-3}	c.m.c./ mol m^{-3}	α	10^4 $u_{c.m.c.}$/ $cm^2 V^{-1} s^{-1}$	slope du/dc/ $cm^5 V^{-1} s^{-1} mol^{-1}$
0.0	8.12	0.287	4.55	-8.69
0.01	5.29	0.281	4.26	-7.01
0.03	3.13	0.285	3.84	-3.62
0.05	2.27	0.295	3.63	-2.42
0.10	1.46	0.324	3.42	-1.66

Unfortunately the concentration range studied is such that there are not many data at constant ionic strength but calculations for several pairs of points can be done. The surfactant concentration corresponding to the chosen value of ionic strength, I, is calculated using equation 5.1.35

$$c = \left(\frac{I - [salt] - c.m.c.}{\alpha}\right) + c.m.c. \quad \ldots\ldots 5.1.35$$

and the mobility at this concentration is found using the data in table 5.1.25. Results are shown in figure 5.1.22 and table 5.1.26. If the mobility is independent of micelle concentration then the calculated pairs of mobility values should be equal at constant ionic strength. It is seen from table 5.1.26 that this is so to within 1% in most cases and therefore it is likely that the reduction in mobility is due solely to the increase in ionic strength and micelle-micelle interactions play little, if any, part.

Although a similar study cannot be done on the CTAB/$C_{12}E_6$ data it is instructive to construct a plot of mobility against ionic strength and consider the variation of the slope with x.

Table 5.1.27 contains the relevant data which is plotted in figure 5.1.23. The values of α used in the calculation are those derived in section 5.2 from conductance and mobility data.

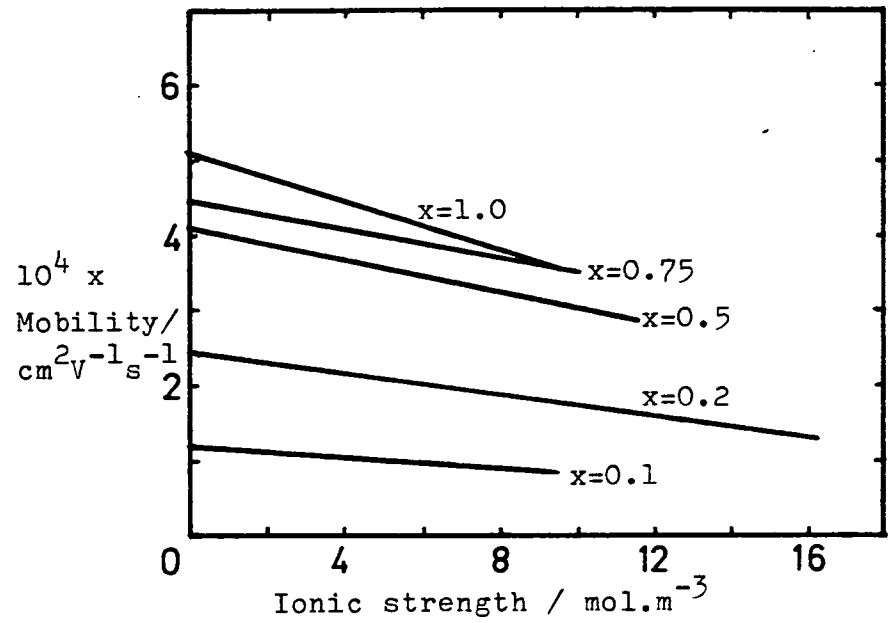

Figure 5.1.23 Plot of electrophoretic mobility of CTAB / $C_{12}E_6$ micelles at 298.15 K as a function of ionic strength.

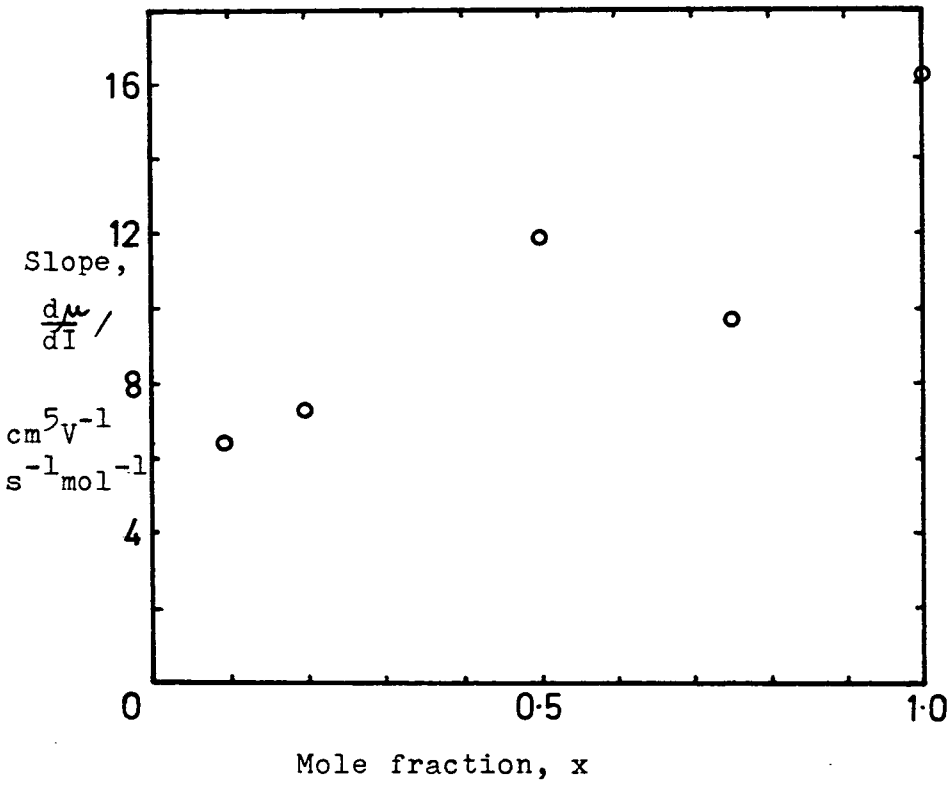

Figure 5.1.24 Plot of the slope of the mobility against ionic strength (see Figure 5.1.23) plot against mole fraction, x.

Table 5.1.26 Mobility of SDS Micelles at Constant Ionic Strength

I/mol m^{-3}	FIRST POINT			SECOND POINT			$10^4 u_1$/ $cm^2 V^{-1} s^{-1}$	$10^4 u_2$/ $cm^2 V^{-1} s^{-1}$
	Added salt concentration/ mol m^{-3}	c.m.c./ mol m^{-3}	c/ mol m^{-3}	Added salt concentration/ mol m^{-3}	c.m.c./ mol m^{-3}	c/ mol m^{-3}		
25	10	5.29	39.85	0	8.12	66.94	4.02	4.04
22.5	10	5.29	30.95	0	8.12	58.23	4.08	4.11
20	10	5.29	22.05	0	8.12	49.51	4.14	4.19
15.3	10	5.29	5.29	0	8.12	33.14	4.26	4.33
33.1	30	3.13	3.13	10	5.29	68.78	3.84	3.82
52.3	50	2.27	2.27	30	3.13	70.29	3.63	3.60
101.5	100	1.46	1.46	50	2.27	169.0	3.43	3.23

Table 5.1.27 Mobility Data for CTAB/$C_{12}E_6$ at 298 K

Mobility as a Function of Ionic Strength

x	α	slope du/dI/ $cm^5V^{-1}s^{-1}mol^{-1}$	10^4 intercept/ $cm^2V^{-1}s^{-1}$
1	0.166	-16.14	5.12
0.75	0.247	- 9.68	4.48
0.5	0.333	-11.91	4.13
0.2	0.519	- 7.23	2.45
0.1	0.655	- 6.42	1.69

From the data in table 5.1.27 a plot of slope du/dI against x is constructed and is shown in figure 5.1.24. Examination of this graph reveals that there is a slight increase in the slope of the mobility against ionic strength plot as x increases. In the absence of micelle-micelle interactions the slopes du/dI are expected to be equal so it is concluded that ionic strength effects are not the sole cause of the decrease of mobility with concentration in this case. The positive slope of figure 5.1.24 indicates that the greater the ionic content of the micelle, the greater the micellar interaction. For example, at given constant ionic strength of 10 mol m^{-3} the total surfactant concentration at x = 1 is 55.6 mol m^{-3} and at x = 0.1 it is 150.9 mol m^{-3}, and therefore there is more micellar material present in the x = 0.1 solution than in the x = 1 solution of ionic strength

10 mol m^{-3}. If micellar interactions were dependent only on micellar concentration then the expected slope of figure 5.1.24 would be negative. It is therefore concluded that both ionic strength effects and micelle-micelle interactions contribute to the variation in electrophoretic mobility with concentration and that the latter are greater in ionic rich systems.

5.1.4 Surface Tension

Surface tension data were obtained by the drop weight method and used to check the purity of the surfactant samples mentioned in section 4.1, in addition to c.m.c. determinations. Results are not expected to be highly precise due to the primitive nature of the apparatus. Drops formed at an approximate rate of one per second which is considerably faster than recommended[115] and no precautions such as use of a dust free box were taken to prevent contamination. However, the surface tension method was particularly useful in the case of CTAB/$C_{12}E_6$ solutions, the c.m.c.'s of which are not readily determined by the conductivity method due to the difficulty in obtaining precise data at very low ionic surfactant concentrations (see section 5.1).

SDS/Salt Solutions

Surface tension data as a function of surfactant concentration and ionic strength yield information about the variation of c.m.c. with salt concentration and α can be calculated by the method of section 2.1.2. Two salts,

NaCl and Na_2SO_4 were added to SDS solutions at 291 K for comparison of a univalent and divalent electrolyte. Results are presented in table 5.1.28, appendix 2 and figure 5.1.25.

Table 5.1.28 C.m.c.'s of SDS/salt Solutions at 291 K

A) SDS/NaCl

Added salt concentration/ mol m^{-3} = I	c.m.c./ mol m^{-3}
0	8.56
10	5.80
30	3.57
100	1.67

B) SDS/Na_2SO_4

Added salt concentration/ mol m^{-3}	Ionic Strength/ mol m^{-3}	c.m.c./ mol m^{-3}
0	0	8.56
10	30	4.53
33.3	100	2.52

The data of table 5.1.28 are plotted in figure 5.1.26 as ln c.m.c. against $\ln[Na^+]$ and the equations of the lines are:

A) SDS/NaCl: $\ln \text{c.m.c.} = -0.661 \ln[Na^+] - 7.894$ 5.1.36

B) SDS/Na_2SO_4: $\ln \text{c.m.c.} = -0.585 \ln[Na^+] - 7.553$ 5.1.37

The corresponding α values are

A) SDS/NaCl $\alpha = 0.339 \pm 0.009$

B) SDS/Na_2SO_4 $\alpha = 0.415 \pm 0.011$

The two salts do not give the same value of α, indicating that the nature and concentration of the coion has some effect in determining α as well as the concentration of the counterion.

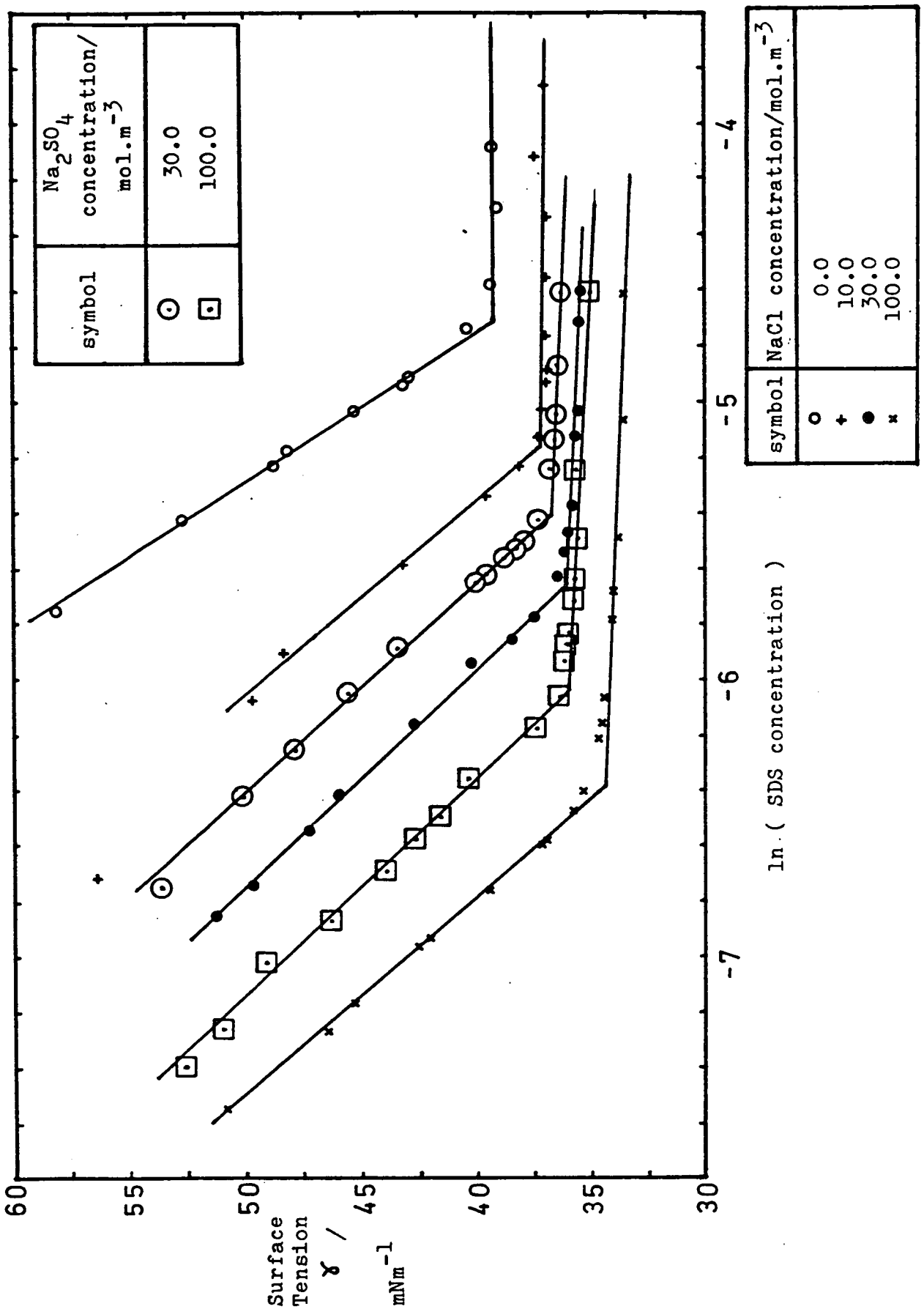

Figure 5.1.25 Plot of surface tension against ln (SDS concentration)

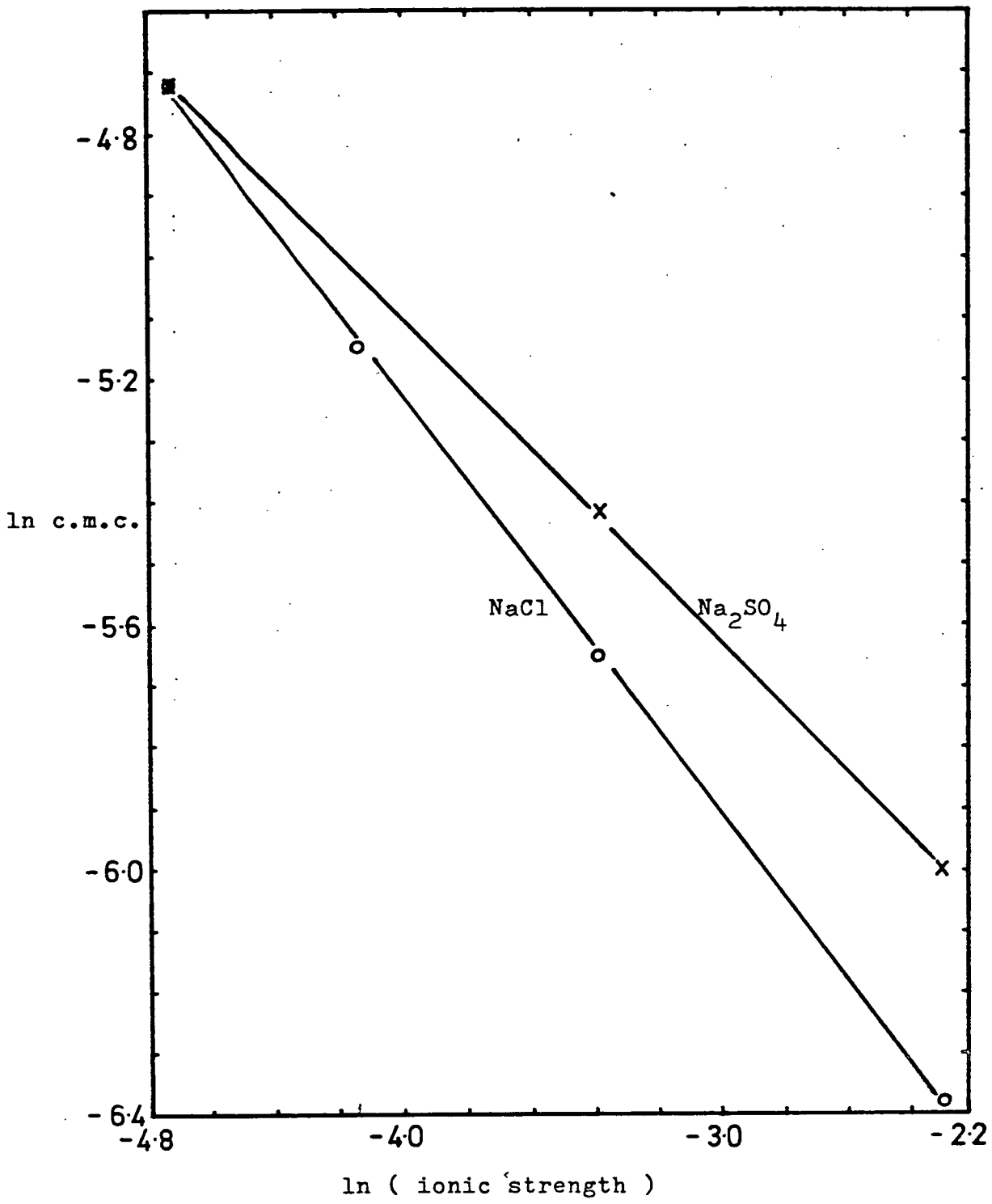

Figure 5.1.26 Plot of ln c.m.c. against ln (ionic strength) for SDS solutions in NaCl and Na_2SO_4 solutions.

SDS/Octanol

This system was studied as a function of composition of the bulk solution at 287 K and results are given in figure 5.1.27, table 5.1.29 and appendix 2.

Table 5.1.29 C.m.c.'s of SDS/Octanol Solutions at 287 K

x	c.m.c./mol m^{-3}
1	8.56 (291 K)
0.938	7.24
0.833	6.11
0.667	4.75
0.50	3.26

For x = 0.938, 0.833 and 0.667 the graph of surface tension against ln concentration has a minimum in the region of the c.m.c. (see section 4.5) and the exact position of the c.m.c. is ill defined. In each case the extrapolation method from points well below and above the c.m.c. was used. For x = 0.5 the plot shows no minimum but a gradual decrease in surface tension in the region of the c.m.c.

Figure 5.1.28 illustrates the variation in c.m.c. with composition. The c.m.c. decreases steadily with increasing alcohol content of the solution and this trend can be understood by examination of the equation for the micellisation process:

Ionic surfactant + alcohol $\rightleftharpoons$ mixed micelle 5.1.38

Due to the complex nature of the micelles formed (see section 2.2) a more quantitative analysis is not possible.

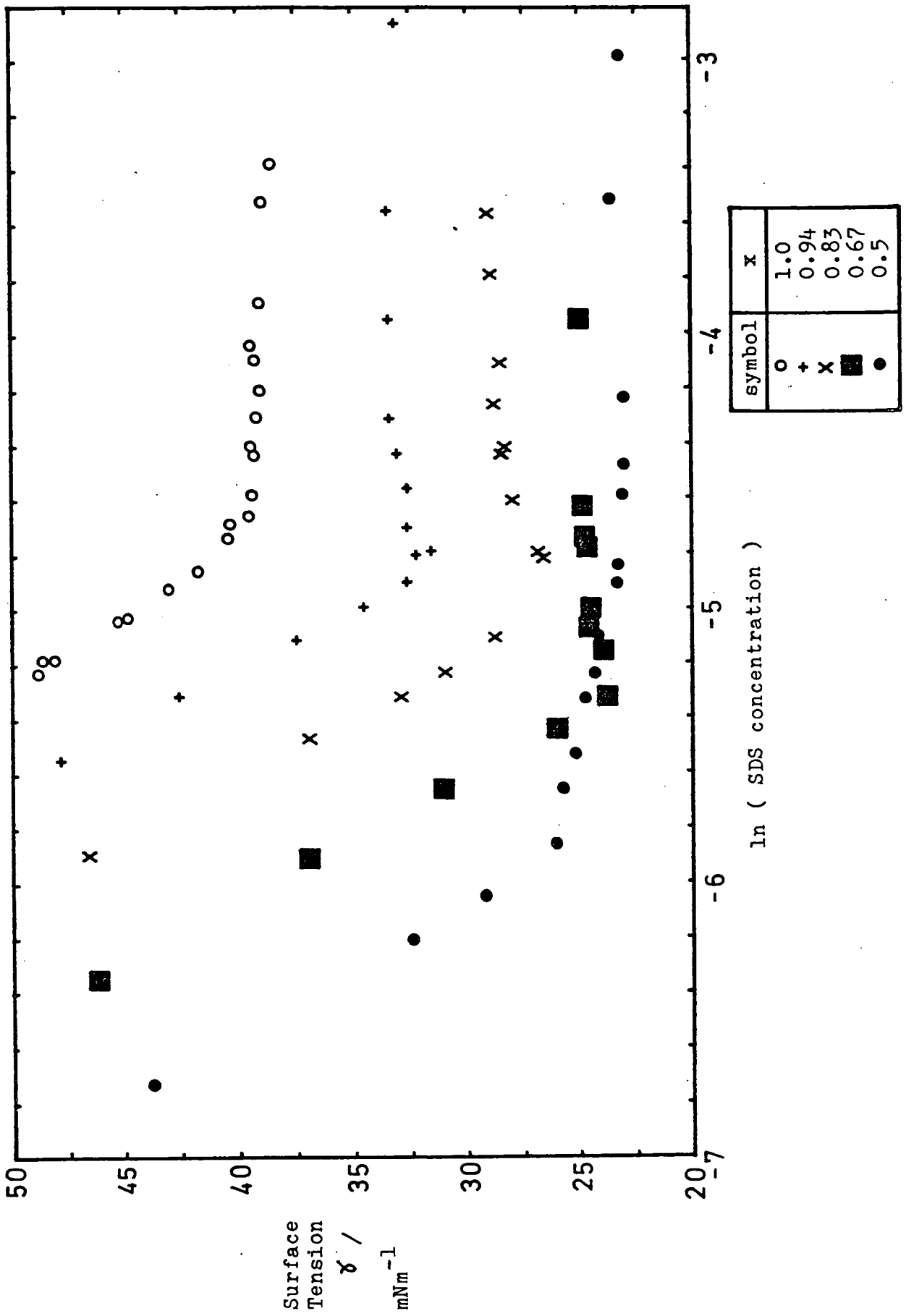

Figure 5.1.27 Plot of surface tension of SDS / octanol solutions against ln (SDS concentration).

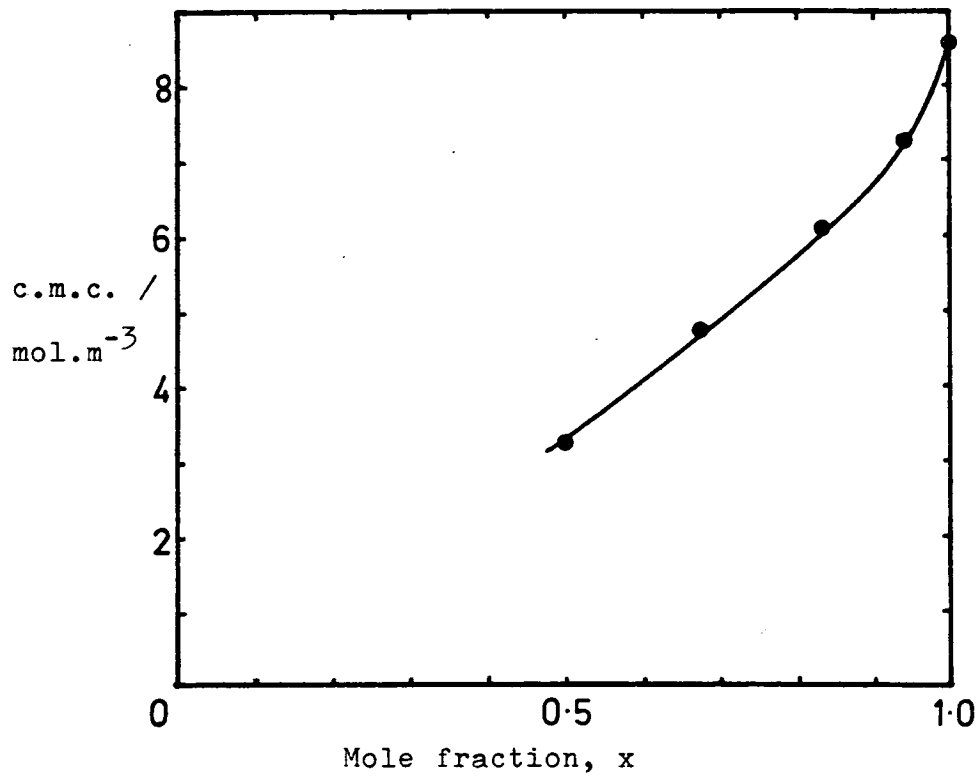

Figure 5.1.28 Plot of the c.m.c. of SDS/octanol solutions against x.

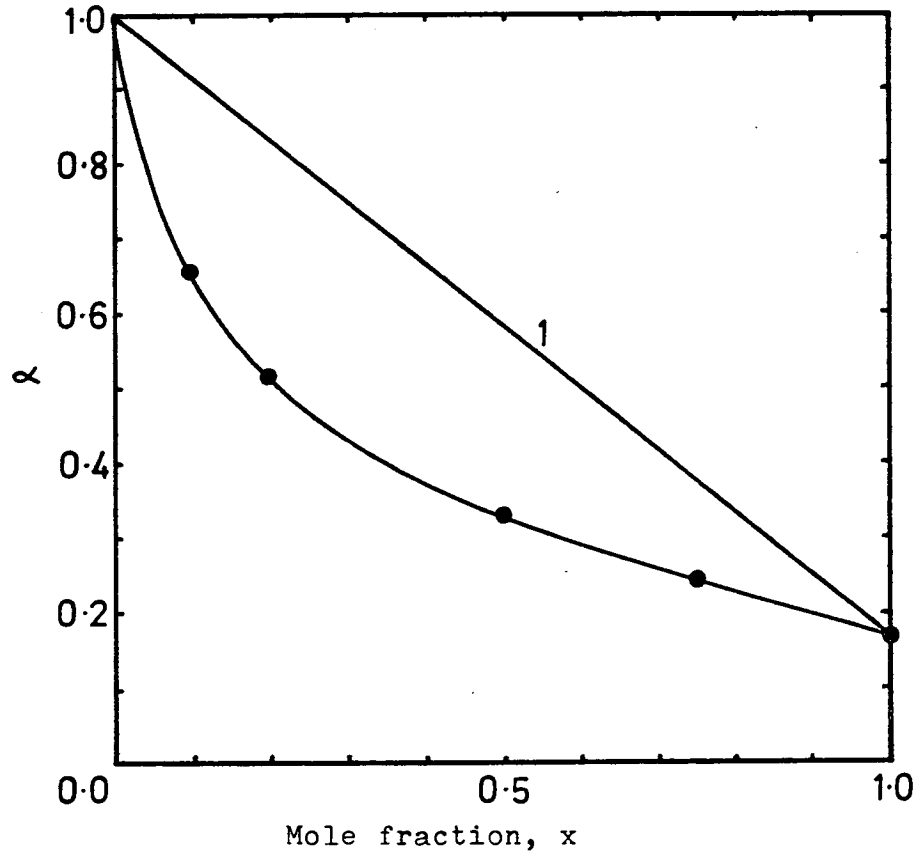

Figure 5.2.1 Plot of the degree of dissociation, α against mole fraction for the system CTAB / $C_{12}E_6$ in water at 298.15K.

CTAB/$C_{12}E_6$

The c.m.c.'s of CTAB/$C_{12}E_6$ systems were determined at 298 K and are given in table 5.1.10. A full set of data is given in appendix 2.

The c.m.c. of the pure $C_{12}E_6$ system in water according to the manufacturers is 0.071 mol m^{-3} and this information, along with that of table 5.1.10 was used to construct a plot of c.m.c. against x as shown in figure 5.1.13(B). This curve is of the form shown in figure 2.2.1(A).

5.2 Discussion

5.2.1 Treatment of the Experimental Results in order to Determine α

The purpose of the present study has been to determine the extent of counterion binding to pure and mixed micelles and several approaches to the solution to this problem are presented below.

A) Law of Mass Action Applied to c.m.c. Data

C.m.c.'s have been determined by conductance and surface tension methods (see sections 4.2, 4.5, and 5.1) and plots of ln c.m.c. against ln ionic strength having slope $-\beta$ or $(\alpha-1)$ constructed. The results of such calculations are summarised in table 5.2.1.

Table 5.2.1 Calculated α values for SDS and CTAB Solutions (Law of Mass Action)

Technique	Surfactant	Salt	T/K	α	error in α
conductance	SDS	NaCl	288	0.308	0.005
conductance	SDS	NaCl	298	0.314	0.015
conductance	SDS	NaCl	308	0.312	0.014
conductance	CTAB	KBr	298	0.172	0.015
surface tension	SDS	NaCl	291	0.339	0.009
surface tension	SDS	Na_2SO_4	291	0.415	0.011

The variation in α with temperature has been discussed in section 5.1.1. There is no inherent reason for the difference in calculated α values for SDS for the two techniques, for although the c.m.c.'s determined by the surface tension method are consistently higher than those determined by conductance due partly to the difference in temperature, it is the variation in c.m.c. with ionic strength which is being studied and this should be the same in each case. Due to the higher precision of the conductance technique the α values calculated from conductance measurements are considered to be the more reliable.

B) Diffusion

The method of Rohde and Sackmann was used to calculate α values for the systems SDS/NaCl and CTAB/KBr and results are given in section 5.1.2. In each case these are unrealistically low and the method dismissed as unreliable.

C) Conductance and Mobility

The simplest approach outlined in section 2.1.8 is used to calculate α for the CTAB/$C_{12}E_6$ system. The expression for κ_{sp} is

$$\kappa_{sp} = F \Sigma u_i c_i z_i \qquad \ldots\ldots 2.1.13$$

Assuming that the c.m.c. is invariant with surfactant concentration the relationship between the slope of the conductance plot above the c.m.c. and α is obtained.

$$\alpha = \frac{\frac{d\kappa_{sp}/F}{dc}}{u_2 + u_{mic}} = \frac{d\kappa_{sp}/dc}{\lambda_2 + \lambda_{mic}} \qquad \ldots\ldots 5.2.1$$

Values of α calculated using this formula are given in table 5.2.2 and a graph of α against x is constructed as shown in figure 5.2.1. In addition one value of α has been calculated for SDS in water using the experimental conductance slope and Stigter's mobility value, and is equal to 0.274.

Table 5.2.1 Values of α calculated from conductance and Mobility Results for CTAB/$C_{12}E_6$ at 298 K in Water

x	c.m.c./ mol m^{-3}	10^4 u_{mic}/ $cm^2V^{-1}s^{-1}$	10^4 u_{Br^-} $cm^2V^{-1}s^{-1}$	slope $d\kappa_{sp}/dc$ $cm^2\Omega^{-1}mol^{-1}$	α	κa
1.0	0.90	4.98	7.98	20.75	0.166	0.31
0.75	0.66	4.40	8.00	29.61	0.247	0.27
0.5	0.31	4.12	8.02	39.06	0.333	0.18
0.2	0.092	2.45	8.05	52.60	0.519	0.10
0.1	0.081	1.69	8.06	61.60	0.655	0.09
0	0.071	0				

As the ionic content of the micelle decreases, α rises slowly at first then as x reaches 0.2 it rises more rapidly approaching α = 1 at x = 0. As the nonionic monomers enter the micelle they have the effect of reducing the surface charge density and as repulsion between head groups decreases, bound counterions can be released. α might therefore be expected to be a linear function of x as indicated by line 1 in figure 5.2.1 but experimentally a significant deviation from this behaviour is found and consideration of the surface charge density of the micelle reveals why this is so. From the photon correlation spectroscopy results the hydrated micellar radii of the pure CTAB, pure $C_{12}E_6$ and mixed micelles are the same and therefore to a first approximation the aggregation number of each type of micelle is the same. On this basis,

considering the change in charge density, that is charge per head group (= αx), proceeding from x = 1 down to x = 0 produces the results shown in table 5.2.3

Table 5.2.3 Surface Charge Densities of CTAB/$C_{12}E_6$ Micelles

x	charge density
1.0	0.166
0.75	0.185
0.5	0.167
0.2	0.104
0.1	0.066

This shows that the charge density is approximately equal over the range x = 1 down to x = 0.4 or 0.3 and then it falls off towards x = 0. This implies that there is a maximum permissible surface charge density for the micelle and if the composition is such that without counterion binding the surface charge density would exceed this value, then counterions will bind to the micelle, reducing the charge density to the permissible level. This is the basis of the counterion condensation theory of polyelectrolytes[144] and since many features of the micelle are similar to those of charged polymers in solution it is to be expected that the same effects will be noted for both systems.

Thus it can be deduced that a micelle with native charge density xn will bind counterions to reduce the charge density

to αxn. However it cannot be that there is a lower limit to the value of αxn as might be predicted from the above model, for as shown in figure 5.2.2 below x = 0.2 counterion binding is still evident and it is possible that geometric factors operate in this region.

The above method relies on the assumption that the monomer concentration above the c.m.c. is constant but if the Mass Action Model of micellisation is used, it is seen from figure 1.2.2 that the concentration of monomer in equilibrium with micelles drops progressively above the c.m.c. From equation 2.1.3

$$1/n \log K = 1/n \log[\text{micelle}] - \log[S^+] - \beta\log[C^-] \quad \ldots\ldots 2.1.3$$

and the condition at the c.m.c. is such that

$$\log[S^+] + \beta\log[C^-] = \log[S^+]^\circ + \beta\log[C^-]^\circ \quad \ldots\ldots 5.2.2$$

$$\text{and} \qquad [S^+] = [C^-]^\circ \quad \ldots\ldots 5.2.3$$

$$\therefore \quad \log[S^+] \doteq (1 + \beta) \log \text{c.m.c.} - \beta\log[C^-] \quad \ldots\ldots 5.2.4$$

$$\text{and} \qquad [S^+] = \frac{\text{c.m.c.}^{(1+\beta)}}{C^{-\beta}} \quad \ldots\ldots 5.2.5$$

The total concentration, c, is given by

$$c = \frac{[C^-] - \beta[S^+]}{1-\beta} \quad \ldots\ldots 5.2.6$$

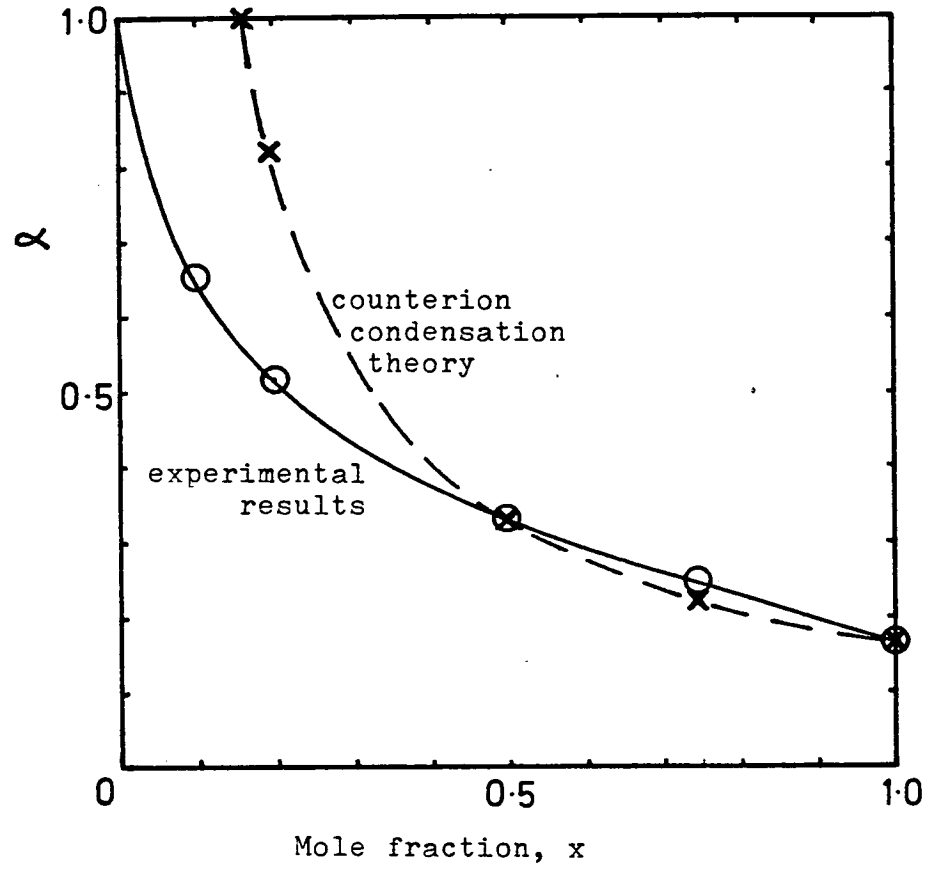

Figure 5.2.2 Plot of α against x - comparison of experimental results and predictions of counterion condensation theory.

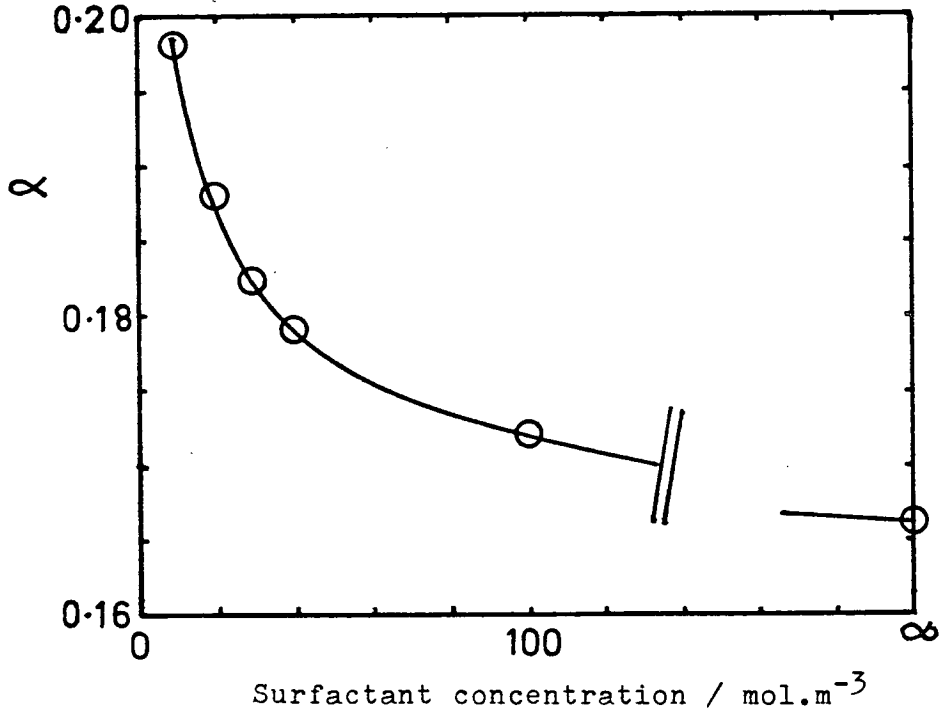

Figure 5.2.3 Plot of α against concentration of CTAB (Mass Action Model).

These equations were used to calculate the monomer and counterion concentrations at several values of c for pure CTAB in water at 298 K with α = 0.166 and results are shown in table 5.2.4.

Table 5.2.4 Monomer and Counterion Concentrations above the c.m.c. as a Function of c for CTAB in water at 298 K (Mass Action Model)

concentration, c/ mol m^{-3}	monomer concentration/ mol m^{-3}	counterion concentration/ mol m^{-3}
0.90	0.900	0.90
10.90	0.432	2.17
20.90	0.277	3.70
30.90	0.205	5.30
40.92	0.164	6.93

The unsimplifed conductance equation above the c.m.c. is

$$\kappa_{sp} = F(u_1c_1 + u_2c_2 + u_{mic}c_{mic}z_{mic}) \quad \ldots\ldots 5.2.7$$

where $|z_1| = |z_2| = 1$

$$\therefore \quad \kappa_{sp} = F[c_1(u_1 + u_2) + \alpha(c - c_1)(u_2 + u_{mic})] \quad \ldots\ldots 5.2.8$$

$$\text{or} \quad \kappa_{sp} = c_1(\lambda_1 + \lambda_2) + \alpha(c - c_1)(\lambda_2 + \lambda_{mic}) \quad \ldots\ldots 5.2.9$$

Inserting the values $\lambda_1 = 34.4\ cm^2\Omega^{-1}mol^{-1}$

$\lambda_2 = 77.01\ cm^2\Omega^{-1}mol^{-1}$

$\lambda_{mic} = 48.06\ cm^2\Omega^{-1}mol^{-1}$

equation 5.2.9 gives for κ_{sp}

$$\kappa_{sp} = 111.41\ c_1 + 125.07\ \alpha(c - c_1) \quad \ldots\ldots\ 5.2.10$$

Using the values of c_1 from table 5.2.4 and the experimental conductance values for the corresponding total surfactant concentrations, equation 5.2.10 can be solved for α. The results are given in table 5.2.5 and plotted graphically in figure 5.2.3

Table 5.2.5 Values of α calculated from equation 5.2.10

$c/mol\ m^{-3}$	$10^4\ \kappa_{sp}/cm^{-1}\Omega^{-1}$	α
10.90	3.078	0.198
20.90	5.152	0.188
30.90	7.226	0.182
40.92	9.304	0.179
100	21.56	0.172

These calculated values of α are not absolutely correct as they are based on calculation of c_1 using $\alpha = 0.166$ and the new values should be inserted in equations 5.2.2 to 5.2.6 to give improved values of α. However this will make very little difference to the absolute values and the trend shown in figure 5.2.3 will still remain. In conclusion, use of the Mass Action Model

produces values of α which vary across the concentration range but approach the 0.166 value calculated using a simpler model. It would seem, therefore, to be an unnecessary complication to use the Mass Action Model method of determining α and so the simpler approach is used in all future calculations.

The plot of α against x of figure 5.2.1 can be fitted to the form of the Langmuir adsorption isotherm by the equation

$$\alpha = \frac{\alpha_i}{\alpha_i + (1 - \alpha_i)x_i} \quad \ldots\ldots 5.2.11$$

where α_i is the value of α at x = 1. This suggests that theory might relate the occurrence of specific sites on the micelle surface with counterion binding. For an ideal mixed micelle with ionic head groups distributed uniformly over the surface these sites could be the head groups themselves or the space between two adjacent or three or more surrounding head groups. Stigter[145] has has suggested such a cell model for an ionic micelle and has calculated the area available to counterions. Figure 5.2.4 illustrates the geometric arrangement of head groups and counterions in the Stern Layer of SDS.

D) Mobility

Values of u_{mic} for CTAB/$C_{12}E_6$ micelles are given in table 5.1.25 and using a suitable theory the zeta potential and charge can be calculated from these figures. As mentioned in section 4.3, older methods, for example those

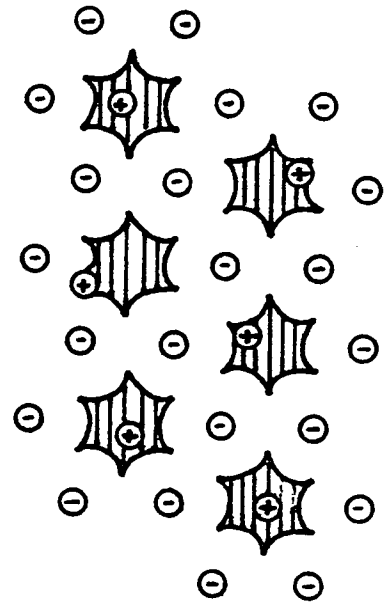

Figure 5.2.4 Model of the Stern layer of SDS at the level of the centres of the fixed sulphate groups.

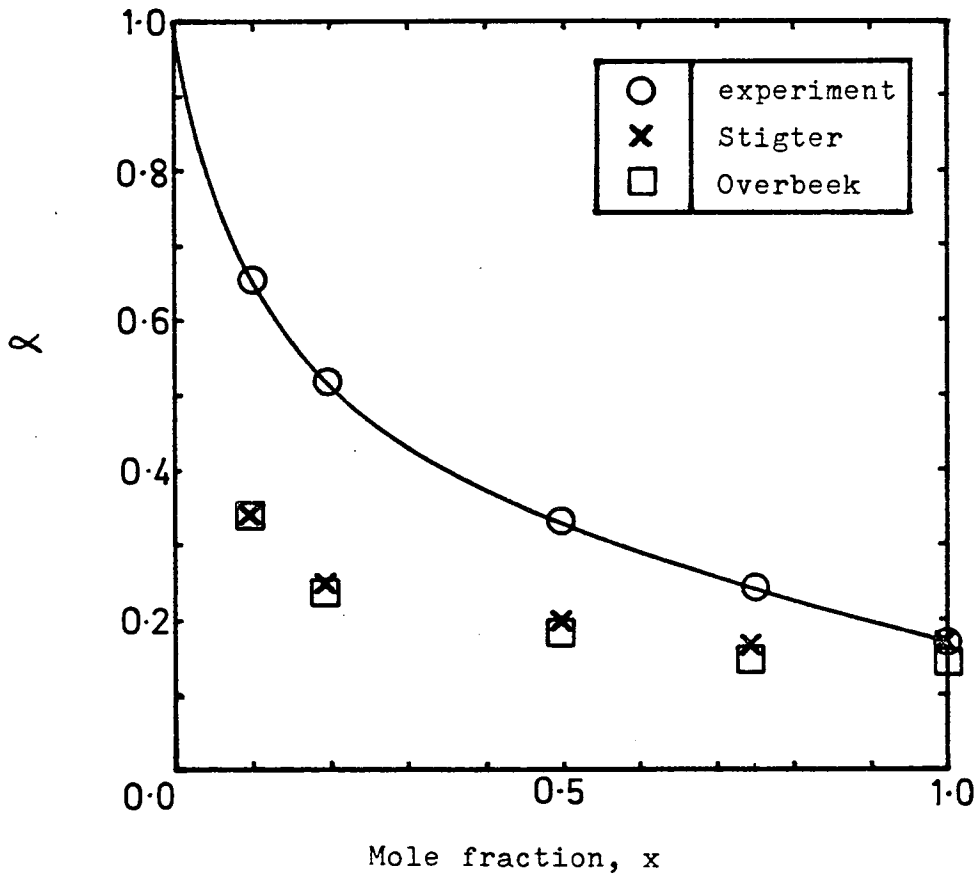

Figure 5.2.5 Plot of α against x for CTAB / $C_{12}E_6$ solutions in water at 298 K - comparison of experimental results and the predictions of the theories of Stigter and Overbeek.

of Hückel,[146] Smoluchowski[55] and Henry[56] are not applicable to micelles of small dimensions and high surface charge, but more recent methods, including those of Loeb, Wiersema and Overbeek,[59] and O'Brien and White[86] are more comprehensive and cover the required range of experimental parameters.

Loeb, Wiersema and Overbeek used the model of figure 3.2.1 and section 3.2 to construct and solve a set of equations relating electrophoretic mobility and zeta potential. The required parameters are listed below

$$E = \frac{6\pi\eta eu}{\epsilon kT}$$

z_+ , z_-

$$q_o = \frac{\kappa a}{\lambda} \quad \text{where } \lambda^2 = \frac{z_+ + z_-}{2z_-}$$

$$y_o = \frac{e\zeta}{KT}$$

$$m_{\pm} = \frac{\epsilon KT}{6\pi\eta e^2} f_{\pm} \quad \text{where } f_{\pm} = Ne^2 \frac{z_{\pm}}{\lambda^o_{\pm}}$$

where λ^o is the limiting ionic conductance.
The details of the method of calculation are to be found in the original work and only a rough outline and the results are presented here (see table 5.2.6). A graph is constructed of E as a function of q_o at several constant values of y_o from which values of y_o corresponding to the experimental conditions and parameters are extracted.

Table 5.2.6 Zeta potentials of CTAB/$C_{12}E_6$ micelles as calculated by the method of Loeb, Wiersema and Overbeek[59]

x	$10^4 u/cm^2V^{-1}s^{-1}$	E	κa	y_o	ζ/mV
1.0	4.98	3.736	0.31	4.387	113.0
0.75	4.40	3.301	0.27	3.638	93.5
0.5	4.12	3.091	0.18	3.290	84.5
0.2	2.45	1.838	0.10	1.864	47.9
0.1	1.69	1.268	0.09	1.274	32.7

O'Brien and White[86] have derived new expressions for the forces acting on a colloidal particle and have solved the governing equations for the case of a spherical particle. This method is more flexible than the Wiersema graphs and is free of the high zeta potential convergence difficulties encountered in the Wiersema approach. Numerical solutions are available using a computer program supplied by the authors or alternatively a graphical method very similar to that of Loeb, Wiersema and Overbeek can be used if precision is not vital. A graph of E against y_o at several constant values of κa is provided for this purpose.

In general the two methods yield the same results to within the accuracy of the graphical method although if the zeta potentials were only slightly higher, over 125 mV, the first method would be expected to fail and use of the method of O'Brien and White would be necessary. For comparison, zeta potentials calculated by the latter method are shown in table 5.2.7.

Table 5.2.7 Zeta potentials of CTAB/$C_{12}E_6$ micelles calculated by the method of O'Brien and White[86]

x	y_o	ζ/mV	% difference from results of table 5.2.6
1.0	4.513	115.9	2.5
0.75	3.704	95.1	1.7
0.5	3.322	85.3	0.9
0.2	1.889	48.5	1.2
0.1	1.294	33.2	1.5

To obtain values of α from the estimated zeta potentials the charge, Q on the micelle must first be evaluated and then α calculated using equation 5.2.12

$$\alpha = \frac{Q}{xn} \qquad \ldots\ldots 5.2.12$$

Two approximate solutions to the charge problem have been used here which yield similar results.

A) Stigter's Method

The details of this method are given in appendix 1 of reference 41 and the expression for the charge is

$$Q = \frac{a\varepsilon\zeta}{e} \beta(1 + \kappa a) \quad \ldots\ldots 5.2.13$$

where β is given by the expression

$$D_Q(y_o,\kappa a) = \frac{\beta(y_o,\kappa a) - 1}{\beta_f(y_o) - 1} \quad \ldots\ldots 5.2.14$$

A graph of D_Q against κa for several values of y_o is plotted so that the ratio of equation 5.2.14 can be evaluated. Substituting for β_f

$$\beta_f = \frac{2kT}{e\zeta} \sin h \frac{e\zeta}{2kT} \quad \ldots\ldots 5.2.15$$

$$Q = \frac{a\varepsilon\zeta}{e} (1 + \kappa a)\left[\left(\frac{2kT}{e\zeta} \sin h \frac{e\zeta}{2kT} - 1\right)D + 1\right] \quad \ldots\ldots 5.2.16$$

B) Overbeek's Method

The expression for the charge density σ was given by Overbeek[147]

$$\sigma = \frac{\varepsilon kT\kappa}{4\pi e}\left[2 \sin h \frac{e\zeta}{kT} + \frac{4}{\kappa a} \tan h \frac{e\zeta}{4kT}\right] \quad \ldots\ldots 5.2.17$$

For a spherical micelle $Q = 4\pi a^2\sigma$

$$\therefore Q = \frac{\varepsilon kT\kappa a^2}{e}\left[2 \sin h \frac{e\zeta}{kT} + \frac{4}{\kappa a} \tan h \frac{e\zeta}{4kT}\right] \quad \ldots\ldots 5.2.18$$

It is to be noted that both methods are best applied in the range $\kappa a > 1$ and for CTAB/$C_{12}E_6$ micelles κa is less than 0.4 but the error involved is probably not great. Results are presented in table 5.2.8.

Table 5.2.8 Charge on CTAB/$C_{12}E_6$ micelles as calculated by the methods of Stigter and Overbeek

x	$y_o = \frac{e\zeta}{kT}$	$Q_{Stigter}$	$Q_{Overbeek}$	$n_i = 180x$	$\alpha_{Stigter}$	$\alpha_{Overbeek}$
1.0	4.387	29.9	26.1	180	0.166	0.145
0.75	3.638	22.3	19.4	135	0.165	0.144
0.5	3.290	18.0	16.0	90	0.200	0.178
0.2	1.864	9.0	8.5	36	0.250	0.236
0.1	1.274	6.1	6.1	18	0.339	0.341

As discussed in section 5.1.2 methods of calculating n are varied and often ambiguous but the value of n chosen here for simplicity is 180 for all x. Results are plotted graphically in figure 5.2.5. Both approaches produce the same trends in α with x but neither agrees quantitatively with experiment. One possible reason is the miscalculation of n and in table 5.2.9 the values of n required to satisfy equation 5.2.12, where α is the experimental value and Q is the calculated value of table 5.2.8, are given.

Table 5.2.9 Aggregation numbers of CTAB/$C_{12}E_6$ micelles calculated from charge and α

x	Stigter's calculation		Overbeek's calculation		Deviation from n = 180	
	n_{ionic}	n_{total}	n_{ionic}	n_{total}	Stigter	Overbeek
1.0	180	180	157	157	0	-23
0.75	90	120	79	105	-60	-75
0.5	54	108	48	96	-72	-84
0.2	17	87	16	82	-93	-98
0.1	9	93	9	94	-87	-96

The question of whether or not these calculated values of n are reasonable on the basis that the hydrodynamic radii of micelles of all compositions are 31.4Å, now arises. Leaving aside the complication that the micelles are ellipsoidal and assuming a spherical shape of volume $V = 4/3\ (31.4Å)^3$, consider the size of the hydrocarbon cores of micelles with aggregation numbers n_{total}(Stigter). The mass of the core is given by

$$M = 225xn + 169(1 - x)n \qquad \ldots\ldots 5.2.19$$

and the volume of the core, V' is

$$V' = d/M \qquad \ldots\ldots 5.2.20$$

where d is the density and is equal to 0.8 g cm^{-3}. From V' the equivalent spherical core radius is calculated and

the difference $\Delta V = V - V'$ is taken to be the volume occupied by the head groups. From the data at x = 1 the volume per ionic head group is calculated to be 152.7 $cm^3 mol^{-1}$ and the contribution to the volume of the ionic head groups V" in each micelle of different composition can be calculated as 152.7 xn $cm^3 mol^{-1}$. The remaining volume which is equal to V - V' - V" is then the volume occupied by the nonionic head groups. The density of this nonionic head group region is then calculated as

$$(1 - x)n\ 281/(V - V' - V")$$

where 281 g mol^{-1} is the molecular weight of the E_6 portion. The results of these calculations are shown in table 5.2.10.

Table 5.2.10 Calculated densities of nonionic head group regions of $CTAB/C_{12}E_6$ micelles

x	n_{total} Stigter	Core weight/ g mol^{-1}	Core volume/ $cm^3 mol^{-1}$	equiv. core radius/Å	$\Delta V=V-V'$	V-V'-V"	density
1.0	180	40500	50630	27.2	27480	0	-
0.75	120	25320	31650	23.2	46460	32710	0.258
0.5	108	21280	26600	21.9	51510	43270	0.351
0.2	87	15680	19600	19.8	58510	55850	0.350
0.1	93	16240	20300	20.0	57810	56390	0.417

Figure 5.2.6 illustrates the cross sections of mixed micelles described above. The densities of the nonionic head group regions vary between 0.26 and 0.42 g cm^{-3} and are never as

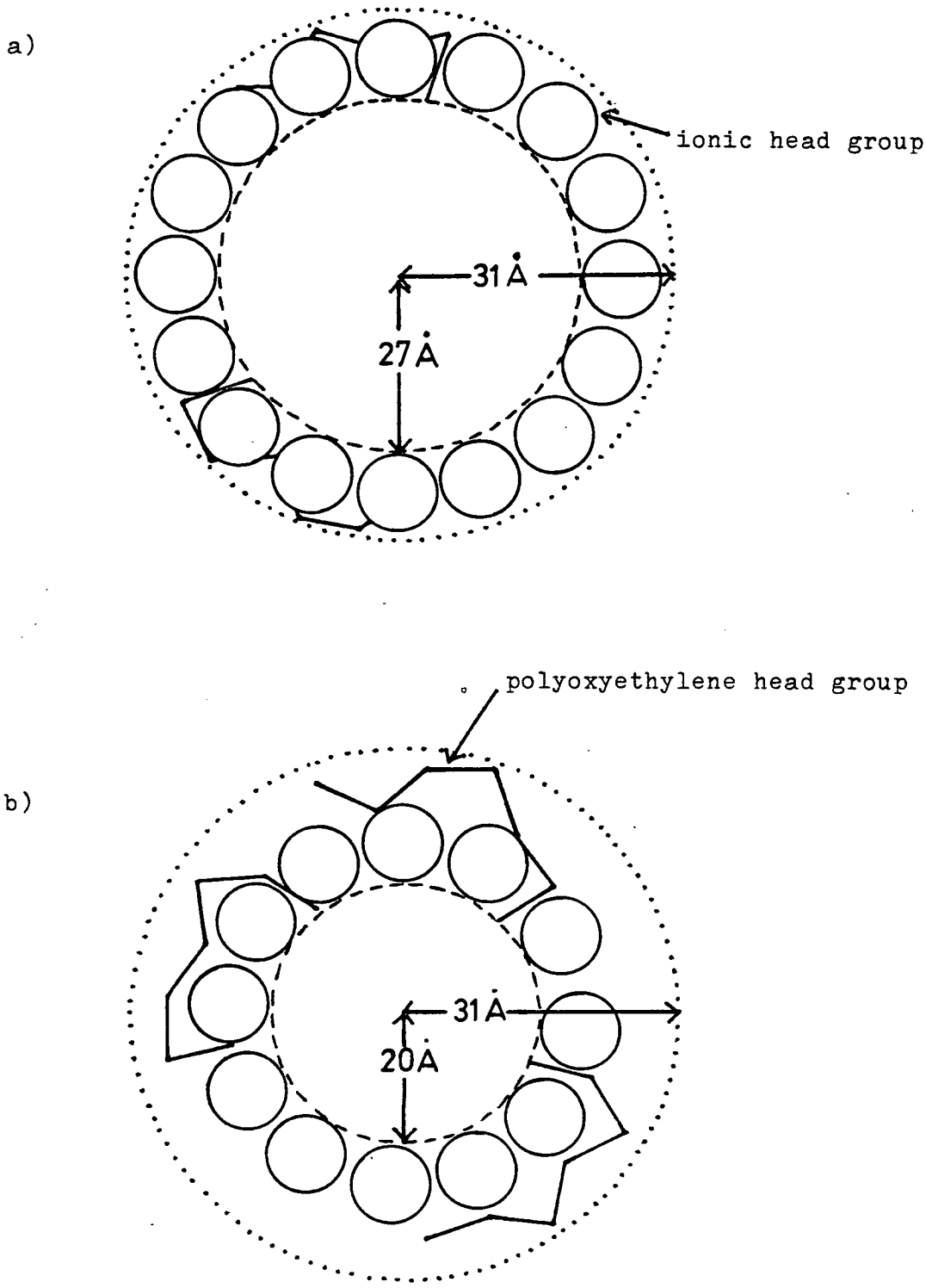

Figure 5.2.6 Two possible cross sections of mixed micelles, showing limits of the head group regions.

high as the density of the hydrocarbon core (0.8 g cm^{-3}). This is to be expected as the polyoxyethylene chains are hydrophilic due to the presence of the ether oxygens and the chains must be heavily hydrated, thereby reducing their density. At low x the chains are more constricted as their concentration increases at the micelle surface and they form a denser layer around the micelle. In general they appear to extend a distance of approximately 10 to 11 Å from the hydrocarbon core surface which fits in well with the staggered conformation shown in figure 5.1.18.

It is instructive to consider the charge densities at the surface of the two types of micelle

A) n is fixed at 180

B) n varies according to the values of table 5.2.9.(Stigter) and results are illustrated in figure 5.2.7. In the first case the charge density rises rapidly with increasing x then levels off above x = 0.5 and in the second case the charge density increases steadily with x. For SDS, α has been claculated from Stigter's[41] electrophoretic mobility data at the c.m.c., at 298 K.

Thus for $u_{c.m.c.}$ = 4.55×10^{-4} cm^2 V^{-1} s^{-1}

and κa = 0.61

the calculated zeta potential is 113 mV and the micellar charge 27.7. The only problem remaining in the determination of α concerns the choice of aggregation number to insert in

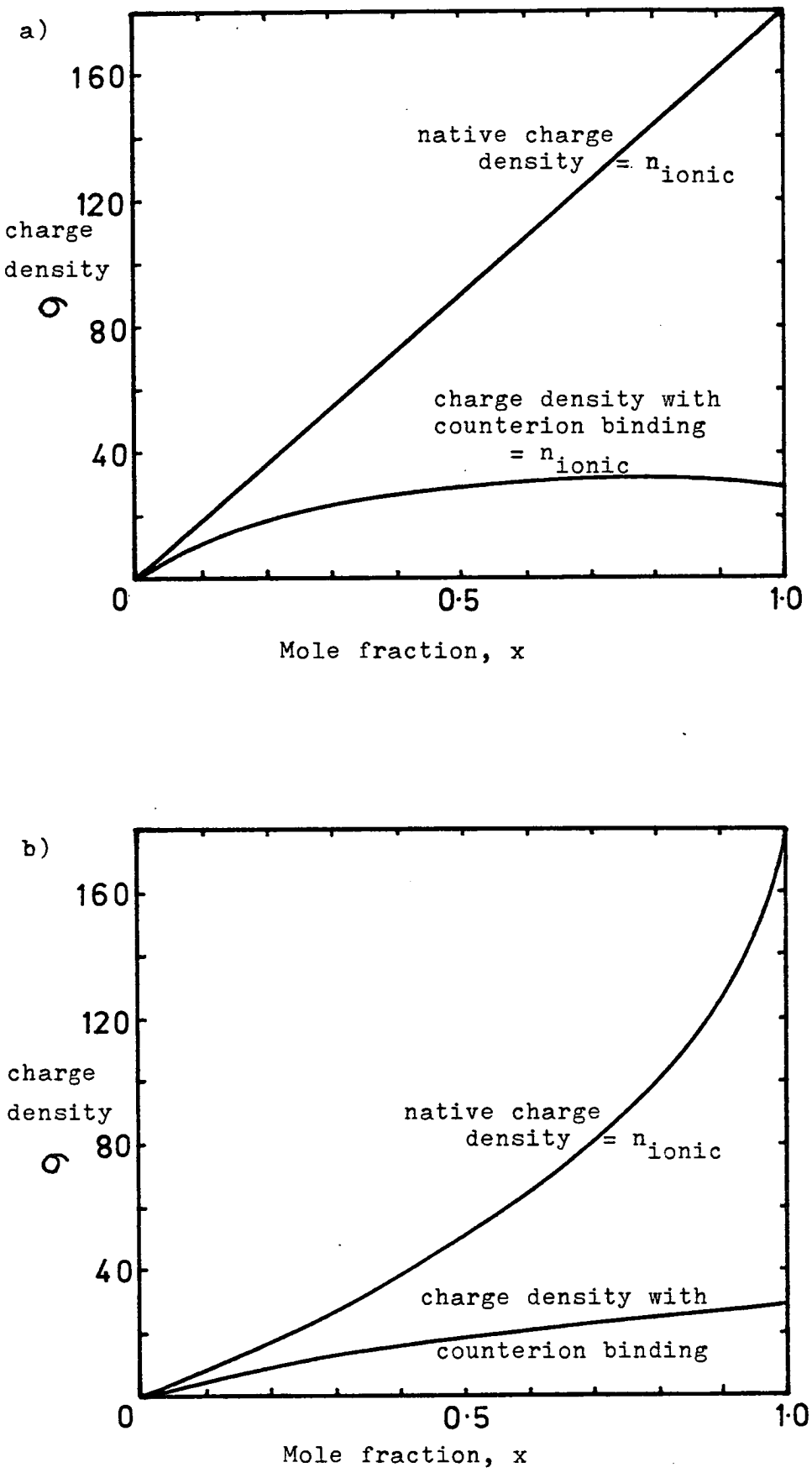

Figure 5.2.7 Plot of charge density, σ against mole fraction.

equation 5.2.12. Stigter's latest estimation[44] of n is 64.4 but the present study suggests a value of nearer 100 using the diffusion data. These values of n produce the results $\alpha = 0.430$ and $\alpha = 0.277$ respectively.

(E) Stigter's Conductivity Treatment[44]

Stigter's method of determining α from conductivity and mobility measurements outlined in section 2.1.8 can in theory be applied to the experimental data for CTAB but due to the invalidity at low ionic strength, (or low κa) the values of α which are produced are virtually meaningless. One example of such a calculation will suffice to illustrate this point. Using the basic conductivity equation

$$\Lambda_2 = 1000 \frac{d\kappa_{sp}}{dc} (1 + A_1 c_3^*) - A_1 c_3^* \Lambda_3 \quad \ldots\ldots 2.1.39$$

and inserting the experimentally determined conductivity slopes and c.m.c. value

$$\Lambda_2 = 24.60[1 + 0.9A_1] - 93.35[0.9A_1] \quad \ldots\ldots 5.2.21$$

Then α is given by

$$\alpha = \frac{\Lambda_2}{\lambda_{coll}^{+}\lambda_{-} + \lambda_{eh}^{+}\lambda_{rel}^{+} + \lambda_{rel}^{-}} \quad \ldots\ldots 2.1.48$$

For this system κa = 0.31 and A_1 is -0.839. A_1 is a correction factor for the excluded volume occupied by the micelles and in solutions containing moderate salt concentrations would be expected to be of the order of -0.1. A value of -0.839 implies that 84% of the volume of solution is occupied by micelles and the corresponding double layer thickness is 100 Å. In such dilute solutions as are present here micelle-micelle interactions are negligible and double layer theory breaks down.

So equation 5.2.21 gives

$$\Lambda_2 = 24.60[0.245] + 70.489 \quad \text{..... 5.2.22}$$

$$\therefore \Lambda_2 = 76.52 \quad \text{..... 5.2.23}$$

The terms λ_{eh}, λ^+_{rel} and λ^-_{rel} combined are negligible

$$\therefore \alpha = \frac{\Lambda_2}{\lambda_{coll} + \lambda_-} \quad \text{..... 5.2.24}$$

$$\therefore \alpha = \frac{76.52}{78.1 + 48.0} = 0.61 \quad \text{..... 5.2.25}$$

The value of α of 0.61 is much higher than values calculated by other methods and is clearly in error due to the inapplicability of the theory for low κa.

5.2.2 Conclusions

Comparison of Methods for the calculation of α

Discounting the results of method 5.2.1(B) which are unrealistically low due to deficiencies of the basic theories

employed, and the results of method 5.2.1(E) which also suffer from an inadequate theoretical base, the methods of calculating α are compared below in table 5.2.11.

Table 5.2.11 Values of α calculated by different methods

Method	Technique	Temp/ K	Surfactant	α	
(A) Mass	conductivity	298	SDS	0.314	
Action	surface tension	291	SDS	0.339	
	conductivity	298	CTAB	0.172	
(C) Conduct-	conductivity	298	SDS	0.274	
ivity and	and mobility	298	CTAB	0.166	
mobility	and diffusion				
(D) Mobility	mobility and	298	SDS	0.277	n=64.4(Stigter)
	diffusion	298	SDS	0.430	n=100(PCS)
		298	CTAB	0.166	Stigter
		298	CTAB	0.145	Overbeek

It is immediately obvious that there is good agreement between the α values produced and it is interesting to note that thermodynamic methods and non-equilibrium studies give such similar results. This is further confirmed by comparing the CTAB/$C_{12}E_6$ data in table 5.2.1 with the data of T.J. Price[148] who measured Na^+ and Br^- ion activities in CTAB/$C_{12}E_6$/NaBr solutions in order to determine α for the mixed system. Both sets of data

are shown in figure 5.2.8. Thus it appears that all the reliable methods of determination of α are in agreement for pure surfactant systems. However,for the mixed CTAB/$C_{12}E_6$ system experimental α values do not agree with those calculated using the theories of Stigter and Overbeek, and in fact the divergence increases at low mole fractions of CTAB. Such a great discrepancy is unlikely to be due solely to inaccuracies of the theories and it is probable that the root of the problem lies in the uncertainty in the aggregation numbers. For method (C) calculated values of α do not depend directly on n, that is the calculation of α can be performed without knowledge of n (see equation 5.2.1) whereas method (D) requires a value of n for the solution of equation 5.2.12. Therefore, assuming that method (C) gives reliable results the deviations of method (D) are due mainly to inaccurate determination of n.

It is recalled that conductivity and mobility measurements were performed either in the absence of salt or in the presence of low salt concentrations, whereas it was necessary to carry out the diffusion studies from which micellar size and hence, n were derived, in the presence of moderate salt concentrations. It is well documented that in general the addition of salt causes an increase in micellar size (see section 2.1.2) and thus the diffusion coefficient results may not be applicable or consistent with other measurements. This effect could be tested by performing the diffusion studies as a function of ionic strength and of surfactant concentration and

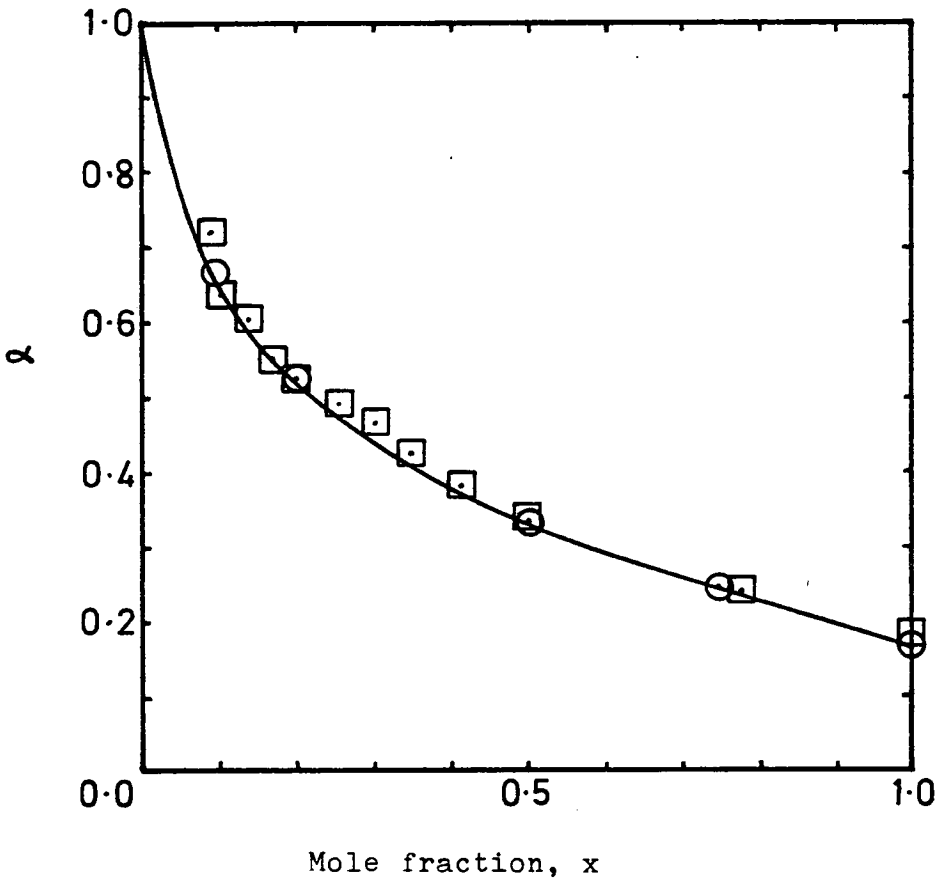

Figure 5.2.8 Plot of α against x for the system CTAB/$C_{12}E_6$ in water at 298K.

⊙ Experimental results

⊡ Data of T.J.Price[148]

extrapolating to the c.m.c. at the minimum possible ionic strength, but for reasons outlined in section 5.1.2 this is very difficult and there may not be much, if any improvement obtained. For example Rohde and Sackmann[149] have performed such a study of the change of diffusion coefficient of SDS as a function of NaCl and SDS concentration and all the lines of constant ionic strength appear to extrapolate to the same point at the c.m.c. suggesting constant micellar size independent of ionic strength, which most workers in the field would dispute. The Photon Correlation Spectroscopy technique may therefore not be well suited to the determination of micellar aggregation numbers.

An alternative way to consistently compare results of the three techniques would be to perform all experiments at the same moderate ionic strength. The accuracy of the conductivity results would therefore be reduced due to the small difference in conductivity over the concentration range but observation of the conductivity curves already constructed shows that the slopes of the κ_{sp} against concentration plots above the c.m.c. do not differ much with increasing salt concentration (see table 5.1.3, 6% decrease in slope from 0 - 10 mol dm^{-3} added salt concentration). Mobility results would be decreased by the addition of salt, for example see reference 41, and by a comparable amount to the conductivity slopes so that α may not change much as a function of ionic strength. Indeed, Method (A), which employs the Mass Action Model, is based on the assumption that α is constant and the linearity of the ln c.m.c. against ln I plots supports this.

Future Work

Some ideas for future work have already been mentioned in the text but are summarised here to present an overall view of possible extensions to the work.

Only one system has been studied thoroughly in detail, namely CTAB/$C_{12}E_6$ but even more information could be obtained to clarify the picture which has emerged so far. In section 5.1.3 it was noted that it would have been useful to have had electrophoretic mobility data at varying ionic strength to compare the effects of micelle concentration and salt concentration on the decrease in mobility with surfactant concentration. If the two effects were found to be separable then the variation of mobility with surfactant concentration and composition could be analysed in terms of micelle-micelle interactions or simple salt effects.

An improved method of determination of micellar aggregation numbers would be invaluable to the study of any pure or mixed system. In addition to diffusion coefficients, sedimentation coefficients could be determined and the intensity of scattered light as a function of scattering angle could be measured to provide information on the interactions in surfactant solutions as described in section 5.1.2.

Conductance data have been obtained for the system SDS/C_8E_4 and determinations of electrophoretic mobility comparable to those for CTAB/$C_{12}E_6$ could be made. It

would then be possible to compare an anionic/nonionic and cationic/nonionic system and perhaps correlate differences with the different types of interaction between the polyoxyethylene chains and the charged head groups. It is interesting to note from figure 5.1.15 that the slopes of the $d\kappa_{sp}/dc$ against x plot are virtually identical for the two systems but the reason for this is by no means obvious and could be coincidence. However, since the mobility against x plots are likely to be of the same form it may indicate that the α against x plot for SDS/C_8E_4 is similar to that for CTAB/$C_{12}E_6$.

On a wider basis it would be possible to change other parameters of the mixed system and study the variation in behaviour. For example substitution of the Br^- anion for Cl^- is known to change the shape of CTA^+ micelles from ellipsoidal or cylindrical to spheroidal and it would be interesting to note the effect of added nonionic surfactant on the shape and size of the micelles, bearing in mind that the pure nonionic and nonionic rich micelles are not likely to be spheroidal. It would also be possible to vary the length of the polyoxyethylene chain without fundamentally altering the types of interaction present in the micelle. There is indication, however, that $C_{12}E_8$ behaves differently from $C_{12}E_6$ in its manner of aggregation at moderate concentrations (see section 5.1.2) so CTAB and $C_{12}E_8$ may form a different type of micelle at low ionic mole fractions from CTAB and $C_{12}E_6$ mixtures.

More drastic alterations of the components could involve the replacement of the ionic head group $-N^+Me_3$ by either $-N^+H_3$ or $-N^+Et_3$ and by alteration of the size of the head group, the counterion binding would undoubtedly differ.

REFERENCES

1. J.N. Phillips, Trans.Faraday Soc., 1955, 51, 561.
2. P. Mukerjee, K.J. Mysels, 'Critical Micelle Concentrations of Aqueous Surfactant Systems', Nat.Stand.Ref.Data Ser., Nat.Bur.Stand. U.S., 36, 1971.
3. C. Tanford in 'The Hydrophobic Effect', Wiley Interscience, U.S., 1973.
4. D. Stigter, J.Phys.Chem., 1964, 68, 3603.
5. J.W. McBain, Trans. Faraday Soc., 1913, 9, 99.
6. P. Mukerjee, Adv.Colloid Interface Sci., 1967, 1, 241.
7. F. Franks (ed.), 'Water - A Comprehensive Treatise, Vol. 4', Plenum Press, New York, 1975.
8. M.J. Schick (ed.), Surfactant Science Series, Vol.2, 'Nonionic Surfactants', Marcel Dekker Inc., New York, 1967.
9. H. Wennerström, B. Lindman, Physics Reports, 1979, 52, 1.
10. G.S. Hartley, 'Aqueous Solutions of Paraffin Chain Salts', Hermann et Cie, Paris, 1936.
11. E.R. Jones, C.R. Bury, Philos.Mag.,1927, 4, 841.
12. J.M. Corkill, J.F. Goodman, T. Walker, J. Wyer, Proc.R.Soc.,Ser.A, 1969, A312, 243.
13. K. Shinoda, T. Nakagawa, B. Tamamushi, T. Isemura, 'Colloidal Surfactants', Academic Press, New York, 1963.
14. J.T. Davies, E.K. Rideal, 'Interfacial Phenomena', Academic Press, New York, 1961.

15. T.L. Hill, 'Thermodynamics of Small Systems', Benjamin, New York, 1964.

16. D.G. Hall, B.A. Pethica, in reference 8, chapter 16.

17. G.C. Kresheck, E. Hamori, G. Davenport, H.A. Scheraga, J.Am.Chem.Soc., 1966, 88, 246.

18. P.F. Minjlieff, R. Ditmarsch, Nature, 1965, 208, 889.

19. J. Lang, J.J. Auborn, E.M. Eyring, J.Colloid Interface Sci., 1972, 41, 484.

20. E.A.G. Aniansson, S.N. Wall, J.Phys.Chem., 1974, 78, 1024.

21. H. Helmholtz, Ann.Physik., 1879, 7, 337.

22. G. Gouy, J.Phys., 1910, 9, 457.

23. D.L. Chapman, Philos.Mag., 1913, 25, 475.

24. O. Stern, Z.Elektrochem., 1924, 30, 508.

25. I. Langmuir, J.Am.Chem.Soc., 1918, 40, 1361.

26. G.S. Hartley, J.Chem.Soc., 1938, 1968.

27. L. Benjamin, J.Phys.Chem., 1966, 70, 3790.

28. A.S. Waggoner, A.D. Keith, O.H. Griffith, J.Phys.Chem., 1968, 72, 4129.

29. S. Levine, G.M. Bell, B.A. Pethica, J.Chem.Phys., 1964, 40, 2304.

30. P. Mukerjee, A.Y.S. Yang, J.Phys.Chem., 1976, 80, 1388.

31. A. Ray, G. Némethy, J.Am.Chem.Soc., 1971, 93, 6787.

32. P.H. Elworthy, A.T. Florence, C.B. MacFarlane, 'Solubilisation by Surface Active Agents', Chapman and Hall, London, 1968.

33. W.B. Gogarty, U.S. P. 3495661, 1970.

34. I.J. Lin, Israel J. Technol., 1971, 9, 621.

35. J.H. Fendler, E.J. Fendler, 'Catalysis in Micellar and Macromolecular Systems', Academic Press, New York, 1975.

36. K.J. Mysels, J.Colloid Sci., 1955, 10, 507.

37. E.W. Anacker, R.M. Rush, J.S. Johnson, J.Phys.Chem., 1964, 68, 81.

38. T. Gilanyi, Acta Chem.Scand., 1973, 27, 729.

39. C. Botré, V.L. Crescenzi, A. Mele, J.Phys.Chem., 1959, 63, 650.

40. L. Shedlovsky, C.W. Jakob, M.B. Epstein, J.Phys.Chem., 1963, 67, 2075.

41. D. Stigter, K.J. Mysels, J.Phys.Chem., 1955, 59, 45.

42. D. Stigter, J.Colloid Interface Sci., 1967, 23, 379.

43. D. Stigter, J.Phys.Chem., 1979, 83, 1663.

44. D. Stigter, J.Phys.Chem., 1979, 83, 1670.

45. J. Clifford, B.A. Pethica, Trans.Faraday Soc., 1964, 60, 216.

46. K.J. Mysels, C.I.Dulin, J.Colloid Sci., 1955, 10, 461.

47. M.L. Corrin, J.Colloid Sci., 1948, 3, 333.

48. P. Debye, J.App.Phys., 1946, 17, 392.

49. W. Prins, J.J. Hermans, Proc.Kon.Neder.Akad.Wet., 1956, B59, 298.

50. K.J. Mysels, L.H. Princen, J.Phys.Chem., 1959, 63, 1696.

51. H. Gustavsson, B. Lindman, J.Am.Chem.Soc., 1975, 97, 3923.

52. H.C. Evans, J.Chem.Soc., 1956, 579.

53. G.G. Stokes, Trans.Camb.Phil.Soc., 1845, VIII, 287.

54. G.S. Hartley, B. Collie, C.S. Samis, Trans. Faraday Soc., 1936, 32, 795.

55. M. Smoluchowski, Z.Physik.Chem., 1918, 93, 129.

56. D.C. Henry, Proc.R.Soc.London.Ser.A., 1931, A133, 106.

57. F. Booth, Proc.R.Soc.(London), 1950, A203, 514.

58. J.Th.G. Overbeek, Koll.Beih., 1943, 54, 316, Thesis, Utrecht, 1941.

59. P.H. Wiersema, A.L. Loeb, J.Th.G. Overbeek, J.Colloid Sci., 1966, 22, 78.

60. W.G. McMillan, J.E. Mayer, J.Chem.Phys., 1945, 13, 276.

61. D. Stigter, T.L. Hill, J.Phys.Chem., 1959, 63, 551.

62. T. Nakagawa, H. Inoue, Nippon Kagaku Zasshi, 1957, 78, 636, C.A. 52, 2429h, 1958.

63. K.J. Mysels, R.J. Otter, J.Colloid Sci., 1961, 16, 462.

64. H. Lange, Kolloid Z.-Z.Polym., 1953, 131, 96.

65. H. Lange, K.H. Beck, Kolloid Z.-Z.Polym., 1973, 251, 424.

66. K. Shinoda, J.Phys.Chem., 1954, 58, 541.

67. J. Clint, J.Chem.Soc., Faraday Trans.1, 1975, 71, 1327.

68. Y. Moroi, N.Nishikido, M. Saito, R. Matuura, J.Colloid Interface Sci., 1975, 52, 356.

69. D.N. Rubingh, 'Solution Chemistry of Surfactants, Vol.1', ed. K.L. Mittal, Plenum Press, New York, 1979.

70. J.M. Corkill, J.F. Goodman, C.P. Ogden, J.R. Tate, Proc.R.Soc. London, 1963, 273, 84.

71. M.J. Schwuger, J.Colloid Interface Sci., 1973, 43, 491.

72. J.M. Corkill, J.F. Goodman, J.R. Tate, Trans.Faraday Soc., 1964, 60, 986.

73. F. Tokiwa, N. Moriyama, J.Colloid Interface Sci., 1969, 30, 338.

74. M.J. Schick, D.J. Manning, J.Am.Oil Chem.Soc., 1966, 43, 133.

75. A.S.C. Lawrence, J.T. Pearson, Trans.Faraday Soc., 1967, 63, 495.

76. K. Hayase, S. Hayano, J.Colloid Interface Sci., 1978, 63, 446.

77. J.D. Bernal, R.H. Fowler, J.Chem.Phys., 1933, 1, 515.

78. R.A. Robinson, R.H. Stokes, 'Electrolyte Solutions', Butterworths, London, 1970.

79. P. Debye, E. Hückel, Phys.Z., 1923, 24, 185.

80. N. Bjerrum, Klg.Danske Videnskab Selskab, 1926, 7, no. 9.

81. D.C. Grahame, Chem.Rev., 1947, 41, 441.

82. L. Onsager, Phys.Z., 1927, 28, 277.

83. H. Falkenhagen, 'Elektrolyte', 2nd Edn., S. Hirzal Verlag, Leipzig, 1953.

84. R.M. Fuoss, F. Accascina, 'Electrolytic Conductance', Interscience, New York, 1959.

85. E. Pitts, Proc.R.Soc. London, 1953, A217, 43.

86. R.W. O'Brien, L.R. White, J.Chem.Soc., Faraday Trans.2, 1978, 74, 1607.

87. M. Miura, M. Kodama, Bull.Chem.Soc.Jpn., 1972, 45, 428.

88. P.H. Elworthy, K.J. Mysels, J.Colloid Sci., 1966, 21, 331.

89. B.D. Flockhart, J.Colloid Sci., 1961, 16, 484.

90. P. Mukerjee, P. Kapauan, H.G. Meyer, J.Phys.Chem., 1966, 70, 783.

91. M.J. Schick, J.Am.Oil Chem.Soc., 1966, 43, 681.

92. M. Czerniawski, Roczn.Chem., 1966, 40, 1935.

93. A.B. Scott, H.V. Tartar, J.Am.Chem.Soc., 1943, 65, 692.

94. H.N. Singh, S. Singh, D.S. Mahalwar, J.Colloid Interface Sci., 1977, 59, 386.

95. G.D. Miles, J.Phys.Chem., 1945, 49, 71.

96. T. Barr, J. Oliver, W.V. Stubbings, J.Soc.Chem.Ind., 1948, 67, 45.

97. T. Shedlovsky, J.Am.Chem.Soc., 1932, 54, 1405.

98. P. Mukerjee, K.J. Mysels, C.I. Dulin, J.Phys.Chem., 1958, 62, 1390.

99. E.J. Bair, C.A. Kraus, J.Am.Chem.Soc., 1951, 73, 1129.

100. F. Kohlrausch, Wied.Ann., 1897, 60, 315.

101. G. Jones, G.M. Bollinger, J.Am.Chem.Soc., 1931, 53, 411.

102. G. Jones, R.C. Josephs, J.Am.Chem.Soc., 1928, 50, 1049.

103. Reference 78, chapter 4.

104. D.A. MacInnes, L.G. Longsworth, Chem.Rev., 1932, 11, 171.

105. G.S. Hartley, E. Drew, B. Collie, Trans.Faraday Soc., 1934, 30, 648.

106. A. Tiselius, Trans.Faraday Soc., 1937, 33, 524.

107. A.P. Brady, J.Am.Chem.Soc., 1948, 70, 911.

108. H.W. Hoyer, K.J. Mysels, D. Stigter, J.Phys.Chem., 1954, 58, 385.

109. K.J. Mysels, J.Colloid Interface Sci., 1967, 23, 474.

110. A. Einstein, Ann.Physik., 1906, 19, 371.

111. M. Von Smoluchowski, Ann. Physik., 1906, 21, 756.

112. H.Z. Cummins, E.R. Pike, (ed.), 'Photon Correlation Spectroscopy and Velocimetry', Plenum Press, 1977.

113. K.J. Randle, Chemistry and Industry, 1980, 74.

114. A.W. Adamson, 'Physical Chemistry of Surfaces', 2nd edn., page 21, Interscience/John Wiley, New York, 1967.

115. W.D. Harkins, F.E. Brown, J.Am.Chem.Soc., 1919, 41, 499.

116. G.D. Parfitt, A.L. Smith, J.Phys.Chem., 1962, 66, 942.

117. R.M. Fuoss, L. Onsager, J.Phys.Chem., 1957, 61, 668.

118. R.M. Fuoss, L. Onsager, J.Phys.Chem., 1958, 62, 1339.

119. B.D. Flockhart, J.Colloid Sci., 1961, 16, 484.

120. E.D. Goddard, G.C. Benson, Can.J.Chem., 1957, 35, 986.

121. J.E. Adderson, H. Taylor, J.Colloid Sci., 1964, 19, 495.

122. A.W. Ralston, D.N. Eggenberger, J.Am.Chem.Soc., 1948, 70, 436.

123. P. Mukerjee, K.J. Mysels, P. Kapauan, J.Phys.Chem., 1967, 71, 4166.

124. J.W. Larsen, L.J. Magid, J.Am.Chem.Soc., 1974, 96, 5774.

125. F. Reiss-Husson, V. Luzzati, J.Phys.Chem., 1964, 68, 3504.

126. J. Ulmius, B. Lindman, G. Lindblom, T. Drakenberg, J.Colloid Interface Sci., 1978, 65, 88.

127. M. Algren, J.E. Löfroth, R. Rydholm, Chem.Phys.Lett., 1979, 63, 265.

128. P. Ekwall, L. Mandell, K. Fontell, J.Colloid Interface Sci., 1969, 29, 639.

129. M.J. Stephen, J.Chem.Phys., 1971, 55, 3878.

130. A. Rohde, E. Sackmann, J.Colloid Interface Sci., 1979, 70, 494.

131. P.N. Pusey, 'Photon Correlation and Light Beating Spectroscopy', Cummins, Pike, (ed.), Nato Adv. Study Institutes Series B3, 1973.

132. N.A. Mazer, G.B. Benedek, M.C. Carey, J.Phys.Chem., 1976, 80, 1075.

133. G.N. Krykova, Deposited Document 1978, VINITI 1805-78, 83-7, C.A. 92:135831s.

134. M. Corti, V. Degiorgio, Chem.Phys.Lett., 1978, 53, 237.

135. C. Tanford, Y. Nozaki, M.F. Rohde, J.Phys.Chem., 1977, 81, 1555.

136. M. Rösch, Kolloid-Z., 1957, 150, 153.

137. M.N. Jones, J.Colloid Interface Sci., 1967, 23, 36.

138. D. Stigter, 'Electromagnetic Scattering', M. Kerker, (ed.), Pergammon Press, London, 1963, page 303.

139. H.F. Huisman, Proc.Koninkl.Ned.Akad.Wetenschap, 1964, 67B, 367, 376, 388, 407.

140. H. Coll, J.Phys.Chem., 1970, 74, 520.

141. H.J.L. Trap, J.J. Hermans, Proc.Kononkl.Ned.Akad.Wetenschap, 1955, 58B, 97.

142. D. Attwood, P.H. Elworthy, S.B. Kayne, J.Phys.Chem., 1970, 74, 3529.

143. K.S. Birdi, Kolloid-Z.u.Z.Polymere, 1972, 250, 731.

144. G.S. Manning, J.Chem.Phys., 1969, 51, 924.

145. D. Stigter, J.Phys.Chem., 1975, 79, 1008.

146. E. Hückel, Physik Z., 1924, 25, 204.

147. A.L. Loeb, J.Th.G. Overbeek, P.H. Wiersema, 'The Electrical Double Layer Around a Spherical Colloid Particle', M.I.T. Press, Cambridge, 1961.

148. T.J. Price, to be published.

149. A. Rohde, E. Sackmann, J.Phys.Chem., 1980, 84, 1598.

APPENDIX 1

Conductance Data

I - SDS

(i) 298K

(A) SDS in water at 298K

concentration/ mol m^{-3}	$10^4 \kappa_{sp}$/ $cm^{-1}\Omega^{-1}$
0.495	0.354
0.856	0.605
0.981	0.692
1.529	1.066
2.092	1.447
2.368	1.630
2.858	1.962
2.920	2.006
3.272	2.242
3.995	2.727
4.522	3.065
4.683	3.179
5.356	3.624
5.358	3.625
5.733	3.876
6.354	4.281
6.448	4.352
6.489	4.359
7.267	4.869
7.327	4.918
7.419	4.972

concentration/ mol m^{-3}	$10^4 \kappa_{sp}$/ $cm^{-1}\Omega^{-1}$
7.890	5.272
8.294	5.480
8.794	5.676
9.019	5.729
9.188	5.785
9.305	5.822
9.896	5.977
9.955	5.981
10.15	6.040
10.63	6.154
10.722	6.182
11.40	6.357
11.49	6.371
12.065	6.510
12.57	6.639
12.97	6.717
13.251	6.799
14.23	7.042
15.46	7.344
15.684	7.395

(B) SDS in 1.0 mol m^{-3} NaCl solution at 298K

concentration/ mol m^{-3}	10^4 κ_{sp}/ $cm^{-1}\Omega^{-1}$
0.00	1.240
1.131	2.004
2.143	2.686
3.234	3.409
4.094	3.985
5.147	4.670
5.878	5.155
6.896	5.809
7.516	6.205

concentration/ mol m^{-3}	10^4 κ_{sp}/ $cm^{-1}\Omega^{-1}$
8.501	6.619
9.024	6.766
9.978	7.019
10.42	7.129
11.34	7.360
11.71	7.452
12.61	7.670
13.78	7.957
14.88	8.226

(C) SDS in 2.5 mol m^{-3} NaCl solution at 298K

concentration/ mol m^{-3}	10^4 κ_{sp}/ $cm^{-1}\Omega^{-1}$
0.00	3.043
1.238	3.861
2.065	4.408
3.515	5.350
3.942	5.632
4.564	6.026
5.658	6.734
6.505	7.267
7.231	7.709
8.263	8.058
8.679	8.177
9.081	8.274

concentration/ mol m^{-3}	10^4 κ_{sp}/ $cm^{-1}\Omega^{-1}$
9.862	8.470
10.02	8.512
11.25	8.812
11.32	8.824
12.41	9.090
12.66	9.149
13.48	9.350
13.89	9.446
14.48	9.586
15.03	9.720
16.09	9.973

(D) SDS in 5.0 mol m^{-3} NaCl solution at 298K

concentration/ mol m^{-3}	10^4 κ_{sp}/ $cm^{-1}\Omega^{-1}$
0.00	6.016
1.187	6.780
1.964	7.268
2.309	7.497
3.755	8.405
4.380	8.808
5.393	9.439
6.247	9.967
6.899	10.247
7.114	10.320
7.940	10.550
8.286	10.633

concentration/ mol m^{-3}	10^4 κ_{sp}/ $cm^{-1}\Omega^{-1}$
8.728	10.749
9.570	10.945
10.20	11.107
10.76	11.239
11.55	11.425
11.87	11.497
12.18	11.574
12.90	11.741
13.38	11.855
13.87	11.969
14.48	12.117
15.50	12.358

(E) SDS in 10.0 mol m^{-3} NaCl solution at 298K

concentration/ mol m^{-3}	10^4 κ_{sp}/ $cm^{-1}\Omega^{-1}$
0.00	11.832
1.424	12.710
2.205	13.168
2.763	13.520
3.573	14.018
4.027	14.290
4.212	14.391
5.220	15.080
6.048	15.285
6.640	15.445
7.732	15.703
9.283	16.069

concentration/ mol m^{-3}	10^4 κ_{sp}/ $cm^{-1}\Omega^{-1}$
9.303	16.072
10.72	16.400
11.64	16.612
12.04	16.709
13.28	16.995
13.70	17.090
14.43	17.261
15.50	17.509
15.53	17.519
17.17	17.898
18.65	18.251
19.99	18.569
21.21	18.860

(ii) 288K

(A) SDS in water at 288K

concentration/ mol m^{-3}	$10^4 \kappa_{sp}$/ $cm^{-1}\Omega^{-1}$
0.652	0.365
1.277	0.703
2.735	1.486
3.454	1.866
4.059	2.184
5.266	2.810
6.373	3.380
6.584	3.482
7.390	3.899

concentration/ mol m^{-3}	$10^4 \kappa_{sp}$/ $cm^{-1}\Omega^{-1}$
8.328	4.347
9.435	4.646
12.041	5.134
14.434	5.555
18.675	6.311
22.317	6.973
25.480	7.555
28.252	8.073
30.701	8.543
32.881	8.929

(B) SDS in 1.0 mol m^{-3} NaCl solution at 288K

concentration/ mol m^{-3}	$10^4 \kappa_{sp}$/ $cm^{-1}\Omega^{-1}$
0.00	1.008
1.323	1.711
2.524	2.343
3.356	2.780
4.624	3.429
5.547	3.902
6.393	4.336
6.398	4.334
7.185	4.734

concentration/ mol m^{-3}	$10^4 \kappa_{sp}$/ $cm^{-1}\Omega^{-1}$
7.916	5.076
9.153	5.403
11.673	5.867
13.983	6.280
18.069	6.998
21.571	7.630
24.606	8.198
27.261	8.693
29.604	9.120
31.687	9.512

(C) SDS in 2.5 mol m^{-3} NaCl solution at 288K

concentration/ mol m^{-3}	$10^4 \kappa_{sp}$/ $cm^{-1}\Omega^{-1}$
0.00	2.470
0.922	2.949
1.759	3.378
2.522	3.774
3.220	4.133
3.817	4.437
4.452	4.759
5.506	5.288
6.417	5.745
7.213	6.135

concentration/ mol m^{-3}	$10^4 \kappa_{sp}$/ $cm^{-1}\Omega^{-1}$
7.270	6.160
10.408	6.852
13.273	7.361
15.899	7.822
20.543	8.650
24.523	9.373
27.971	10.005
30.988	10.563
33.649	11.068
36.014	11.518

(D) SDS in 5.0 mol m^{-3} NaCl solutions at 288K

concentration/ mol m^{-3}	$10^4 \kappa_{sp}$/ $cm^{-1}\Omega^{-1}$
0.00	4.870
0.771	5.248
1.472	5.603
2.112	5.920
3.236	6.480
3.401	6.565
4.193	6.966
5.018	7.375
5.735	7.730
6.365	8.035

concentration/ mol m^{-3}	$10^4 \kappa_{sp}$/ $cm^{-1}\Omega^{-1}$
6.478	8.064
9.276	8.691
11.827	9.140
14.168	9.544
18.307	10.263
21.855	10.891
24.930	11.454
27.618	11.937
29.991	12.369
32.100	12.781

(E) SDS in 10.0 mol m^{-3} NaCl solution at 288K

concentration/ mol m^{-3}	$10^4 \kappa_{sp}$/ $cm^{-1}\Omega^{-1}$
0.00	9.526
1.045	9.961
1.992	10.494
2.854	10.902
3.112	10.989
3.643	11.279
4.367	11.625
5.035	11.942
5.651	12.186

concentration/ mol m^{-3}	$10^4 \kappa_{sp}$/ $cm^{-1}\Omega^{-1}$
5.929	12.228
8.490	12.734
10.829	13.115
12.974	13.502
16.769	14.153
20.023	14.711
22.844	15.209
25.312	15.678
27.491	16.070
29.428	16.412

(iii) 308K

(A) SDS in water at 308K

concentration/ mol m^{-3}	$10^4 \kappa_{sp}$/ $cm^{-1}\Omega^{-1}$
1.354	1.181
1.378	1.201
2.631	2.263
2.656	2.281
3.777	3.219
4.827	4.086
5.709	4.805
5.795	4.879
7.516	6.271
8.500	6.968
9.002	7.204
10.297	7.676

concentration/ mol m^{-3}	$10^4 \kappa_{sp}$/ $cm^{-1}\Omega^{-1}$
11.061	7.919
11.436	8.058
12.446	8.383
13.347	8.676
13.419	8.701
17.618	10.040
21.244	11.201
24.406	12.246
27.188	13.155
29.656	13.966
31.858	14.722

(B) SDS in 1.0 mol m^{-3} NaCl solution at 308K

concentration/ mol m^{-3}	$10^4 \kappa_{sp}$/ $cm^{-1}\Omega^{-1}$
0.00	1.521
1.182	2.517
2.259	3.410
3.143	4.135
3.244	4.226
4.148	4.972
4.981	5.644
6.002	6.458
6.465	6.841
7.746	7.828

concentration/ mol m^{-3}	$10^4 \kappa_{sp}$/ $cm^{-1}\Omega^{-1}$
8.613	8.306
8.865	8.396
11.009	9.150
13.214	9.839
17.136	11.095
20.520	12.179
23.469	13.127
26.062	13.979
28.360	14.743
30.411	15.401

(C) SDS in 2.5 mol m^{-3} NaCl solution at 308K

concentration/ mol m^{-3}	$10^4 \kappa_{sp}$/ $cm^{-1}\Omega^{-1}$
0.00	3.733
1.161	4.683
2.218	5.534
3.131	6.277
3.186	6.283
4.075	7.042
4.895	7.702
5.979	8.561
6.356	8.859
7.619	9.741

concentration/ mol m^{-3}	$10^4 \kappa_{sp}$/ $cm^{-1}\Omega^{-1}$
8.579	10.147
9.694	10.517
10.962	10.940
13.155	11.641
17.055	12.874
20.417	13.940
23.346	14.875
25.921	15.711
28.201	16.449
30.235	17.126

(D) SDS in 5.0 mol m^{-3} NaCl solution at 308K

concentration/ mol m^{-3}	$10^4 \kappa_{sp}$/ $cm^{-1}\Omega^{-1}$
0.00	7.350
1.366	8.432
2.609	9.415
2.879	9.632
3.744	10.275
4.785	11.115
5.502	11.685
5.743	11.870
7.448	12.872
7.901	13.052

concentration/ mol m^{-3}	$10^4 \kappa_{sp}$/ $cm^{-1}\Omega^{-1}$
8.919	13.379
10.104	13.771
10.201	13.761
12.134	14.405
15.751	15.536
18.876	16.491
21.604	17.376
24.007	18.147
26.138	18.832
28.042	19.441

(E) SDS in 10.0 mol m^{-3} NaCl solution at 308K

concentration/ mol m^{-3}	$10^4 \kappa_{sp}$/ $cm^{-1}\Omega^{-1}$
0.00	14.413
0.982	15.152
1.878	15.832
2.697	16.457
3.450	17.000
3.708	17.223
4.144	17.562
4.786	18.044
5.381	18.452
7.082	19.109

concentration/ mol m^{-3}	$10^4 \kappa_{sp}$/ $cm^{-1}\Omega^{-1}$
10.165	20.079
12.993	20.949
15.597	21.750
20.231	23.165
24.230	24.405
27.717	25.507
30.784	26.482
33.503	27.319
35.929	28.150

II SDS/Octanol

(A) SDS/Octanol in water at 298K; x = 0.94

SDS concentration/ mol m^{-3}	$10^4 \kappa_{sp}$/ $cm^{-1}\Omega^{-1}$
0.461	0.335
0.463	0.335
0.913	0.650
2.247	1.552
2.647	1.824
3.050	2.101
4.292	2.950
4.638	3.152
4.999	3.397
6.159	4.164
6.459	4.352
6.784	4.566

SDS concentration/ mol m^{-3}	$10^4 \kappa_{sp}$/ $cm^{-1}\Omega^{-1}$
7.871	5.084
8.131	5.178
9.447	5.620
9.672	5.660
10.90	5.998
11.10	6.054
12.25	6.358
12.42	6.406
13.50	6.681
13.65	6.728
15.01	7.022

(B) SDS/Octanol in water at 298K; x = 0.83

SDS concentration/ mol m^{-3}	$10^4 \kappa_{sp}$/ $cm^{-1}\Omega^{-1}$
0.614	0.439
1.480	1.027
2.050	1.412
2.828	1.933
3.359	2.291
4.096	2.760
5.192	3.506

SDS concentration/ mol m^{-3}	$10^4 \kappa_{sp}$/ $cm^{-1}\Omega^{-1}$
6.234	4.108
7.197	4.497
8.085	4.813
8.920	5.091
9.693	5.328
10.42	5.549
11.73	5.931

(C) SDS/Octanol in water at 298 K; x = 0.67

SDS concentration/ mol m^{-3}	$10^4 \kappa_{sp}$/ $cm^{-1}\Omega^{-1}$
0.250	0.186
0.495	0.359
0.499	0.364
0.989	0.703
1.428	0.997
2.294	1.576
3.099	2.117
3.299	2.257
3.849	2.618
4.551	3.045
5.017	3.259
5.208	3.347
5.404	3.449
5.790	3.587
5.825	3.607

SDS concentration/ mol m^{-3}	$10^4 \kappa_{sp}$/ $cm^{-1}\Omega^{-1}$
6.507	3.870
7.173	4.122
7.330	4.193
7.793	4.347
8.373	4.547
8.384	4.544
8.915	4.736
9.098	4.810
9.423	4.908
9.435	4.899
10.36	5.206
10.73	5.346
11.19	5.477
11.93	5.710
12.59	5.860

(D) SDS/Octanol in water at 298 K; x = 0.5

SDS concentration/ mol m^{-3}	$10^4 \kappa_{sp}$/ $cm^{-1}\Omega^{-1}$
0.649	0.459
0.875	0.616
1.235	0.862
1.636	1.131
1.766	1.244
2.250	1.546
2.306	1.583
2.693	1.841
2.898	1.974
3.099	2.088
3.426	2.233

SDS concentration/ mol m^{-3}	$10^4 \kappa_{sp}$/ $cm^{-1}\Omega^{-1}$
3.428	2.225
3.474	2.248
3.820	2.380
3.900	2.410
3.902	2.412
4.142	2.499
4.330	2.564
4.440	2.603
4.718	2.698
5.062	2.821
5.394	2.935

III SDS/C_8E_4

(A) SDS/C_8E_4 in water at 298 K; x = 0.83

SDS concentration/ mol m^{-3}	$10^4 \kappa_{sp}$/ $cm^{-1}\Omega^{-1}$
1.789	1.248
5.736	3.654
9.072	5.069
11.928	6.075
14.401	6.889
16.654	7.601
18.469	8.175

SDS concentration/ mol m^{-3}	$10^4 \kappa_{sp}$/ $cm^{-1}\Omega^{-1}$
20.447	8.784
21.677	9.166
23.075	9.605
24.270	9.964
26.477	10.649
28.209	11.178
31.057	12.054

(B) SDS/C_8E_4 in water at 298 K; x = 0.67

SDS concentration/ mol m^{-3}	$10^4 \kappa_{sp}$/ $cm^{-1}\Omega^{-1}$
1.918	1.330
3.694	2.439
7.614	4.363
10.926	5.739
13.761	6.882
15.475	7.525

SDS concentration/ mol m^{-3}	$10^4 \kappa_{sp}$/ $cm^{-1}\Omega^{-1}$
18.362	8.637
21.934	9.991
23.641	10.613
24.789	11.059
29.064	12.651
32.114	13.785

(C) SDS/C_8E_4 in water at 298 K; x = 0.5

SDS concentration/ mol m^{-3}	$10^4 \kappa_{sp}$/ $cm^{-1}\Omega^{-1}$
1.847	1.279
3.556	2.340
7.322	4.295
10.498	5.861
13.213	7.139
14.758	7.835

SDS concentration/ mol m^{-3}	$10^4 \kappa_{sp}$/ $cm^{-1}\Omega^{-1}$
17.611	9.131
21.019	10.664
22.571	11.349
23.738	11.875
27.803	13.657
30.698	14.935

(D) SDS/C_8E_4/water at 298 K; x = 0.25

SDS concentration/ mol m^{-3}	$10^4 \kappa_{sp}$/ $cm^{-1}\Omega^{-1}$
0.856	0.615
2.467	1.756
5.990	3.955
8.932	5.636
11.427	6.993
14.087	8.403
15.429	9.109

SDS concentration/ mol m^{-3}	$10^4 \kappa_{sp}$/ $cm^{-1}\Omega^{-1}$
17.429	10.137
18.497	10.669
19.775	11.292
20.924	11.899
22.850	12.834
24.521	13.650
27.058	14.867

IV Lithium Dodecyl Sulphate (LiDs) in water at 298 K

concentration/ mol m^{-3}	$10^4 \kappa_{sp}$/ $cm^{-1}\Omega^{-1}$
0.911	0.571
1.739	1.090
2.494	1.559
3.186	1.982
3.597	2.292
3.823	2.361
4.955	3.044
5.930	3.627
6.778	4.126
6.870	4.260
7.524	4.556
8.184	4.915

concentration/ mol m^{-3}	$10^4 \kappa_{sp}$/ $cm^{-1}\Omega^{-1}$
8.773	5.176
9.861	5.672
12.604	6.509
17.462	7.936
18.627	8.295
19.623	8.570
22.941	9.576
23.501	9.747
25.945	10.480
26.881	10.770
29.854	11.685

V CTAB

(A) CTAB in water at 298 K

concentration/ mol m^{-3}	$10^4 \kappa_{sp}$/ $cm^{-1}\Omega^{-1}$
0.126	0.140
0.249	0.257
0.370	0.372
0.487	0.486
0.518	0.516
0.602	0.598
0.715	0.703
0.932	0.885
1.140	0.959
1.339	1.014
1.531	1.066
1.976	1.174
2.749	1.361
2.971	1.413
3.394	1.519
3.529	1.545
5.212	1.937
5.265	1.934
6.672	2.242
9.162	2.798
9.489	2.830
9.696	2.874
12.533	3.481

concentration/ mol m^{-3}	$10^4 \kappa_{sp}$/ $cm^{-1}\Omega^{-1}$
13.478	3.637
14.330	3.804
16.264	4.189
16.744	4.289
18.340	4.609
18.890	4.755
19.132	4.764
19.592	4.882
19.777	4.923
21.125	5.203
21.716	5.297
22.171	5.380
23.960	5.791
24.320	5.846
25.225	6.023
25.797	6.151
27.085	6.414
28.085	6.631
29.255	6.879
30.006	7.036
31.154	7.273
33.704	7.801
35.856	8.267

(B) CTAB in 1.0 mol m^{-3} KBr solution at 298 K

concentration/ mol m^{-3}	$10^4 \kappa_{sp}$/ $cm^{-1}\Omega^{-1}$
0.00	1.511
0.094	1.603
0.185	1.682
0.273	1.765
0.358	1.849
0.376	1.858
0.440	1.923
0.596	2.053
0.743	2.111
0.744	2.110
1.072	2.206
1.101	2.207
1.468	2.300
1.792	2.374
2.172	2.464
2.450	2.521
3.080	2.661
3.620	2.788
3.681	2.793
4.257	2.919

concentration/ mol m^{-3}	$10^4 \kappa_{sp}$/ $cm^{-1}\Omega^{-1}$
4.753	3.033
4.808	3.039
4.937	3.038
5.425	3.142
5.635	3.219
6.089	3.313
6.617	3.425
7.248	3.562
8.284	3.725
9.033	3.893
12.488	4.567
13.086	4.713
15.441	5.189
16.959	5.507
17.993	5.719
20.148	6.169
20.222	6.203
22.184	6.610
26.105	7.401
30.238	8.274

(C) CTAB in 2.5 mol m^{-3} KBr solution at 298 K

concentration/ mol m^{-3}	$10^4 \kappa_{sp}$/ $cm^{-1}\Omega^{-1}$
0.00	3.712
0.054	3.765
0.107	3.812
0.160	3.850
0.211	3.891
0.261	3.946
0.359	4.027
0.453	4.061
0.488	4.077
0.543	4.091
0.631	4.120
0.693	4.120
0.836	4.170
0.953	4.200
1.369	4.289
1.397	4.295
1.650	4.326
1.822	4.384
2.228	4.469
2.617	4.547
2.990	4.629
3.347	4.701
3.691	4.775
4.021	4.848
4.511	4.908

concentration/ mol m^{-3}	$10^4 \kappa_{sp}$/ $cm^{-1}\Omega^{-1}$
4.729	4.961
4.792	5.003
5.495	5.145
6.729	5.398
7.305	5.446
7.777	5.618
8.677	5.805
8.824	5.961
9.459	5.967
9.807	5.950
12.404	6.475
14.100	6.813
15.561	7.097
17.649	7.535
18.365	7.675
20.633	8.135
22.992	8.664
23.127	8.659
23.176	8.674
26.025	9.287
27.020	9.466
29.979	10.055
30.262	10.145
33.003	10.702
35.351	11.194

(D) CTAB in 5.0 mol m^{-3} KBr solution at 298 K

concentration/ mol m^{-3}	$10^4 \kappa_{sp}$/ $cm^{-1}\Omega^{-1}$
0.00	7.316
0.069	7.378
0.138	7.443
0.204	7.499
0.252	7.500
0.270	7.526
0.334	7.549
0.459	7.586
0.498	7.574
0.579	7.611
0.695	7.618
0.864	7.651
0.968	7.679
0.973	7.669
1.426	7.765
1.449	7.760
1.706	7.817
1.859	7.847
2.272	7.929
2.668	8.008
3.047	8.077
3.410	8.136
3.759	8.217
4.094	8.273
4.315	8.310
4.876	8.434

concentration/ mol m^{-3}	$10^4 \kappa_{sp}$/ $cm^{-1}\Omega^{-1}$
5.588	8.561
5.633	8.551
6.835	8.815
7.891	9.000
8.106	9.025
8.223	9.091
8.798	9.182
9.137	9.212
9.585	9.363
11.464	9.665
12.283	9.826
14.459	10.256
15.124	10.357
18.536	11.077
19.572	11.262
20.051	11.292
23.113	11.971
23.776	12.073
24.177	12.139
26.369	12.620
27.294	12.780
27.681	12.864
30.280	13.394
30.693	13.487
30.696	13.438
32.847	13.922

(E) CTAB in 10.0 mol m^{-3} KBr solution at 298 K

concentration/ mol m^{-3}	$10^4 \kappa_{sp}$/ $cm^{-1}\Omega^{-1}$
0.00	14.364
0.007	14.386
0.014	14.362
0.021	14.399
0.035	14.393
0.048	14.396
0.062	14.416
0.074	14.396
0.087	14.446
0.118	14.471
0.174	14.484
0.232	14.504
0.459	14.551
0.782	14.537
0.896	14.629
1.312	14.719
1.710	14.775
2.089	14.851
2.968	15.007
3.759	15.161
3.997	15.160
4.361	15.244
4.474	15.292
5.124	15.418

concentration/ mol m^{-1}	$10^4 \kappa_{sp}$/ $cm^{-1}\Omega^{-1}$
5.249	15.439
6.260	15.629
6.564	15.645
7.221	15.808
7.504	15.850
7.555	15.774
7.567	15.811
8.045	15.962
8.758	16.093
10.743	16.368
13.072	16.784
13.616	16.906
15.521	17.265
17.627	17.658
18.586	17.799
19.112	17.910
21.459	18.366
21.612	18.382
22.735	18.584
24.727	18.972
24.865	18.986
26.252	19.242
29.270	19.812
30.005	19.911

VI CTAB/alcohol

(i) Octanol

(A) CTAB/Octanol in water at 298 K; x = 0.94

CTAB concentration/ mol m^{-3}	$10^4 \kappa_{sp}$/ $cm^{-1}\ \Omega^{-1}$
1.396	1.002
2.738	1.346
4.030	1.663
9.825	2.882
14.705	3.884

CTAB concentration/ mol m^{-3}	$10^4 \kappa_{sp}$/ $cm^{-1}\Omega^{-1}$
18.871	4.750
22.469	5.513
28.370	6.774
33.006	7.733

(B) CTAB/Octanol in water at 298 K; x = 0.83

CTAB concentration/ mol m^{-3}	$10^4 \kappa_{sp}$/ $cm^{-1}\Omega^{-1}$
0.371	0.348
0.734	0.631
1.788	1.025
2.451	1.212
3.416	1.457
4.016	1.599
5.449	1.928
6.267	2.113

CTAB concentration/ mol m^{-3}	$10^4 \kappa_{sp}$/ $cm^{-1}\Omega^{-1}$
6.766	2.221
7.980	2.481
8.683	2.644
10.145	2.959
12.018	3.378
13.369	3.655
16.762	4.394
21.344	5.402

(C) CTAB/Octanol in water at 298 K; x = 0.67

CTAB concentration/ mol m^{-3}	$10^4 \kappa_{sp}$/ $cm^{-1}\Omega^{-1}$
0.444	0.406
1.219	0.824
1.780	0.991
2.677	1.230
3.400	1.402
3.698	1.480
4.882	1.749
5.033	1.768
6.241	2.046

CTAB concentration/ mol m^{-3}	$10^4 \kappa_{sp}$/ $cm^{-1}\Omega^{-1}$
8.650	2.570
9.485	2.686
10.719	3.020
12.515	3.402
16.115	4.171
18.821	4.748
20.931	5.196
24.006	5.818

(ii) Dodecanol

(A) CTAB/Dodecanol in water at 298 K; x = 0.83

CTAB concentration/ mol m^{-3}	$10^4 \kappa_{sp}$/ $cm^{-1}\Omega^{-1}$
0.812	0.623
1.596	0.941
5.134	1.726
8.143	2.329
10.734	2.809
11.049	2.875

CTAB concentration/ mol m^{-3}	$10^4 \kappa_{sp}$/ $cm^{-1}\Omega^{-1}$
14.966	3.649
15.712	3.798
18.277	4.292
20.939	4.818
24.952	5.578
27.192	6.018

(B) CTAB/Dodecanol in water at 298 K; x = 0.5

CTAB concentration/ mol m^{-3}	$10^4 \kappa_{sp}$/ $cm^{-1}\Omega^{-1}$
0.835	0.414
1.638	0.643
5.252	1.229
8.305	1.563
10.918	1.797
14.966	2.111

CTAB concentration/ mol m^{-3}	$10^4 \kappa_{sp}$/ $cm^{-1}\Omega^{-1}$
15.157	2.122
18.449	2.356
21.078	2.550
25.016	2.803
26.529	2.872

(iii) Hexanol

(A) CTAB/Hexanol in water at 298 K; x = 0.83

CTAB concentration/ mol m^{-3}	$10^4 \kappa_{sp}$/ $cm^{-1}\Omega^{-1}$
1.258	0.965
2.469	1.282
3.636	1.572
8.888	2.701
12.455	3.511
13.330	3.654
17.136	4.462

CTAB concentration/ mol m^{-3}	$10^4 \kappa_{sp}$/ $cm^{-1}\Omega^{-1}$
18.388	4.804
20.435	5.195
23.320	5.839
28.128	6.895
31.974	7.731
35.120	8.445

(B) CTAB/Hexanol in water at 298 K; x = 0.5

CTAB concentration/ mol m^{-3}	$10^4 \kappa_{sp}$/ $cm^{-1}\Omega^{-1}$
0.936	0.837
1.837	1.103
2.706	1.324
6.615	2.285
9.922	3.099
12.294	3.820
12.758	3.828

CTAB concentration/ mol m^{-3}	$10^4 \kappa_{sp}$/ $cm^{-1}\Omega^{-1}$
17.365	5.038
17.525	5.158
20.948	6.018
23.815	6.856
27.181	7.743
30.505	8.679

VII $CTAB/C_{12}E_6$

(A) $CTAB/C_{12}E_6$ in water at 298 K; x = 0.83

CTAB concentration/ mol m^{-3}	$10^4 \kappa_{sp}$/ $cm^{-1}\Omega^{-1}$
0.422	0.388
0.835	0.665
1.241	0.868
2.029	1.175
4.705	1.950
8.480	2.998
11.577	3.824

CTAB concentration/ mol m^{-3}	$10^4 \kappa_{sp}$/ $cm^{-1}\Omega^{-1}$
14.162	4.523
16.353	5.107
19.866	6.049
22.558	6.766
24.687	7.320
28.465	8.306

(B) $CTAB/C_{12}E_6$ in water at 298 K; x = 0.75

CTAB concentration/ mol m^{-3}	$10^4 \kappa_{sp}$/ $cm^{-1}\Omega^{-1}$
0.763	0.634
1.496	1.001
4.799	2.136
7.590	3.014
9.980	3.745

CTAB concentration/ mol m^{-3}	$10^4 \kappa_{sp}$/ $cm^{-1}\Omega^{-1}$
13.861	4.897
16.875	5.806
19.285	6.479
22.896	7.562
25.472	8.251

(C) $CTAB/C_{12}E_6$ in water at 298 K; x = 0.5

CTAB concentration/ mol m^{-3}	$10^4 \kappa_{sp}$/ $cm^{-1}\Omega^{-1}$
0.733	0.642
1.440	1.061
2.122	1.416
3.416	2.058
4.479	2.470
6.297	3.347
8.059	4.052

CTAB concentration/ mol m^{-3}	$10^4 \kappa_{sp}$/ $cm^{-1}\Omega^{-1}$
10.986	5.235
13.424	6.208
15.485	7.013
18.782	8.307
21.301	9.249
23.289	10.04
26.226	11.11

(D) CTAB/$C_{12}E_6$ in water at 298 K; x = 0.2

CTAB concentration/ mol m^{-3}	$10^4 \kappa_{sp}$/ $cm^{-1}\Omega^{-1}$
0.717	0.679
1.408	1.208
4.508	3.348
7.123	4.947
9.370	6.242
12.980	8.233

CTAB concentration/ mol m^{-3}	$10^4 \kappa_{sp}$/ $cm^{-1}\Omega^{-1}$
13.810	8.664
15.786	9.703
17.466	10.567
18.024	10.824
21.371	12.380
23.755	13.468

(E) CTAB/$C_{12}E_6$ in water at 298 K; x = 0.1

CTAB concentration/ mol m^{-3}	$10^4 \kappa_{sp}$/ $cm^{-1}\Omega^{-1}$
0.928	0.841
1.781	1.526
3.644	2.883
5.197	3.905
6.511	4.726
7.638	5.389
8.615	5.944

CTAB concentration/ mol m^{-3}	$10^4 \kappa_{sp}$/ $cm^{-1}\Omega^{-1}$
9.470	6.415
10.895	7.111
12.035	7.774
12.969	8.236
13.747	8.612
14.405	8.935

APPENDIX 2

Surface Tension Data

I SDS

(A) SDS in water at 293 K

lnc	γ/mNm^{-1}
-	72.9
-7.571	72.0
-7.426	71.9
-6.648	68.4
-6.774	69.4
-6.301	65.2
-6.128	63.2
-5.942	60.6

lnc	γ/mNm^{-1}
-5.766	58.2
-5.527	55.8
-5.434	52.8
-5.230	48.8
-5.180	48.3
-5.040	45.3
-5.029	44.8
-4.944	43.2

lnc	γ/mNm^{-1}
-4.918	43.1
-4.739	40.5
-4.691	40.3
-4.584	39.4
-4.444	39.4
-4.296	39.2
-4.090	39.4
-3.508	38.9

(B) SDS in 10.0 mol m^{-3} NaCl solution at 295 K

lnc	γ/mNm^{-1}
-	73.23
-6.717	56.56
-6.083	49.80
-5.895	47.45
-5.585	43.26
-5.330	39.52
-5.229	38.26
-5.128	37.56
-5.123	37.49
-5.010	37.28

lnc	γ/mNm^{-1}
-4.925	37.09
-4.879	37.15
-4.850	37.21
-4.760	37.22
-4.654	37.11
-4.557	37.15
-4.328	37.31
-4.108	37.65
-3.863	37.16
-3.219	37.11

(C) SDS in 30.0 mol m^{-3} NaCl solution at 295 K

lnc	γ/mNm^{-1}
-	73.60
-6.862	51.32
-6.754	49.83
-6.545	47.35
-6.418	45.96
-6.165	42.87
-5.945	40.03
-5.862	38.55

lnc	γ/mNm^{-1}
-5.780	37.54
-5.630	36.48
-5.541	36.21
-5.470	36.02
-5.376	35.86
-5.126	35.71
-5.035	35.50
-4.716	35.56
-4.605	35.42

(D) SDS in 100.0 mol m^{-3} NaCl solution at 295 K

lnc	γ/mNm^{-1}
-	74.08
-7.556	50.89
-7.267	46.50
-7.173	45.32
-6.963	42.68
-6.930	42.03
-6.765	39.53
-6.597	37.19
-6.589	36.92

lnc	γ/mNm^{-1}
-6.476	35.75
-6.414	35.41
-6.215	34.75
-6.152	34.57
-6.069	34.47
-5.780	34.01
-5.686	34.10
-5.488	33.82
-5.047	33.53
-4.605	33.53

(E) SDS in 10.0 mol m^{-3} Na_2SO_4 solution at 290 K

lnc	γ/mNm^{-1}
-6.760	53.60
-6.432	50.06
-6.258	47.86
-6.054	45.60
-5.891	43.37
-5.653	39.96
-5.627	39.53
-5.573	38.79

lnc	γ/mNm^{-1}
-5.512	38.04
-5.434	37.33
-5.246	36.81
-5.138	36.63
-5.051	36.68
-4.874	36.52
-4.826	36.94
-4.605	36.40

(F) SDS in 33.3 mol m^{-3} Na_2SO_4 solution at 289 K

lnc	γ/mNm^{-1}
-7.439	54.21
-7.023	49.06
-6.678	44.82
-6.608	43.88
-6.357	40.38
-6.223	38.51
-6.023	36.52
-5.933	36.17

lnc	γ/mNm^{-1}
-5.876	36.02
-5.844	35.94
-5.711	35.78
-5.683	35.67
-5.638	35.75
-5.491	35.64
-5.249	35.98
-4.605	35.89

II SDS/Octanol

(A) SDS/Octanol in water at 288 K; x = 0.94

lnc	γ/mNm^{-1}
-	74.91
-6.837	69.15
-6.148	59.36
-5.865	54.37
-5.557	47.94
-5.316	42.63
-5.113	37.45
-4.997	34.67
-4.902	32.76

lnc	γ/mNm^{-1}
-4.788	32.29
-4.786	31.59
-4.695	32.72
-4.563	32.78
-4.429	33.12
-4.301	33.45
-3.940	33.55
-3.549	33.64
-2.866	33.14

(B) SDS/Octanol in water at 287 K; x = 0.83

lnc	γ/mNm^{-1}
-	75.07
-7.169	69.19
-6.485	58.65
-5.899	46.74
-5.474	36.91
-5.319	33.02
-5.228	31.07
-5.112	28.27
-4.810	26.69

lnc	γ/mNm^{-1}
-4.797	26.98
-4.600	28.00
-4.436	28.58
-4.411	28.41
-4.249	28.85
-4.107	28.64
-3.783	29.10
-3.566	29.13
-2.767	28.67

(C) SDS/Octanol in water at 287 K; x = 0.67

lnc	γ/mNm^{-1}
-	74.65
-7.240	63.26
-6.583	51.10
-6.353	46.40
-5.911	36.93
-5.657	31.18
-5.440	26.01
-5.321	23.86

lnc	γ/mNm^{-1}
-5.152	23.97
-5.070	24.59
-4.994	24.62
-4.772	24.70
-4.744	24.75
-4.611	24.86
-3.935	24.94
-2.984	24.46

(D) SDS/Octanol in water at 288 K; x = 0.5

lnc	γ/mNm^{-1}
-	73.77
-6.997	49.00
-6.735	43.95
-6.204	32.61
-6.048	29.32
-5.849	26.10
-5.655	25.85
-5.532	25.24
-5.318	24.78

lnc	γ/mNm^{-1}
-5.229	24.31
-5.091	24.24
-4.901	23.40
-4.837	23.33
-4.587	23.17
-4.478	23.15
-4.232	23.05
-3.512	23.72
-2.984	23.25

III $CTAB/C_{12}E_6$

(A) $CTAB/C_{12}E_6$ in water at 298 K; x = 1.0

lnc	γ/mNm^{-1}
-2.314	70.60
-1.628	68.02
-0.999	59.59
-0.692	53.93
-0.521	50.50

lnc	γ/mNm^{-1}
-0.358	47.11
-0.232	44.57
-0.103	42.02
-0.006	40.43
0.391	37.82

lnc	γ/mNm^{-1}
0.684	37.35
1.060	36.80
1.431	36.41
2.417	35.28

(B) $CTAB/C_{12}E_6$ in water at 298 K; x = 0.75

lnc	γ/mNm^{-1}
-2.704	70.30
-2.027	65.87
-1.753	61.86
-1.659	60.44
-1.380	56.14
-1.155	52.06

lnc	γ/mNm^{-1}
-0.904	47.15
-0.884	46.84
-0.743	44.45
-0.303	39.20
-0.235	38.76
-0.081	38.24

lnc	γ/mNm^{-1}
0.292	37.12
0.663	36.38
0.750	36.24
1.230	35.52
1.730	34.58
2.969	32.54

(C) $CTAB/C_{12}E_6$ in water at 298 K; x = 0.5

lnc	γ/mNm^{-1}
-2.347	59.81
-1.766	50.11
-1.628	47.62
-1.569	46.46

lnc	γ/mNm^{-1}
-1.418	43.83
-1.281	42.01
-0.438	37.93
0.305	36.26

lnc	γ/mNm^{-1}
0.824	35.15
1.248	34.23
1.676	33.77

(D) $CTAB/C_{12}E_6$ in water at 298 K; x = 0.2

lnc	γ/mNm^{-1}
-3.859	62.99
-3.618	59.70
-3.325	55.23
-3.015	49.06
-2.832	45.55

lnc	γ/mNm^{-1}
-2.682	42.89
-2.543	40.91
-2.403	39.55
-2.302	38.88

lnc	γ/mNm^{-1}
-1.643	36.57
-0.709	34.47
-0.582	34.18
0.601	32.26

APPENDIX 3

Electrophoretic Mobility Data

$CTAB/C_{12}E_6$ in water at 298. K

x	CTAB concentration / mol m^{-3}	$10^4 \mu$ / $cm^2 V^{-1} s^{-1}$
1.0	3.60	4.981
	8.97	4.714
	11.27	4.658
	13.99	4.508
	18.03	4.538
	24.17	4.227
	26.20	4.326
	30.84	4.139
	41.25	3.824
0.75	5.64	4.309
	10.25	4.165
	19.46	3.948
	30.06	3.741

x	CTAB concentration / mol m^{-3}	$10^4 \mu$ / $cm^2 V^{-1} s^{-1}$
0.5	5.34	3.970
	10.05	3.626
	16.90	3.458
	23.14	3.144
	30.13	2.902
0.2	4.92	2.333
	8.91	2.098
	13.88	1.883
	19.27	1.650
	29.99	1.368
0.1	5.14	1.477
	10.12	1.255
	14.40	1.084

APPENDIX 4

Diffusion Coefficient Data

Surfactant	x	Total surfactant concentration/ mol m^{-3}	Salt	Salt concentration/ mol m^{-3}	$10^6 D$/ $cm^2 s^{-1}$
CTAB	1	10.0	-	-	2.2
		50.0	-	-	1.08
		10.0	KBr	5.0	1.30
		10.0	KBr	12.5	0.985
		2.008	KBr	25.0	0.811
		4.987	KBr	25.0	0.823
		8.001	KBr	25.0	0.845
		10.0	KBr	25.0	0.851
		10.00	KBr	25.0	0.856
		19.994	KBr	25.0	0.966
		30.00	KBr	25.0	0.938
		40.011	KBr	25.0	1.16
		50.0	KBr	25.0	1.02
		50.00	KBr	25.0	1.273
CTAB/ $C_{12}E_6$	0.83	12.0	-	-	1.75
		60.0	-	-	3.5
CTAB/ $C_{12}E_6$	0.75	13.33	KBr	2.667	1.84
		13.33	KBr	4.167	1.7
		13.33	KBr	5.00	1.6
		13.33	KBr	8.33	1.26
		13.33	KBr	10.0	1.18
		10.0	KBr	25.0	0.818
		13.33	KBr	25.0	0.877
		20.0	KBr	25.0	0.980
		40.0	KBr	25.0	1.163
CTAB/ $C_{12}E_6$	0.5	20.0	-	-	2.4
		100.0	-	-	2.9
		10.0	KBr	25.0	0.861
		20.0	KBr	25.0	0.974
		40.0	KBr	25.0	1.127

Surfactant	x	Total surfactant concentration/ mol m^{-3}	Salt	Salt concentration/ mol m^{-3}	$10^6 D$/ $cm^2 s^{-1}$
CTAB/	0.25	10.0	KBr	25.0	0.816
$C_{12}E_6$		20.0	KBr	25.0	0.845
		40.0	KBr	25.0	0.873
CTAB/	0.2	50.0	-	-	2.8
$C_{12}E_6$		250.0	-	-	1.9
		50.0	KBr	5.0	1.86
		50.0	KBr	12.5	1.17
		50.0	KBr	25.0	0.734
CTAB/ $C_{12}E_6$	0.1245	32.14	KBr	25.0	0.526
CTAB/	0.1	2.028	KBr	25.0	0.725
$C_{12}E_6$		6.572	KBr	25.0	0.644
		10.0	KBr	25.0	0.601
		20.0	KBr	25.0	0.504
		30.0	KBr	25.0	0.466
		50.0	KBr	25.0	0.447
$C_{12}E_6$	0	10.0	-	-	0.540
		25.0	-	-	0.386
		50.0	-	-	0.336
		10.0	KBr	5.0	0.480
		10.0	KBr	12.5	0.463
		0.990	KBr	25.0	0.755
		2.396	KBr	25.0	0.645
		5.035	KBr	25.0	0.576
		10.0	KBr	25.0	0.471
		10.075	KBr	25.0	0.481
		19.980	KBr	25.0	0.391
		30.0	KBr	25.0	0.387
		50.0	KBr	25.0	0.330
SDS	1	10.013	NaCl	100.0	1.023
		20.028	NaCl	100.0	1.064
		30.008	NaCl	100.0	1.100
		39.991	NaCl	100.0	1.121
		50.00	NaCl	100.0	1.179
C_8E_4	0	10.035	NaCl	100.0	1.23
		20.005	NaCl	100.0	0.770
		30.076	NaCl	100.0	0.671
		50.060	NaCl	100.0	0.582
$C_{12}E_8$		7.922	NaCl	100.0	0.769
		40.535	NaCl	100.0	0.734